Biblioteca Digital
F C E N - U B A

BIBLIOTECA CENTRAL LUIS F LELOIR
BIBLIOTECA CENTRAL LELOIR
FACULTAD DE CIENCIAS EXACTAS Y NATURALES UBA

Tesis Doctoral

Termodinámica y simulaciones cuánticas en trampas de iones

Freitas, José Nahuel

2017-03-23

Este documento forma parte de la colección de tesis doctorales y de maestría de la Biblioteca Central Dr. Luis Federico Leloir, disponible en digital.bl.fcen.uba.ar. Su utilización debe ser acompañada por la cita bibliográfica con reconocimiento de la fuente.

This document is part of the doctoral theses collection of the Central Library Dr. Luis Federico Leloir, available in digital.bl.fcen.uba.ar. It should be used accompanied by the corresponding citation acknowledging the source.

Cita tipo APA:
Freitas, José Nahuel. (2017-03-23). Termodinámica y simulaciones cuánticas en trampas de iones. Facultad de Ciencias Exactas y Naturales. Universidad de Buenos Aires.

Cita tipo Chicago:
Freitas, José Nahuel. "Termodinámica y simulaciones cuánticas en trampas de iones". Facultad de Ciencias Exactas y Naturales. Universidad de Buenos Aires. 2017-03-23.

EXACTAS UBA
Facultad de Ciencias Exactas y Naturales

UBA
Universidad de Buenos Aires

Dirección: Biblioteca Central Dr. Luis F. Leloir, Facultad de Ciencias Exactas y Naturales, Universidad de Buenos Aires. Intendente Güiraldes 2160 - C1428EGA - Tel. (++54 +11) 4789-9293

Contacto: digital@bl.fcen.uba.ar

UNIVERSIDAD DE BUENOS AIRES

Facultad de Ciencias Exactas y Naturales

Departamento de Física

Termodinámica y simulaciones cuánticas en trampas de iones

Trabajo de Tesis para optar al título de
Doctor de la Universidad de Buenos Aires en el Área de Ciencias Físicas

por José Nahuel Freitas

Director de Tesis: Juan Pablo Paz
Consejero de Estudios: Cristina Caputo
Lugar de trabajo: Departamento de Física, FCEyN, UBA

Buenos Aires
Fecha de defensa: 23/03/2017

Resumen

En esta tesis se estudian fundamentos de termodinámica en sistemas cuánticos lineales. Se desarrolla una teoría general que permite estudiar procesos periódicos sobre redes armónicas acopladas a entornos bosónicos. Se muestra cómo las leyes usuales de la termodinámica clásica emergen a partir de la dinámica determinista del sistema. Además, los resultados obtenidos son utilizados para estudiar procesos termodinámicos en situaciones arbitrariamente alejadas del equilibrio térmico y del límite termodinámico.

El formalismo desarrollado aquí es exacto y no requiere de ciertas aproximaciones que son comunmente usadas en la literatura (acoplamiento débil y dinámica Markoviana). Esto permite entender cuáles son las consecuencias de utilizar estas aproximaciones, y establecer precisamente el rango en el que pueden ser aplicadas, lo cuál es de utilidad en otros modelos donde una solución exacta no es posible. Este desarrollo también aclara ciertas confusiones existentes en la literatura respecto de la versión dinámica de la tercera ley de la termodinámica, dado que se obtiene una demostración novedosa de la validez de esta ley para una familia general de máquinas térmicas.

Por último, se proponen experimentos en sistemas de iones atrapados para simular procesos de transporte de energía y transiciones de fase en materiales magnéticos.

Palabras clave: Información cuántica, Termodinámica Cuántica, Simulaciones Cúanticas, Sistemas Cuánticos Abiertos, Refrigeradores Cuánticos

Thermodynamics and quantum simulations in ion traps

Abstract

This thesis studies foundations of thermodynamics in quantum linear systems. A general theory is developed to study periodic processes in harmonic networks that are connected to bosonic reservoirs. It is shown how the usual thermodynamical laws emerge from the deterministic dynamics of the system. Furthermore, the obtained results are employed to study thermodynamical processes in non-equilibrium regimes which are far from the thermodynamical limit.

The developed formalism is exact and does not require some approximations that are commonly used in the literature (the weak coupling and Markovian limits). This feature allows to understand what are the consequences of using these approximations, and to establish precisely when they can be employed, which is useful in other models where an exact solution is not available. This development also clarifies some confusions existing in the literature regarding the dynamical version of the third law of thermodynamics, since it is possible to obtain a novel proof of its validity for a general family of thermal machines.

Finally, some experiments with trapped ions are proposed to simulate energy transport processes and phase transitions in magnetic materials.

Keywords: Quantum Information, Quantum Thermodynamics, Quantum Simulations, Open Quantum Systems, Quantum Refrigerators

Agradecimientos

A Juan Pablo, por el apoyo, la ayuda, y la renovada confianza.

A mis viejos y mis abuelos, por poner siempre el hombro para que yo haya podido hacer lo que quise (imposible no pensar en ellos cada vez que veo la frase 'sobre hombros de gigantes' en google scholar).

A Suyi, Aye, Jero y Tilo, por alegrarme tanto estos últimos meses de doctorado y escritura.

A Sabrina, por todo ♡.

A mi otra familia que son los pibes de la facu. A Gaby, Juli, Mario, Fede, Vir, PP, Mechi, Marian, Anita, Ari, Fer, Andres, Ioni, Leo, Pablo, Mariana, Nahuel A. y Nahuel S.

A los compañeros de QUFIBA de los que aprendí tanto en las reuniones. A Augusto, Diego, Pablo, Marcos, Fede, Richi, Ariel, Christian, Laura y Nacho.

A los grandes docentes con los que me tocó cursar o trabajar durante estos años en exactas. En especial a Ricardo Piegaia, Diego Mazzitelli, Mariano Sigman, y Guillem Perez Nadal.

Al estado nacional, a la eduación pública y gratuita, y al sistema científico argentino. Al pueblo argentino que financió mis estudios.

A los compañeros de Científicos y Universitarios Autoconvocados, por permitirme no ser indiferente ante las políticas neoliberales y la estafa electoral de Cambiemos.

A la comunidad Open Source.

Contents

I Introduction **1**

1 Quantum thermodynamics **8**
1.1 Fluctuation theorems . . . 9
1.2 Thermodynamics as a resource theory . . . 10
1.3 The theory of quantum open systems . . . 12

2 Floquet Theory **16**
2.1 Classical Floquet theory . . . 16
2.2 Floquet theory for quantum systems . . . 17
2.2.1 Floquet theory and quantum dissipation . . . 18

3 Trapped ions **21**
3.1 Linear Paul traps . . . 21
3.2 Ion crystals . . . 22
3.3 Electronic degrees of freedom and basic Hamiltonian . . . 23
3.3.1 Carrier and sideband resonances . . . 24
3.4 Laser cooling . . . 25
3.5 Quantum simulation of magnetic systems . . . 26
3.5.1 Ising-like systems with transverse magnetic field . . . 26
3.5.2 A single ion in a bi-chromatic field . . . 26
3.5.3 Generalization to many ions and the Magnus expansion . . . 27
3.5.4 Initialization and readout of the internal state . . . 29

II Driven open systems with continuous variables **32**

4 An exactly solvable model **33**
4.1 Heisenberg's equations of motion . . . 34
4.2 An integro-differential equation for the system's operators . . . 35
4.2.1 Dissipation kernel . . . 36
4.2.2 Solution of the equation of motion . . . 36
4.2.3 Renormalization and damping kernel . . . 36
4.3 Evolution of quantum states . . . 37
4.3.1 Evolution of the covariance matrix . . . 37
4.3.2 Evolution of the Wigner characteristic function . . . 38
4.3.3 Evolution of the Wigner quasiprobability distribution . . . 39

5 Periodic processes **41**
5.1 Asymptotic state for stable systems . . . 41
5.2 Periodic driving . . . 42
5.3 Calculation of the function $p(t, \omega)$ . . . 43

III Emergence of thermodynamical laws **46**

6 Definitions of work and heat rates **47**
6.1 Total work and heat rates . . . 47
6.2 Local heat rates . . . 48
6.3 Work and heat in the asymptotic state . . . 48
6.4 Heat transfer matrix . . . 49
6.5 Heat rates in terms of elementary processes . . . 50
6.6 Dynamical Casimir effect as a fundamental limit for cooling . . . 52
6.7 Time independent systems . . . 53
6.8 A further extension of the model . . . 54

7 Validity of the second law **57**
7.1 The Planck proposition . . . 57
7.2 Irreversible entropy generation . . . 58

8 Fundamental limits for cooling processes **61**
8.1 Laser cooling . . . 62
8.1.1 Power spectrum of the radiation emitted into the EM field . . . 63
8.2 An adaptative cooling strategy . . . 66

IV Experimental proposals **71**

9 Heat transport through ion crystals **72**
9.1 Anomalous transport and the failure of the Fourier's Law . . . 72
9.2 The model . . . 73
9.3 Results . . . 76

10 Simulation of the ANNNI model with trapped ions **81**
10.1 Adiabatic quantum simulations with trapped ions . . . 81
10.1.1 Controlling the range and sign of the Ising interactions . . . 82
10.2 Many spectral pairs and approximation of target interactions . . . 84
10.3 The ANNNI model . . . 85
10.4 Approximating the ideal ANNNI model . . . 86
10.4.1 An iterative procedure . . . 87
10.4.2 Phase transitions at zero temperature . . . 89

V Conclusions **92**

VI Supplementary Material **95**

A Structural phases in ion crystals **96**

B Integration techniques for undriven systems **99**
B.1 Green's function and the cubic eigenvalue problem 99
B.2 Frequency integrals for the covariance matrix and heat currents 101

C Weak coupling approximation, minimum cooling temperature, and numerical evaluation of the heat rates **104**
C.1 Weak coupling approximation 104
C.2 Minimum temperature 105
C.3 Numerical evaluation of the heat rates for a simple case 106

Part I

Introduction

In the last decades the research in Quantum Mechanics was increasingly dominated by the fields of 'Quantum Information' and 'Quantum Computation' [1]. One of the objectives in these areas is to understand what are the implications of the unique properties of Quantum Mechanics (like entangled states or the wave function collapse) for the manipulation, transmission, and processing of information. The seminal ideas were originally introduced by Richard Feynman in 1982 when he proposed to employ well controlled quantum systems in order to simulate the physics of other target system [2]. Few years later it was shown by Bennet and Bassard that the properties of quantum mechanics could be employed to design fundamentally secure schemes of key distribution for cryptography [3]. Also, it was shown that quantum computers could offer significant advantages for solving problems that were intractable for classical computers, in particular the factorization of large integers [4].

These and later ideas stimulated the interest in building quantum systems capable of implementing the envisioned quantum processing of information. The subsequent interplay between theoretical and experimental progress led to the development of experimental platforms in which individual quantum systems can be controlled with an astonishing level of precision. Today, it is possible to precisely control the quantum state of individual ions confined in electromagnetic traps [5,6]. Arrays of tens of these ions were employed as a quantum register to run elementary quantum algorithms [7–10]. Pairs of entangled photons are routinely produced in many laboratories in the world to perform quantum key distribution for cryptography or quantum state teleportation [11–14]. Quantum optical technology is even commercially available [15], and being tested is space [16]. Also, increasingly complex and powerful superconducting circuits are constructed in which the quantum state of Josephson junctions and microwave cavities is employed to store and process quantum information [17–20]. Many more quantum technologies are currently under development [21].

Although a full fledged and large quantum computer is still not a reality, this impressive experimental progress also open the door for new research in fundamental questions, or unexplored regimes in which quantum systems have not been yet tested or employed. For example, although a completely programmable quantum computer is needed to *digitally simulate* the physics of an arbitrary quantum system, another less demanding kind of simulation is possible. This alternative is known as *'analogous quantum simulation'* and consists on engineering the natural and continuous time evolution of a highly controllable quantum system in order for it to mimic the evolution of a real or hypothetical target system that is not accessible [21]. Of course, only a limited family of systems can be simulated in this way with a given experimental platform. Examples along this line include the simulation of: Ising models of magnetic materials with trapped ions [22, 23] or superconducting qubits [18] (the commercial platform D-Wave might be another example of the second case [24]), controlled decoherence in open quantum systems [25], the dynamics of lattice gauge theories [26], and the Bose-Hubbard model [27].

Another area that received much attention in recent years is that of 'Quantum Thermodynamics', in which thermodynamical processes are studied from a quantum mechanical and dynamical viewpoint [28, 29]. There are many ways in which the mentioned progress in Quantum Mechanics can be related to thermodynamics. In first place, the precise control of individual quantum systems is closely related to the common thermodynamical process of cooling. Atoms, optical cavities, mechanical resonators, and electronic systems must often be cooled to ultra low temperatures in order to avoid spurious thermal excitations. In ion traps, ions are cooled down close to its motional ground

state as the first step of any quantum algorithm. Second, as the connection between classical information theory and statistical mechanics is well known [30, 31], the development of quantum information theory has a natural application to the study and revision of fundamental concepts in thermodynamics [32, 33]. Finally, the new experimental platforms allow to study individual, microscopic or mesoscopic quantum systems in non-equilibrium situations where usual thermodynamical treatments break down. An engine composed of a single ion has been recently constructed [34], the distribution or work performed on a single quantum harmonic oscillator was measured [35, 36], and single electrons can be transported between quantum dots [37]. Thus, new theoretical developments are needed to extend the limits of classical thermodynamics.

The results presented in this thesis aim to contribute to the fields of quantum thermodynamics and quantum simulations. An exact formalism is developed to study thermodynamical processes on a restricted family of linear quantum thermal machines. The fundamental limits for cooling in this setting are identified, showing that they are related to the well known Dynamical Casimir Effect (DCE). Importantly, it is shown that common approximations fail to capture this effect. Also, new experiments with trapped ions are proposed to simulate the transport of heat across microscopic crystalline structures, as a function of relevant parameters such as disorder and dimensionality. The quantum simulation of magnetic materials with trapped ions is also explored.

This thesis is organized as follows. The first three chapters are introductory material. In chapter 1 a brief review of different topics in quantum thermodynamics is provided, in order to put into context the work later presented. Chapter 2 is a very general description of Floquet Theory, that contains some concepts that might be useful later on. Ending the introductory part, Chapter 3 gives a very basic picture of how an ion trap works, and how the motion of an ion and its internal state is manipulated. This is necessary to understand the experimental proposals presented in the last two chapters.

In chapters 4 and 5 the main model of this thesis is introduced: a family of linear quantum machines consisting in arbitrary networks of harmonic oscillators, connected to several bosonic reservoirs at different temperatures, and whose parameters can be driven in a periodic fashion. It is shown that this model can be solved without requiring any approximation such as weak coupling or Markovian hypothesis.

The following three chapter explains how the usual thermodynamical laws emerge in the family of thermal machines previously presented. Chapter 6 presents and discusses the microscopic definitions of thermodynamical quantities such as heat and work. From this definitions the first law of thermodynamics follows trivially. An exact expression for the heat current between the system and each thermal reservoir is obtained. A physical interpretation of this expression is put forward, from which it follows that the fundamental limit for cooling in this family of thermal machines is given by a pairs creation mechanism analogous to the DCE. Then, chapter 7 analyses the validity of the second law of thermodynamics, and chapter 8 discusses the validity of the dynamical third law, or unattainability principle, and shows how to employ the developed formalism to calculate the minimum achievable temperature in some relevant cooling schemes.

Finally, the last two chapters describe experimental proposals. In chapter 9 the heat transport through crystals of trapped ions is studied. It is shown that the flow of heat strongly depends on the disorder and dimensionality of the crystal, and that these systems are promising candidates to observe the transition from normal or diffusive heat transport, to an abnormal or 'ballistic' regime. Chapter 10 explores the possibility of extending state of the art experiments on the simulation of magnetic materials with trapped

ions in order to simulate more complex models, with special emphasis in the ANNNI [1] model.

[1] ANNNI stands for Anisotropic Next-Nearest-Neighbor Interactions

Introducción

En las últimas décadas la investigación en mecánica cuántica fue progresivamente dominada por las áreas de 'Información cuántica' y 'Mecánica Cuántica' [1]. Uno de los objetivos en estas áreas es entender cuáles son las implicaciones de las propiedades únicas de la mecánica cuántica (como los estados entrelazados o el colapso de la función de onda) para la manipulación, transmisión, y procesamiento de información. El inicio de estas ideas fue originalmente introducido por Richard Feynman en 1982 cuando propuso el empleo de sistemas cuánticos como elementos de cómputo para la simulación de la física de otros sistemas cuánticos a los que no se tiene acceso [2]. Pocos años mas tarde Bennet y Bassard mostraron que las propiedades de la mecánica cuántica pueden ser usadas para diseñar esquemas fundamentalmente seguros de distribución de claves para criptografía [2]. También, se demostró teóricamente que las computadoras cuánticas podrían ofrecer ventajas significativas para resolver problemas que eran intratables para computadoras clásicas, en particular la factorización de números enteros [4].

Estas ideas estimularon el interés en la construcción de sistemas cuánticos capaces de implementar el procesamiento cuántico de la información. La interacción subsiguiente entre progresos experimentales y teóricos llevó al desarrollo de plataformas experimentales donde sistemas cuánticos individuales pueden ser controlados con un sorprendente nivel de precisión. Hoy, es posible controlar el estado cuántico de iones individuales confinados en trampas electromagnéticas [5,6]. Arreglos de decenas de estos iones fueron empleados como registro cuántico para ejecutar algoritmos cuánticos elementales [7–10]. Pares de fotones entrelazados son rutinariamente producidos en muchos laboratorios del mundo para realizar distribución de claves criptográficas o teleportación cuántica [11–14]. Tecnologías basadas en óptica cuántica están incluso disponibles comercialmente [15], y siendo actualmente probadas en el espacio [16]. También son construidos circuitos superconductores cada vez más complejos y poderosos, en donde el estado cuántico de junturas de Josephson y cavidades de microondas es utilizado para almacenar y procesar información [17–20]. Muchas otras tecnologías cuánticas se encuentras actualmente en desarrollo [21].

Aunque una computadora cuántica completamente desarrollada no es todavía una realidad, este impresionante progreso experimental abre las puertas para nuevas investigaciones en preguntas fundamentales, o hacia nuevos regímenes en donde los sistemas cuánticos aún no han sido utilizados o examinados. Por ejemplo, aunque una computadora cuántica completamente programable es necesaria para *simular digitalmente* la física de un sistema cuántico arbitrario, otro tipo menos demandante de simulación es posible. Esta alternativa se conoce como *simulación cuántica analógica*, y consiste en el control y diseño de la evolución natural y continua de un sistema cuántico controlable, de forma que esta simule la evolución de otro sistema cuántico, real o hipotético, al que no se tiene acceso [21]. Por supuesto, solo una familia limitada de sistemas pueden ser simulados de esta manera con una dada plataforma experimental. Ejemplos de este tipo incluyen la

simulación de: modelos tipo Ising de materiales magnéticos con iones atrapados [22, 23] o qubits superconductores [18] (la plataforma comercial D-Wave podría ser otro ejemplo [24]), decoherencia controlada en sistemas cuánticos abiertos [25], la dinámica de teorías de gauge [26], o el modelo de Bose-Hubbard [27].

Otra área que recibió mucha atención en los último años se conoce como 'Termodinámica Cuántica', en la cuaĺ se estudian procesos termodinámicos desde el punto de vista de la dinámica cuántica subyacente [28, 29]. El progreso mencionado anteriormente en mecánica cuántica está relacionado de muchas maneras con la termodinámica. En primer lugar, el control preciso de sistemas cuánticos individuales esta fuertemente ligado al proceso termodinámico de refrigeración. Átomos, cavidades ópticas, resonadores mecánicos, y sistemas electrónicos deben ser enfriados a temperaturas ultra bajas para evitar excitaciones cuánticas espurias. En experimentos con iones atrapado, estos son enfriados hasta que su estado de movimiento alcanza casi el estado fundamental, como primer paso de cualquier cómputo cuántico. En segundo lugar, dado que la conexión entre la teoría de la información clásica y la mecánica estadística se conoce ampliamente [30, 31], el desarrollo de la teoría de la información cuántica tiene una aplicación natural en el estudio y revisión de conceptos fundamentales en termodinámica [32, 33]. Finalmente, las nuevas plataformas experimentales permiten estudiar sistemas cuánticos individuales, microscópicos, o mesoscópicos en situaciones fuera del equilibrio térmico donde las herramientas usuales de la termodinámica no pueden ser aplicadas. Un motor compuesto de un único ion fue construido recientemente [34], se midió la distribución de trabajo realizado sobre un único oscilador armónico cuántico [35,36], y electrones únicos pueden ser transportados entre puntos cuánticos[2] [37]. Por lo tanto, nuevos desarrollos teóricos son necesarios para extender los límites de la termodinámica clásica.

Los resultados presentados en esta tesis pretenden contribuir a las áreas de Termodinámica Cuántica y Simulaciones Cuánticas. Un formalismo exacto es desarrollado para estudiar procesos termodinámicos en una familia restringida de máquinas térmicas cuánticas. Los límites fundamentales de estas máquinas para la refrigeración fueron identificados, mostrando que estos están relacionados con el Efecto Casimir Dinámico (ECD). Se muestra también que este efecto no es capturado por tratamientos comunes que emplean ciertas aproximaciones. Además, se proponen nuevos experimentos con iones atrapados para simular el transporte de calor a través de estructuras cristalinas microscópicas, como función de parámetros relevantes como el desorden y la dimensionalidad. También se explora la simulación cuántica de materiales magnéticos.

Esta tesis está organizada de la siguiente manera. Los primeros tres capítulos son material introductorio. En el capítulo 1 se repasan brevemente diferentes temas de termodinámica cuántica, para poner en contexto el trabajo que se presenta más adelante. El capítulo 2 es una descripción muy general de la teoría de Floquet, que contiene algunos conceptos que pueden ser útiles más adelante. Finalizando la introducción, en el capítulo 3 se da se da una explicación básica de como funciona una trampa de iones, y como el movimiento y estado interno de los iones es manipulado. Esto es necesario para poder entender las propuestas experimentales que se dan en los últimos dos capítulos.

En los capítulos 4 y 5 se introduce el modelo principal de esta tesis: una familia de maquinas térmicas lineales que consiste en redes arbitrarias de osciladores armónicos conectados a varios entornos bosónicos a distinta temperatura, y cuyos parámetros pueden ser variados en el tiempo de forma periódica. Se muestra que este modelo puede ser resuelto exactamente, sin requerir ninguna aproximación (como por ejemplo las aproximaciones Markovianas o de acoplamiento débil que son ampliamente uti-

[2] Quantum dots

lizadas).

Los siguientes tres capítulos explican como emergen las leyes usuales de la termodinámica en la familia de máquinas térmicas consideradas previamente. En el capítulo 6 se presentan y discuten definiciones microscópicas de cantidades termodinámicas como calor y trabajo. A partir de estas definiciones la primera ley de la termodinámica se obtiene trivialmente. Se obtiene una expresión exacta para las corrientes de calor entre el sistema central y cada reservorio térmico. Se da una interpretación física de esta expresión, de la cual se deduce que que el límite fundamental para el enfriamiento en esta familia de máquinas esta dado por un mecanismo de creación de pares análogo al ECD. Luego, el capítulo 7 analiza la validez de la segunda ley de la termodinámica, y el capítulo 8 discute la validez de la versión dinámica de la tercera ley, y muestra como emplear el formalismo desarrollado para calcular la mínima temperatura alcanzable en algunos esquemas de enfriamiento relevantes.

Finalmente, los últimos dos capítulos describen propuestas experimentales. En el capítulo 9 se estudia la corriente de calor transportada a través de cristales formados por iones atrapados. Se muestra que el flujo de calor depende fuertemente del desorden y la dimensionalidad del cristal, y que estos sistemas son candidatos prometedores para observar la transición entre los regímenes de transporte difusivo y 'balístico'. En el capítulo 10 se explora la posibilidad de extender algunos experimentos actuales sobre la simulación cuántica de materiales magnéticos con iones atrapados, de forma de simular modelos mas complejos. Se pone especial énfasis en el modelo ANNNI [3].

[3] ANNNI son las siglas en inglés para Interacciones anisotrópicas a segundos vecinos.

Chapter 1

Quantum thermodynamics

The relation between thermodynamics and quantum mechanics goes back to the birth of quantum mechanics. As is well known, the analysis of the observed energy distribution of the electromagnetic field at thermal equilibrium led Max Planck to the idea that the energy of harmonic oscillators was quantized. This idea was later expanded by Albert Einstein, when he proposed that light was in fact composed of discrete packets of energy, now called photons. Thus, it is possible to say that quantum mechanics emerged from the search of consistency between microscopic models of radiation and matter and macroscopic thermodynamics. Later on, quantum mechanics had an independent development, although consistency with the main thermodynamical laws was always maintained. Highly successful dynamical models of matter and radiation were proposed and tested in non-equilibrium regimes where classical thermodynamics had not much to say. Nowadays, quantum mechanics is a general and well developed theory which gives a consistent framework to describe the ultimate components of matter and its interactions.

In the last decades the relation between quantum mechanics and thermodynamics was somewhat inverted with respect to its origin: now, many researchers try to understand how and to what extent the usual macroscopic laws of thermodynamics emerge from a given quantum substrate. This line of inquiry, called Quantum Thermodynamics [28, 29, 33], is perhaps motivated by the following reasons:

- *Reductionist understanding of macroscopic laws*. The decomposition of complex and macroscopic behaviors in terms of simpler processes operating at lower spatial and temporal scales is a basic method of all science. When this method can be applied to composite systems, it usually provides a detailed understanding of emergent phenomena in terms of more elementary laws. The ubiquity of thermal states and the dynamical approach to them [38, 39], the apparent inconsistency between the Second Law of thermodynamics and the time-invariant character of quantum mechanical evolution [40–42], the relation between the notion of information and the physical origin of entropy [30, 33, 43, 44], are all examples of problems and questions in which a microscopic understanding of thermodynamical laws seems to be needed.

- *Expansion of the limits of classical thermodynamics*. Classical thermodynamics can only make statements about the properties of systems at thermal equilibrium, and about the possibility of reaching a particular equilibrium state from another one. Dynamical processes can only be analyzed in the quasiestationary regime in which at all times the system in question is in equilibrium with its environment. There is

no notion of time in classical equilibrium thermodynamics. Later developments in non-equilibrium thermodynamics enabled the analysis of settings in which energy, charge or mass is transported between thermal reservoirs at different temperature or chemical potential [45, 46]. However, general results were initially restricted to the so called 'linear regime', in which the deviations from thermal equilibrium are small. A description of thermodynamical processes from a quantum dynamical point of view would allow to consider situations arbitrarily away from thermal equilibrium.

- *Description of new machines working at the quantum level*. Technological progress in the manipulation of individual quantum systems has enabled the fabrication of thermal machines operating at quantum regimes: individual atoms can be trapped and cooled close to the ground state by means of their interaction with individual photons, a thermal engine in which the working substance is composed of a single trapped ion has been proposed [47] and constructed [34], the electronic and spin transport between quantum dots can be controlled at the single electron level [48, 49]. At variance with macroscopic systems at finite temperature, these devices are dominated by quantum fluctuations. Thus, a fully quantum description of their operation is needed.

Quantum thermodynamics is therefore a very wide subject comprising physical implementations of thermal machines in different experimental platforms, as well as general concepts, ideas, and methods involved in the description of non-equilibrium processes that are out of the reach of previous developments. We will briefly review here three general and modern approaches to the treatment of thermodynamical processes from a quantum perspective. First we mention the general concepts behind fluctuation theorems. Then we mention the treatment of thermodynamics as a 'resource theory', that is inspired in the theory of entangled states. The last, more traditional, approach is based on the theory of quantum open systems, in which the exact quantum dynamics of a system that is interacting with an environment (in general considered to be another quantum system) is studied.

1.1 Fluctuation theorems

Statistical mechanics, quantum or classical, gives a connection between the microscopic dynamics of a system and its macroscopic state at thermal equilibrium. From this connection it is possible to predict the expected values of macroscopic variables like energy, pressure or volume, and also their fluctuations about these expected values. For example, we know how the average speed of molecules escaping from an oven with a hot gas is related to the temperature of the oven, but we also know that the velocities of individual molecules are distributed according to the Maxwell-Boltzmann distribution. What fluctuation theorems address are the fluctuations in macroscopic variables related to processes that drive the system out of thermal equilibrium, typically heat or work, about which statistical mechanics gives no information (except in cases where the final state is also at themal equillibrium).

Fluctuation relations have a long history, with the first general results appearing in the decade of 1950 in the work of Green and Kubo, although they were valid only in the linear regime close to thermal equilibrium. In the last decade of the past century general relations were established that accounted for the fluctuations in completely general non-equilibrium and quantum settings. A short review of the main historical points in the

development of the fluctuation theorems can be found in [50], but perhaps the most famous of the recent results is the Jarzynski equality [51].

Jarzynski considered a quantum or classical system that is at thermal equilibrium at temperature T and is driven out of it by a time dependent process that change the Hamiltonian of the system from H_a to H_b in a given period of time. Since the initial state is thermal, the system can start the process in different configurations, with different probabilities. Therefore the work performed on the system by the driving will be different for each run. Jarzynski showed that the probability $P(W)$ of performing work W is such that the following equality is satisfied:

$$\left\langle e^{-\beta W} \right\rangle = e^{-\beta \Delta F} \tag{1.1}$$

with $\beta = (k_b T)^{-1}$ and $\Delta F = F_b - F_a$ is the free energy difference between the final and initial Hamiltonians, i.e, F_x is the Helmholtz free energy corresponding to a thermal state of the Hamiltonian H_x at temperature T. Thus, the Jarzynski equality relates properties of thermal equilibrium (ΔF), to properties of arbitrary non-equilibrium processes ($P(W)$). Applying the Jensen's inequality to Eq. (1.1), it can be easily deduced that $\langle W \rangle \leq \Delta F$, which is a well known result for irreversible processes.

The Jarzynski equality can be derived from an independent result known as the Tasaki-Crooks relation [52], that reads:

$$\frac{P_f(W)}{P_b(W)} = e^{-\beta(\Delta F - W)} \tag{1.2}$$

where $P_f(W)$ is the probability of performing work W during the *'forward'* execution of a process, while $P_b(W)$ correspond to the time reversed (*'backwards'*) version of the same process. Fluctuations theorems with the same form as Eq. (1.2) has been derived also for the transport of mass, charge, and energy [53].

1.2 Thermodynamics as a resource theory

A resource theory is defined by a set of of quantum states and operations that are considered 'free'. A state or operation that is not free is then a 'resource' that can be employed to perform tasks that are not initially accessible via free states or operations. A prominent example is the theory of entangled states, which are the resources that emerge when the free states considered are the separable states and the free operations are the local operations aided with classical communication. Thus, entangled states enable the realization of tasks that are otherwise impossible, like quantum teleportation, for example.

Thermodynamic transformations at background temperature T can also be put in the framework of a resource theory. In this case the free states are thermal states at temperature T. The free operations are those in which the system of interest can interact with an arbitrary auxiliary system, or ancilla, that is initially in a thermal state at temperature T, via an energy conserving interaction. These are called 'thermal operations'. Explicitly, if ρ is the density matrix of the system, the allowed transformations $\mathcal{E}$ are parametrized by [54, 55]:

$$\mathcal{E}(\rho) = \mathrm{Tr}_A[U(\rho \otimes \rho_A)U^\dagger] \tag{1.3}$$

where, if the Hamiltonians of the system and the ancilla are respectively H and H_A, $\rho_A \propto e^{-H_A/(k_b T)}$ is a thermal state of the ancilla at temperature T, and U is an arbitrary

unitary operation acting on both system and ancilla with the restriction of conserving the total energy, i.e., it must satisfy $[U, H \otimes \mathbb{1} + \mathbb{1} \otimes H_A] = 0$. In this case, the resource states are states out of thermal equilibrium, or at thermal equilibrium at a temperature $T' \neq T$. A feature of thermal operations is that they cannot perform work by themselves. However, they can be employed to extract work from resource states.

A number of important results can be obtained in this framework. We only mention here the generalization of the Second Law of thermodynamics presented by Brandao and others in [56]. They have found that a initial state ρ of a system with Hamiltonian H can be transformed to a final state ρ' via thermal operations if and only if $F_\alpha(\rho, \rho_\beta) \geq F_\alpha(\rho', \rho_\beta)$ for all $\alpha \geq 0$, where $\rho_\beta = e^{-\beta H}/Z$ is a thermal state of the system at inverse temperature $\beta = (k_b T)^{-1}$, $Z = \mathrm{Tr}[e^{-\beta H}]$, and the functions F_α are defined as[1]:

$$F_\alpha(\rho, \rho_\beta) = k_b T \left[D_\alpha(\rho || \rho_\beta) - \log(Z) \right] \tag{1.4}$$

where the function $D_\alpha(\rho||\rho_\beta)$ is the Rényi divergence of state ρ from state ρ_β. It is defined in the following way:

$$D_\alpha(\rho||\rho_\beta) = \frac{\mathrm{sgn}(\alpha)}{\alpha - 1} \log \left(p_i^\alpha q_i^{1-\alpha} \right) \tag{1.5}$$

where $\{p_i\}$ and $\{q_i\}$ are the eigenvalues of ρ and ρ_β, respectively. The continuous family of functions $F_{\alpha \geq 0}$ is a generalization of the usual Helmholtz free energy $F(\rho) = \langle E \rangle - k_b T S$, where $\langle E \rangle = \mathrm{Tr}[\rho H]$ and S is the von Neumann entropy $S(\rho) = -\mathrm{Tr}[\rho \log(\rho)]$. In fact, the Helmholtz free energy is recovered in the limit $\alpha \to 1$, i.e, $\lim_{\alpha \to 1} F_\alpha(\rho||\rho_\beta) \to F_1(\rho, \rho_\beta) = F(\rho)$. Thus we see that the family of conditions $F_\alpha(\rho, \rho_\beta) \geq F_\alpha(\rho', \rho_\beta)$ (for all $\alpha \geq 0$) includes the common version of the Second Law that states that when interacting with a thermal reservoir the Helmholtz free energy can only decrease. However, in the general case there are more constraints to possible state transitions. Not only the usual Helmholtz free energy must decrease in order for a transition $\rho \to \rho'$ to be thermodynamically possible, all the generalized free energies $F_\alpha(\rho, \rho_\beta)$ must decrease. This result can be considered a generalization of the Second Law of thermodynamics to the quantum regime. Interestingly, it is also shown in [56] that in the limit in which the system is macroscopic all the family of free energies collapses to the Helmholtz free energy, i.e., $F_\alpha(\rho, \rho_\beta) \simeq F_1(\rho, \rho_\beta) = F(\rho)$. Thus, we see that the additional restrictions on possible state transitions are only relevant away from the thermodynamical limit.

The connection between the functions F_α and the usual notion of free energy becomes stronger when analyzing how much work can be extracted in a transition $\rho \to \rho'$. It is found that the maximum amount of extractable work W is given by:

$$W = k_b T \inf_\alpha \left[F_\alpha(\rho, \rho_\beta) - F(\rho, \rho_\beta) \right] \tag{1.6}$$

which again is compatible with the usual limit to the work that can be extracted as the difference in the Helmholtz free energy, although it is more stringent in the general case.

The results presented in the second and third parts of this thesis can also be understood as an example of a resource theory. We will consider a restricted but sufficiently general class of thermal machines where the resources are: i) access to bosonic reservoirs in thermal equilibrium states ii) access to arbitrary networks of harmonic oscillators, whose parameters can be driven periodically in time, and iii) the implementation of dipolar interactions between the harmonic network and the thermal reservoirs. Then, we will try to answer the following questions: are the usual laws of thermodynamics

[1] This results are actually restricted, for simplicity, to states that are block diagonal in the energy eigenbasis

valid in this setting? how do they emerge? how the exchange of energy between the harmonic network and the reservoirs (heat currents) depends on the driving, the temperatures, and other parameters? Under which conditions is it possible to extract energy (to cool) a given reservoir? If it is possible, what is the minimum temperature that can be achieved? What are the limitations imposing this minimum temperature?. We can summarize these questions in the simple one: what tasks it is possible to perform with the given resources?. An example of the kind of answers that can be obtained can be found in [57], where the same family of linear thermal machines was considered, but without the possibility of driving the system parameters. It was found that it was not possible with the given resources to construct what is known as 'quantum absorption refrigerators' [58, 59]. In this kind of refrigerators, a non-equilibrium current established by a thermal gradient between two thermal reservoirs connected to a central system generates the cooling of a third thermal reservoir, even if the temperature of this last reservoir is lower than the other two. Thus, it was concluded that non-linear resources are crucial to construct absorption refrigerators.

1.3 The theory of quantum open systems

The previous approaches aim at identifying general and exact thermodynamic relations valid even if the system is away of thermal equilibrium or the thermodynamic limit. There is another widely used strategy, in some sense more traditional, that is based in solving the dynamics of a quantum system that is interacting with an environment. Although it does not directly offer any insight into general principles, it is perhaps better suited to deal with situations in which a steady non-equilibrium state is established. It also allows to take into account details of the thermal reservoirs, like its spectral content.

This is the approach employed in this thesis, so it will be described in detail. We consider a quantum system S that is interacting with a number of thermal reservoirs E_α, that are coupled to the system via interaction terms $H_{int,\alpha}$. Then, the total Hamiltonian is:

$$H(t) = H_S(t) + \sum_\alpha H_{E,\alpha} + \sum_\alpha H_{int,\alpha} \tag{1.7}$$

where $H_S(t)$ is the system's Hamiltonian, possibly time dependent, and $H_{E,\alpha}$ is the Hamiltonian of the α-th reservoir. Thus, if $\rho_T(s)$ is the total density matrix of system and reservoirs, it evolves according to the von Neumann equation

$$i\hbar \, \frac{d\rho_T}{dt} = [H(t), \rho_T(t)] \tag{1.8}$$

which describes an unitary evolution for the global state. The previous equation can be integrated given an initial state $\rho_T(0)$. This state is usually taken to be a product state of the form $\rho_T(0) = \rho_S(0) \otimes \rho_E(0)$, where the system and the environment are uncorrelated ($\rho_S(0)$ and $\rho_E(0)$ are the initial states of the system and environment, respectively). Also, in the initial state of the environment each reservoir is in a thermal state and uncorrelated with the others, i.e, $\rho_E(0) = \bigotimes_\alpha e^{-\beta_\alpha H_{E,\alpha}} / \operatorname{Tr}[e^{-\beta_\alpha H_{E,\alpha}}]$, where $\beta_\alpha = (k_b T_\alpha)^{-1}$ is the initial inverse temperature of each reservoir.

Once the Eq. (1.8) is integrated up to time t, the reduced state of the system can be obtained as $\rho_S(t) = \operatorname{Tr}_E \rho_T(t)$. From the reduced state of the system we can obtain the expectation values of observables of interest as $\langle A \rangle (t) = \operatorname{Tr}[\rho_S(t) A]$. From such observables it is possible to calculate thermodynamic variables like the energy of the system, the energy interchanged with each reservoir (heat), the work performed by the

driving of the Hamiltonian, etc. Thus, we can describe in this way thermodynamical processes where the system is driven away of equilibrium by two mechanisms: (i) the arbitrary time dependence of the system's Hamiltonian $H(t)$, and (ii) the fact that it can be in simultaneous contact with several reservoirs at different temperatures.

Of course, this general program face several difficulties. In first place, in almost all realistic situations at least one thermal reservoir is a system with many, if not infinite, degrees of freedom. Thus, the description and analytical manipulation of the global quantum state (which may be simple initially) can turn out to be prohibitively demanding. Also, for arbitrary variations in time of the Hamiltonian $H_S(t)$ the Eq. (1.8) can only be integrated numerically. The theory of Quantum Open Systems developed in the last 50 years offers some tools to deal with the first of these problems [60]. A possible solution is to derive, from the global unitary evolution of Eq. (1.8) an evolution equation for the reduced state $\rho_S(t)$, where the environmental degrees of freedom are traced out. These are called 'master equations' and generally adopt the following form:

$$i\hbar \, \frac{d\rho_S}{dt} = [H_R(t), \rho_S(t)] + \int_0^t dt' \; \mathcal{K}(t,t') \; \rho_S(t'). \tag{1.9}$$

The first term describes the unitary part of the evolution, which is associated to a renormalized Hamiltonian $H_R(t)$ that in general does not coincide with the original $H_S(t)$. The second term takes into account the non-unitary part of the evolution (dissipation and diffusion, for example), as well as non-Markovian memory effects. It depends on the kernel $\mathcal{K}(t,t')$ that is in general a super-operator acting on the state ρ_S. Thus, now we only need to track the evolution of the system, since the environmental degrees of freedom were eliminated.

A paradigmatic example of quantum open system is the Caldeira-Legget model of Quantum Brownian Motion (QBM) [61]. In this model the system is a single harmonic oscillator that is interacting in a bilinear way with a bath also formed by a continuous distribution of harmonic oscillators. Due to its linearity, an exact master equation can be obtained for this model [62, 63]. It reads:

$$\begin{aligned} \frac{d}{dt}\rho(x,x') = \frac{1}{i\hbar} \langle x| \, [H_R(t), \rho] \, |x'\rangle &- \gamma(t)(x-x') \left(\frac{\partial}{\partial x} - \frac{\partial}{\partial x'} \right) \rho(x,x') \\ &- D(t)(x-x')^2 \rho(x,x') \\ &+ if(t)(x-x') \left(\frac{\partial}{\partial x} + \frac{\partial}{\partial x'} \right) \rho(x,x') \end{aligned} \tag{1.10}$$

where $\rho(x,x') = \langle x| \, \rho \, |x'\rangle$. We see that, at variance with the general form of Eq. (1.9), the exact master equation for the QBM is local in time. However, non-Markovian memory effects are still captured by the time dependence of the coefficients $\gamma(t)$, $D(t)$, and $f(t)$ which respectively describe dissipation, diffusion, and anomalous diffusion effects [63], and also of the renormalized Hamiltonian $H_R(t)$.

In some situations where the characteristic decay time of the environment correlation functions is much shorter than the time scales of the system dynamics it is valid to employ the Markovian approximation, which disregards the memory effects induced by the environment. This correspond to using a kernel $\mathcal{K}(t,t')$ in Eq. (1.9) that is local in time, i.e, such that $\mathcal{K}(t,t') \propto \delta(t-t')$, since in that case the $\frac{d\rho_S}{dt}$ only depends on the instantaneous state $\rho_S(t)$ and not on its history. When the Markovian approximation is applied to the Caldeira-Legget model of QBM a master equation with the same form as

Eq. (1.10) is obtained, but with time independent coefficients[2].

It can be proven that the most general Markovian evolution of a quantum state (preserving the positivity of the density matrix) can always be described by a local differential equation of the form [64]:

$$\frac{d\rho}{dt} = \frac{1}{i\hbar}[H,\rho] - \sum_n \gamma_n (L_n^\dagger L_n \rho + \rho L_n^\dagger L_n - 2L_n \rho L_n^\dagger) \tag{1.11}$$

for some positive constants γ_n and operators L_n. This is known as the 'Lindblad form' for master equations and is widely employed in the theory of quantum open systems. Master equations in Lindblad form can be derived from a phenomenological point of view, in which one chooses the operators L_n in order to obtain an effective description of an observed behavior (the spontaneous decay of an atom, for example), or from a microscopic model of the environment and its interaction with the system [60]. In the latter case the following approximations are often employed (apart from the Markovian assumption):

- *Weak coupling.* It is very common to assume that the interaction between system and environment is weak, and in that case the derived master equations are usually only valid to second order in the interaction Hamiltonian.
- *Born approximation.* It is assumed that the environment is much larger than the system and that the interaction between them does not significantly affects the environmental state. Also, it is considered that system and environment remain uncorrelated. This assumption is also related to the weak coupling and Markovian approximations.
- *Secular or 'Rotating wave' approximation.* All fast rotating terms of the total Hamiltonian in the Interaction Picture are disregarded. This approximation is often justified by noting that only the 'slow' or 'average' dynamic of the system is of interest.

Only few models of quantum open system can be solved without requiring any of these approximations. The Caldeira-Legget model of QBM is one of them. However, as is explained in the next section, further complications arise if the system is externally driven. In chapter 4 we define a general family of linear quantum systems that are interacting with different thermal environments and are also externally driven. We show how to exactly solve the dynamics of the system, without employing any of the previously mentioned approximations. We will use this simple model of driven open system to study thermodynamical processes in which energy is transported between thermal environments. Based on the exact solution, we will analyze some of the consequences of employing the weak coupling approximation. We show that some processes cannot be captured by the second order weak coupling approximation, and that they are relevant to analyze the fundamental limits for cooling.

[2]In this case the obtained equation does not preserve the positivity of the density matrix. Therefore, it cannot be cast in Lindblad form.

Termodinámica Cuántica

La relación entre la termodinámica y la mecánica cuántica se remonta al origen mismo de esta última. Como es bien sabido, el análisis de la distribución de energía del campo electromagnético en equilibrio térmico llevó a Max Planck a la idea de que la energía de los osciladores armónicos estaba cuantizada. Esta idea fue posteriormente expandida por Albert Einstein, al proponer que la luz estaba de hecho compuesta por paquetes discretos de energía, ahora conocidos como fotones. Por lo tanto, es posible decir que la mecánica cuántica surgió de la búsqueda de consistencia entre la termodinámica y los modelos microscópicos de la materia y la radiación. Luego la mecánica cuántica tuvo un desarrollo independiente, aunque siempre se mantuvo la consistencia con las leyes de la termodinámica. Modelos altamente exitosos de la materia y la radiación fueron propuestos y contrastados en regímenes fuera del equilibrio térmico donde la termodinámica no estuvo involucrada. Hoy en día, la mecánica cuántica es un teoría muy general y bien desarrollada que provee un marco teórico consistente y que permite describir los componentes fundamentales de la materia y sus interacciones.

En las últimas décadas la relación entre la mecánica cuántica y la termodinámica ha sido de alguna forma invertida con respecto a su origen: ahora, muchos investigadores intentan entender cómo, o bajo qué condiciones, las leyes usuales de la termodinámica surgen a partir de un substrato cuántico.

Chapter 2

Floquet Theory

In this chapter we review the basic concepts of Floquet Theory. As mentioned in the previous chapter, we are interested in the study of driven quantum systems that are also open. When the system is driven in an arbitrary way only a numerical approach to solve its dynamics is in general possible. However, if it is assumed that the driving is periodic significant analytical progress can be achieved. For this, Floquet theory is a well known and developed tool. We first review the main ideas in the context of their origin: classical systems of time-dependent linear differential equations. Then we discuss the generalization of Floquet theory to quantum *closed* systems. Finally, we consider the case of driven *open* system, whose exact treatment is a subject of current research.

2.1 Classical Floquet theory

Floquet theory was original developed to study general systems of linear differential equations with coefficients that are time-dependent and periodic [65]. The basic theorem underlying Floquet theory is very easy to understand. Lets consider a vector of n complex or real variables $\bar{x} = (x_1, x_2, ..., x_n)^T$ and the following differential equation:

$$\frac{d\bar{x}}{dt} = A(t)\bar{x} \tag{2.1}$$

where $A(t) = A(t+\tau)$ is a $n \times n$ τ-periodic matrix. What the Floquet theorem states is that it is always possible to find a family of independent solutions to Eq. (2.1) such that, although they are not periodic in general, each of them can be written as:

$$\bar{x}(t) = e^{\mu t}\bar{p}(t) \tag{2.2}$$

where $\bar{p}(t)$ is also τ-periodic. The proof of this theorem is very simple and can be found in many books [66]. The exponent μ is called *characteristic* or *Floquet* exponent. There are n Floquet exponents, one for each independent solution. They are not univocally defined, since we could replace the solution $\bar{x}(t) = e^{\mu t}\bar{p}(t)$ by $\bar{x}'(t) = e^{\mu' t}\bar{p}'(t)$, with $\mu' = \mu + i2\pi k/\tau$ and $p'(t) = e^{-i(2\pi k/\tau)t}p(t)$ for any integer k. However, they always satisfy:

$$\prod_{j=1}^{n} e^{\mu_j \tau} = e^{\int_0^\tau \mathrm{Tr}[A(t)]dt} \tag{2.3}$$

Thus, we see that the fundamental solutions of periodic systems of linear differential equations can always be cast as the product of a periodic function (with the same periodicity as the coefficients) and a exponential function.

The calculation of the Floquet exponents is difficult even for the simplest examples, and closed form expressions cannot be obtained in general. They can be obtained numerically by integrating the differential equation up to the period τ of the driving (since, for a fundamental solution, $\bar{x}(\tau) = e^{\mu\tau}\bar{x}(0)$). However, this simple approach is not accurate.

From Eq. 2.2 it follows that:

$$\bar{x}(t + K\tau) = (e^{\mu\tau})^K \bar{x}(t) \tag{2.4}$$

Therefore, we can identify three different regimes for the long time behavior of $\bar{x}(t)$, depending on the value of μ:

- If $\mathrm{Re}\,[\mu] < 0$ then $\bar{x}(t) \to 0$ for $t \to +\infty$.
- If $\mathrm{Re}\,[\mu] = 0$ then $\bar{x}(t)$ is quasi-periodic. It is exactly τ-periodic if $\mu = ik\pi/\tau$ for any integer k.
- If $\mathrm{Re}\,[\mu] > 0$ then $|\bar{x}(t)| \to +\infty$ for $t \to +\infty$.

The last case, in which the solution is divergent, has a clear physical interpretation in the context of parametrically driven harmonic oscillators. This is a typical example in which Floquet theory can be applied. We consider the dissipative Mathieu equation:

$$\frac{d^2x}{dt^2} + \gamma\frac{dx}{dt} + \omega^2(t)x^2 = 0 \tag{2.5}$$

where the time-dependent frequency is $\omega^2(t) = \omega_0^2 + \epsilon\cos(\Omega t)$. This equation can be expressed as a first order differential equation in two variables (x and dx/dt, for example), and consequently has two Floquet exponents. However, since the equation is invariant to complex conjugation, they are a complex conjugate pair. Thus, the only relevant parameter to determine the stability of the dynamics is the real part of any of them. Figure 2.1 shows the stability diagram as a function of ϵ and ω_0^2 for $\Omega = 1$. The stable region for null damping is colored. We see that at certain frequencies ω_0 the dynamics becomes unstable for any value of ϵ, the driving amplitude. This phenomenon is known as 'parametric resonance' and can be shown to occur at frequencies $\omega_0^2 = (n\Omega/2)^2$, for any integer $n \geq 0$ (for no damping). In Figure 2.1 only the first three resonances are shown ($n = 0, 1, 2$). At these points, the relation between the natural frequency of the oscillator and the frequency of the parametric driving is such that it delivers energy into the system. When the damping is turned on (dashed lines) a minimum driving amplitude is needed in order to enter the unstable phase. What happens in this case is that the rate at which energy is injected into the system by the parametric driving must overcome the rate of energy dissipation. In Chapter 4 we will show that if the analysis is restricted to the stable regime, then the asymptotic state of the system can be found without requiring the calculation of the Floquet exponents. Also, this asymptotic state is periodic, with the same period as the parametric driving.

2.2 Floquet theory for quantum systems

The ideas of the previous section can be applied to the problem of evolving quantum states. The connection is very straightforward. Lets consider a quantum system with a time-dependent Hamiltonian $H(t)$ which is periodic in time (with period τ). Quantum states in the Schrodinger's picture will evolve according to:

$$i\hbar\frac{\partial}{\partial t}|\Psi\rangle = H(t)|\Psi\rangle \tag{2.6}$$

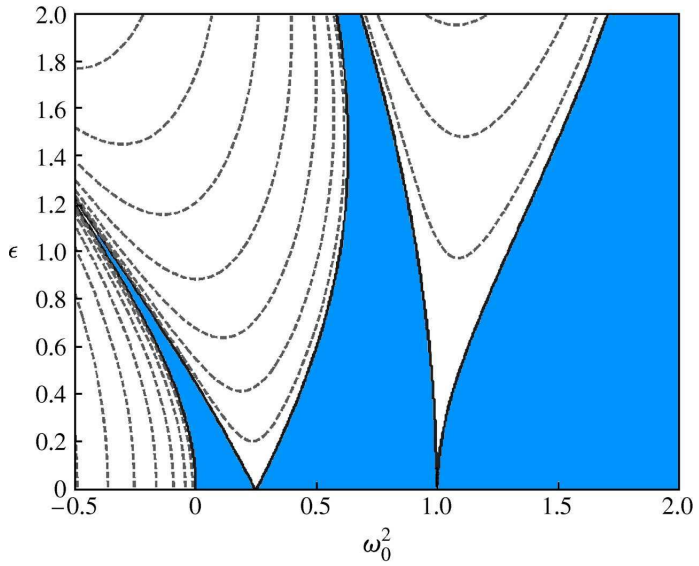

Figure 2.1: Stability diagram for the damped Mathieu equation for $\Omega = 1$. The stable region for no damping is colored. Dashed lines mark the boundary between stability and instability as the damping is increased. Figure obtained from [67]

.

This equation is completely analogous to Eq. (2.1). Therefore, the Floquet theorem ensures that there exists a set of independent solutions of the form:

$$|\psi_\alpha(t)\rangle = e^{-i\epsilon_\alpha t/\hbar}\,|\Phi_\alpha(t)\rangle \tag{2.7}$$

Where $|\Phi_\alpha(t+\tau)\rangle = |\Phi_\alpha(t)\rangle$ is a τ-periodic state in Hilbert space, known as 'Floquet mode', and ϵ_α is a real number that is called 'Floquet quasienergy'. These quasienergies play the role of the Floquet exponents (apart from a factor $(i\hbar)^{-1}$) but, in contrast, can only be real. The reason is that the unitary evolution given by Eq. (2.6) always preserves the norm of the state (and therefore the real part of the Floquet exponents must be zero, see Eq. 2.4). For the same reasons as before, the quasienergies are only defined up to multiples of $\hbar 2\pi/T = \hbar\omega_d$, where $\omega_d = 2\pi/\tau$ is the fundamental angular frequency of the driving. Thus, they can always be consider to belong to the first 'Brillouin Zone' $-\hbar\omega_d/2 < \epsilon_\alpha < \hbar\omega_d/2$.

2.2.1 Floquet theory and quantum dissipation

The Born-Markov and weak coupling approximations described in the previous chapters to obtain the master equations for the dynamics of open quantum systems can be combined with the tools and ideas of Floquet theory. An interesting comparison of different approaches and methods can be found in [68]. As explained there, incompatible results are obtained depending on whether the Markovian approximation is performed with respect to the timescales given by the eigenenergies of the undriven system, or by the Floquet quasienergies of the driven system. In any case, if the weak coupling approximation is performed, the regime of validity is restricted by the conditions [68]:

$$\gamma \ll \Delta_{\alpha,\beta} \qquad \text{and} \qquad \gamma \ll \frac{k_b T}{\hbar} \tag{2.8}$$

where γ is the dissipation rate, $k_b T/\hbar$ is the timescale given by the thermal energy at some characteristic environmental temperature T, and $\Delta_{\alpha,\beta}$ are the transition rates of

the system. For undriven systems $\Delta_{\alpha,\beta} = (E_\alpha - E_\beta)/\hbar$, where E_α are the eigenenergies, but for driven systems $\Delta_{\alpha,\beta} = (\mu_\alpha - \mu_\beta)/\hbar$. Therefore, it is clear that the weak coupling approximation prevents the analysis of ultra-low temperatures. Although this fact is not at all unknown, it is not sufficiently clear in the literature [69–71]. Also, to the best of our knowledge there are not clear physical interpretations available of what kind of processes are missed by performing the weak coupling approximation at low temperatures. The results presented in Chapters 4, 5 and 6, which are exact, offer a simple answer to this problem.

Teoría de Floquet

En este capítulo se describen conceptos básicos de la teoría de Floquet. Como se menciona en el capítulo anterior, estamos interesados en el estudio de sistemas cuánticos dependientes del tiempo que además son abiertos. Cuando la dependencia en el tiempo es arbitraria en general solo una solución numérica es posible. Sin embargo, si se asume que esta dependencia es periódica es posible avanzar analíticamente. Para esto, la teoría de Floquet es una herramienta muy conocida y desarrollada. En primer lugar se discuten las ideas principales en el contexto de sistemas lineales de ecuaciones diferenciales dependientes del tiempo, donde tuvieron origen. Luego se aplican estas ideas a sistemas cuánticos cerrados. Finalmente se consideran sistemas cuánticos forzados y con disipación, cuyo tratamiento exacto es un tema de investigación actual.

Chapter 3

Trapped ions

In this chapter we give a basic description of systems of trapped ions. We review some basic concepts involved in the manipulation of these systems, which will be needed in the last part of this thesis to understand some experimental proposals. We mainly follow [72], [73] and [5]. Trapped ions constitute an experimental platform in which quantum degrees of freedom can be controlled with great accuracy. In these systems, positively charged ions are spatially confined by means of electromagnetic fields inside a vacuum chamber. They are promising candidates for quantum information processing. Crystals with about fifteen ions have been manipulated to create multipartite entangled states implementing small versions of quantum algorithms [74, 75]. More recently, they have been used to simulate frustrated magnetic materials [76], the creation of topological defects during phase transitions, [77], and the dynamics of lattice gauge theories [10]. Their potential to simulate energy flow through complex networks has also been noticed [78–81]. In the last part of this thesis we propose some experiments to study energy transport through ion crystals with emphasis in the effects of dimensionality and disorder (Chapter 9), and to simulate magnetic materials with non-trivial interactions (Chapter 10).

3.1 Linear Paul traps

It is easy to see that it is not possible to trap charges using an static electric field: the Laplace equation $\nabla^2\phi = 0$ cannot be satisfied by a potential $\phi(\bar{r})$ which is attractive in the three spatial directions, i.e, $\phi(\bar{r}) \propto 1/2(\omega_x x^2 + \omega_y y^2 + \omega_z z^2)$, where $\bar{r} = (x, y, z)$ is the distance to the center of the trap and $\omega_k \geq 0$. Some traps, known as Penning traps, use a combination of static electric and magnetic fields. An static electric field confine the particles in the longitudinal direction, while a magnetic field achieves the radial confinement. Another alternative, which is the one employed in the so called Paul traps, is to employ time dependent electric fields. In the following we will focus on this type of traps. Figure 3.1 shows a scheme of a linear Paul trap. The radial confinement is achieved by a time dependent quadrupolar potential of the form $V_q(t) = V_0/2(1+(x^2-y^2)/R^2)\cos(\Omega_{RF}t)$ (near the center of the trap), which results from the application of radio frequency signals (of frequency Ω_{RF}) to four parallel electrodes with cylindrical shapes. The quadrupolar potential $V_q(t)$ is actually repulsive along one transverse direction, which change in time, but for sufficiently high Ω_{RF} a charged particle in the center of the trap will feel an effective harmonic trapping potential along all transverse directions. Two additional electrodes located along the longitudinal axis and

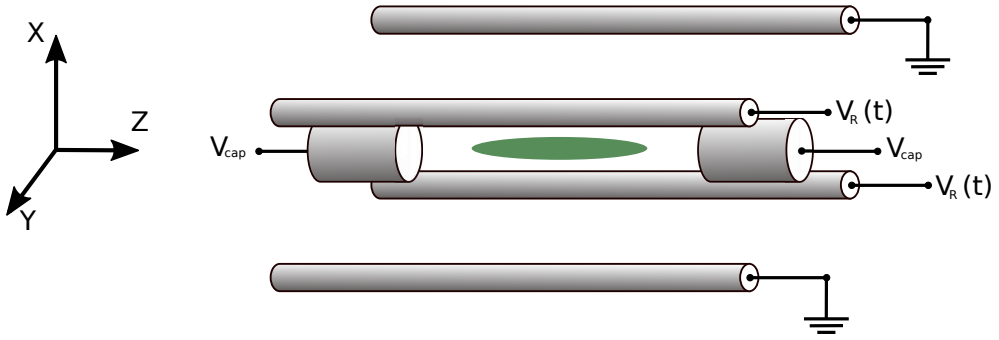

Figure 3.1: A scheme of a linear Paul trap. A high voltage radio frequency signal $V_R(t)$ is applied to two of four parallel cylindrical electrodes (while the other two are grounded). Two additional electrodes along the longitudinal axis are maintained at a fixed potential V_{cap}. The green volume is the trapping region.

maintained at the same constant potential create a confining field along the $\hat{z}$ direction. Therefore, the dynamics of the trapped ions near the axis of the trap can be described by the following effective potential:

$$V_{\text{eff}} = \frac{m}{2q}[\omega_r(x^2 + y^2) + \omega_z z^2] \tag{3.1}$$

where m and q are the mass and electric charge of the ions, and the trapping frequencies $\omega_r, \omega_z > 0$ can be controlled by changing the voltages applied to the electrodes. Typical values of the radial frequency ω_r are between 4 and 10 Mhz, while the longitudinal frequency ω_z is in general smaller, ranging from 0.5 to 5 Mhz. The dynamics induced by the previous potential is a first approximation to the motion of the ions. The actual motion has weak modulations at the frequency Ω_{RF} of the time dependent trapping fields, which are called micromotion. The micromotion can be neglected for ions near the longitudinal axis of the trap, and will be ignored in the following.

3.2 Ion crystals

If the trap contains two or more ions, and they are cooled to sufficiently low temperatures, they organize themselves in regular structures called Coulomb or Wigner crystals [82, 83]. These structures arise as a result of the competing effects of the confining potential of the trap and the mutual Coulomb repulsion of the ions. For strong transverse confinement ($\omega_r \gg \omega_z$) the equilibrium structure is a string of ions along the longitudinal axis, as shown in Figure 3.2-(a). If the transverse confinement is relaxed below a critical value an structural phase transition takes place: instabilities grow from the center of the chain and a two-dimensional zigzag pattern emerges (Figure 3.2-(b)). Another phase transition occurs if the transverse confinement is further relaxed, and the equilibrium structure changes from the two-dimensional zigzag to a three-dimensional helix (Figure 3.2-(c)). Finally, in the opposite limit of strong axial confinement ($\omega_z \gg \omega_r$) the equilibrium structure is again two-dimensional: the ions form a disc at $z = 0$ (not shown). These structural phase transitions have been used to explore the processes of spontaneous symmetry breaking and defect formation [77, 84]. Also, the interaction of ion crystals with optical lattices was experimentally studied as a way of testing microscopic models of friction between surfaces [85]. In appendix A we perform a detailed numerical analysis of these phase transitions.

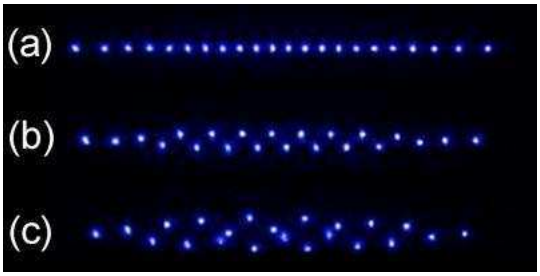

Figure 3.2: Different equilibrium structures: (a) linear string of ions, (b) two-dimensional zig-zag structure and (c) three-dimensional helix. Images like these are obtained by irradiating the ions with laser light of the appropriate frequency and detecting its fluorescence with a CCD camera.

3.3 Electronic degrees of freedom and basic Hamiltonian

So far we have only considered the motional degrees of freedom of the trapped ions. However, the internal electronic degrees of freedom can also be precisely controlled via light fields. In many experimental settings only two of the many electronic states are employed to define an effective two-level system, or qubit. Additional levels can also be used to implement laser cooling or to measure the electronic state, as explained later. The simplified description of the internal state of the ion as a two-level system will be valid if the frequency of the electromagnetic field that is interacting with it is in resonance with the transition between the two selected levels, and other possible transitions can be ignored. Thus, if $|g\rangle$ and $|e\rangle$ are the two selected electronic states, while $\hbar\omega_e = E_e - E_g$ is the energy difference between them, then the Hamiltonian corresponding to the internal and motional degrees of freedom is:

$$H_0 = H_e + H_m = \hbar\frac{\omega_e}{2}\sigma_z + \hbar\omega_z a^\dagger a \tag{3.2}$$

where $\sigma_z = |e\rangle\langle e| - |g\rangle\langle g|$ and a is the destruction operator associated to the harmonic motion in the longitudinal direction of the trap. For simplicity, we ignore motion along the transverse directions.

We now consider that the ion is interacting by a classical electromagnetic wave of frequency ω_L with electric field $\bar{E}(z,t) = \bar{E}_0 e^{i(kz-\omega_L t+\phi)}$ propagating along the z direction. If the frequency ω_L is close to resonance with ω_e then transitions between the levels $|e\rangle$ and $|g\rangle$ will be induced. They are described by the following interaction Hamiltonian:

$$H_I = \frac{\hbar}{2}\Omega\left(\sigma_+ \, e^{i(k\hat{z}-\omega_L t+\phi)} + h.c\right) \tag{3.3}$$

where $\sigma_+ = |e\rangle\langle g|$ and $\Omega = 2e_-/\hbar\bar{E}_0$. $\langle e|\,\bar{x}\,|g\rangle$ is the Rabi frequency of the induced transitions and measures the strength of the electron-light interaction (e_- is the electron charge and $e_-\langle e|\,\bar{x}\,|g\rangle$ is the dipole moment of the transition). The previous Hamiltonian is also useful to describe transitions between levels that are not allowed by dipole interactions, for example quadruple transitions or stimulated Raman transitions. In these cases the form of the interaction Hamiltonian is the same but the identification of the parameters Ω, ω_L and k changes [86]. In the interaction picture given by H_0 the interaction Hamiltonian is:

$$H_I \simeq \frac{\hbar}{2}\Omega\left(\sigma_+ e^{i(k\hat{z}-\Delta t+\phi)} + h.c\right) \tag{3.4}$$

where $\Delta = \omega_L - \omega_e$ and the terms oscillating at frequency $\omega_L + \omega_e$ were discarded (this is known as the 'rotating wave' approximation, which is justified if one is interested in the slow dynamics of the system). This interaction Hamiltonian can be further simplified in the so called Lambd-Dicke regime. In this regime the spatial extension of the atomic wave packet is assumed to be much smaller than the wavelength $2\pi/k$ of the incident light. Therefore, we can approximate $e^{ik\hat{z}} \simeq 1 + ik\hat{z}$, and since $\hat{z} = \sqrt{\hbar/(2m\omega_z)}\left(ae^{-i\omega_z t} + a^\dagger e^{i\omega_z t}\right)$, we obtain:

$$H_I^{\text{LD}} = \frac{\hbar}{2}\Omega\ \sigma_+\ e^{i(\phi-\Delta t)}\left[1 + i\eta\left(ae^{-i\omega_z t} + a^\dagger e^{i\omega_z t}\right)\right] + h.c \tag{3.5}$$

where we defined the Lambd-Dicke parameter as $\eta = k\sqrt{\hbar/(2m\omega_z)}$. The previous expression is a valid approximation to first order in $\eta \ll 1$.

3.3.1 Carrier and sideband resonances

The slow dynamics of the system can be changed drastically by controlling the detuning Δ. There are three main possibilities which correspond to the three resonances of the previous equation. For $\Delta = 0$ the only time independent term is:

$$H_I^{\text{carrier}} = \frac{\hbar}{2}\Omega\ \left(\sigma_+\ e^{i\phi} + \sigma_- e^{-i\phi}\right) \tag{3.6}$$

which does not affect the motional state and generates rotations in the Bloch sphere defined by the two levels $|e\rangle$ and $|g\rangle$, around an axis that can be controlled by changing the phase ϕ of the incident light. This is the 'carrier' resonance.

If $\Delta = -\omega_z$ then we obtain the 'red sideband' resonance, which reads:

$$H_I^{\text{rsb}} = \frac{\hbar}{2}\Omega\eta\ \left(\sigma_+ a\ e^{i\phi} + \sigma_- a^\dagger\ e^{-i\phi}\right) \tag{3.7}$$

At variance with the carrier resonance, this interaction couples the electronic and motional degrees of freedom. It will generate transitions between the levels $|g\rangle\,|n\rangle$ and $|e\rangle\,|n-1\rangle$, where $|n\rangle$ are the eigenstates of $a^\dagger a$. The effective Rabi frequency of these transitions is $\Omega_{n,n-1} = \Omega\eta\sqrt{n}$. We observe that in this case the number of excitations is conserved: if the electronic state is excited, a vibrational quantum must be destroyed, and viceversa.

Finally, the 'blue sideband' resonance is obtained for $\Delta = \omega_z$:

$$H_I^{\text{bsb}} = \frac{\hbar}{2}\Omega\eta\ \left(\sigma_+ a^\dagger\ e^{i\phi} + \sigma_- a\ e^{-i\phi}\right) \tag{3.8}$$

this interaction will generate transitions between the levels $|g\rangle\,|n\rangle$ and $|e\rangle\,|n+1\rangle$ with effective Rabi frequency $\Omega_{n,n+1} = \Omega\eta\sqrt{n+1}$. In this case the number of excitations is not conserved: electronic and vibrational excitations can be created or destroyed simultaneously.

As explained in the following, these interactions, and the spontaneous decay process $|e\rangle \to |g\rangle$ (which was not taken into account yet), can be used to cool the motional degrees of freedom to low temperatures.

3.4 Laser cooling

The aim of any process for cooling a trapped ion is to bring the mean occupation number $\bar{n}$ to low values. This is expected to happen if somehow the transitions $|g,n\rangle \rightarrow |g,n-1\rangle$ are more probable than $|g,n\rangle \rightarrow |g,n+1\rangle$. We will briefly explain how to do this in a simple case. We consider, as before, that the ion can only move in a single direction and that it is interacting with a laser field in the Lambd-Dicke regime, in which the carrier and sideband transitions dominate. Also, we take into account the process of spontaneous emission where the electronic state decay from $|e\rangle$ to $|g\rangle$ via the emission of a photon. The rate of these spontaneous emissions is Γ, that also determines the line width of the electronic transition. We first consider the case of 'resolved-sideband' cooling, which can be implemented when $\Gamma \ll \omega_z$, i.e, when the red and blue sidebands can be well resolved between them and the carrier. The relevant transitions for this case are shown in Figure 3.3. In the resolved-sideband regime the optimal cooling

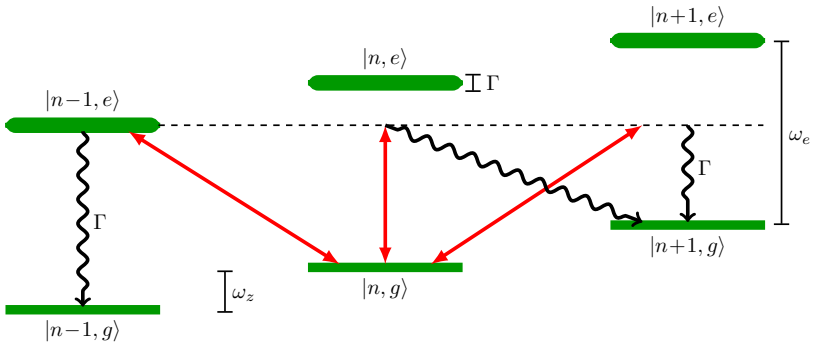

Figure 3.3: State transitions involved in resolved-sideband cooling (only the more relevant transitions are shown).

condition is achieved by driving the red sideband at $\Delta = -\omega_z$. Then, coherent oscillations between the levels $|n,g\rangle$ and $|n-1,e\rangle$, interrupted by the spontaneous decay $|n-1,e\rangle \rightarrow |n-1,g\rangle$, drive the transition $|n,g\rangle \rightarrow |n-1,g\rangle$. The opposite transition $|n-1,g\rangle \rightarrow |n,g\rangle$, being off-resonant, is suppressed. However, it can take place via coherent excitations to a virtual off-resonant level followed by spontaneous emission processes, as depicted in Figure 3.3.

In general, the total rates $R_\pm$ of the transitions $|g,n\rangle \rightarrow |g,n\pm 1\rangle$ have the form $R_+ = (n+1)A_+$ and $R_- = nA_-$, where the coefficients $A_\pm$ depend on the decay rate Γ, the laser detuning Δ, the trap frequency ω_z, and are proportional to $(\Omega\eta)^2$ [72]:

$$A_\pm = \frac{(\Omega\eta)^2}{\Gamma}\left[\alpha W(\Delta) + \beta W(\Delta \mp \omega_z)\right] \tag{3.9}$$

where α and β are geometrical factors, and $W(\Delta) = (4\Delta^2/\Gamma^2 + 1)^{-1}$. Therefore, the evolution of the mean occupation number is:

$$\dot{\bar{n}} = -(A_- - A_+)\bar{n} + A_+. \tag{3.10}$$

For $A_- < A_+$ the previous equation indicate that $\bar{n}$ exponentially approach the asymptotic value $\bar{n} = A_+/(A_- - A_+)$. Thus, lower temperatures are achieved for higher values of A_-/A_+. In this way, the final occupation number, or the effective temperature, can be controlled by varying the detuning Δ. There are two relevant regimes depending on whether the line width Γ of the electronic transition is wide or narrow compared to the

trap frequency ω_z. In the weak confinement regime in which $\omega_z \ll \Gamma$, the maximum value of A_-/A_+ is obtained for $\Delta = -\Gamma/2$, and in that case we have $\bar{n} \simeq \Gamma/(2\omega_z) > 1$. This case correspond to the 'Doppler cooling' limit. In the opposite regime, $\omega_z \gg \Gamma$, the blue and red sideband can be individually resolved, and the optimal occupation number is $\bar{n} \simeq (\Gamma/\omega_z)^2$, which occurs when $\Delta = -\omega_z$ (i.e., when the laser is in resonance with the red sideband). Thus, in this resolved-sideband cooling regime occupation numbers $\bar{n} \ll 1$ can be achieved. In Chapter 8 we will re obtain these results by analyzing laser cooling as a thermodynamic cycle.

3.5 Quantum simulation of magnetic systems

The simulation of quantum systems is a hard problem that is in general intractable with classical computers. The main reason is the exponential explosion in the resources needed to describe a quantum state of a composite system, with respect to the number of subsystems. For example, if we consider a collection of N two-level systems, we only need N bits of information to give a classical description of its state. However, if each two-level subsystem is quantum, we need $\simeq 2^N$ complex numbers to completely specify a pure state of the total system. Similarly, observables like the energy and operations like the time evolution of the state are represented by matrices that act on a space of dimension 2^N. For moderate values of N (for example, $N \simeq 40$), the treatment of general quantum systems is intractable even for the largest computers that exists today.

A solution proposed in the early eighties by Feynman and others was to employ a highly controllable quantum system to simulate the physics of another, target, system. This idea, which also led to the concept of quantum computing, was experimentally realized in recent years in a variety of systems like cold atoms, trapped ions, or superconducting qubits. In this section we review the main concepts involved in the simulation of magnetic materials using arrays of trapped ions. We mainly follow [23].

3.5.1 Ising-like systems with transverse magnetic field

In the following we will explain how to employ trapped ions to simulate Hamiltonian's of the form:

$$H = \sum_{i,j} J_{i,j}\sigma_x^i\sigma_x^j - \sum_i B_y\sigma_y^i \tag{3.11}$$

where σ_q^i are the usual Pauli matrix associated with a two-level subsystem i which, as before, is represented by the internal electronic state of each trapped ion. The properties of the Hamiltonian H_I for different choices of the interaction constants $J_{i,j}$ and external field B_y will be discussed in detail in Chapter 10.

3.5.2 A single ion in a bi-chromatic field

We consider again a single ion moving in only one direction and interacting with a laser field. This time, the laser field has two spectral components with the same amplitude and frequencies $\omega_L^{\pm}$ such that the detuning with respect to the electronic transitions are $\Delta^{\pm} = \omega_L^{\pm} - \omega_e = \pm\mu$. When $\mu \simeq \omega_z$, then the red and blue sidebands are driven simultaneously[1]. It is easy to see that in that case the interaction Hamiltonian is:

$$H_I = H_I^{\text{bsb}} + H_I^{\text{rsb}} = \frac{\hbar}{2}\Omega\, k\hat{z}\, \sigma_\phi \tag{3.12}$$

[1]The simultaneous driving of the red and blue sidebands is known as the Molmer-Sorensen scheme [87]

where $\hat{z} = \sqrt{\hbar/(2m\omega_z)}(a + a^\dagger)$ and $\sigma_\phi = \sigma_+ e^{i\phi} + \sigma_- e^{-i\phi}$. Thus, we see that the ion position in the trap is coupled to the projection of the internal state along a direction (given by the angle ϕ) in the equatorial plane of the Bloch sphere defined by the levels $|e\rangle$ and $|g\rangle$.

If the detuning μ is not necessarily close to the trap frequency ω_z, we can obtain the interaction Hamiltonian by adding a term like Eq. (3.5) for each spectral component of the laser field. Thus, we obtain:

$$H_I(t) = \hbar\Omega \cos(\mu t)\ \sigma_\phi\ +\ \hbar\Omega \cos(\mu t)\ k\hat{z}(t)\ \sigma_\phi \tag{3.13}$$

where this time we have $\hat{z}(t) = \sqrt{\hbar/(2m\omega_z)}(ae^{-i\omega_z t} + a^\dagger e^{i\omega_z t})$. Now we generalize this interaction Hamiltonian to the case with many trapped ions forming a linear string.

3.5.3 Generalization to many ions and the Magnus expansion

We consider a situation like the one depicted in Figure 3.4. A string of N ions is interacting with two coherent laser fields traveling at oblique directions. One of this

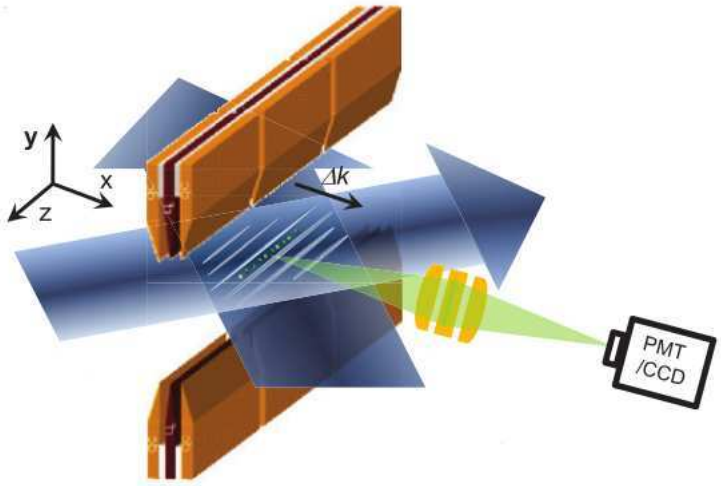

Figure 3.4: A string of trapped ions driven by two oblique laser beams (blue). The orange and purple blocks are the electrodes of the trap. Figure taken from [23].

lasers has a single spectral component at frequency ω_L, while the other has two spectral components at frequencies $\omega_L^\pm = \omega_L + \omega_e \pm \mu$. In the region where the two laser beams overlap, they form an interference wave pattern that oscillates at the beatnote frequencies $\omega_e \pm \mu$ and moves with a wave vector $\Delta\bar{k} = \bar{k}_1 - \bar{k}_2$, if $\bar{k}_1$ and $\bar{k}_2$ are the wave vectors of each laser. Thus, we can think that the ions interact with a bi-chromatic field with wavevector $\Delta\bar{k}$ and spectral components at frequencies $\omega_e \pm \mu$, as in the previous section. If the system is aligned such that $\Delta\bar{k} = \delta k\ \bar{x}$, then the internal state of the ions will be coupled to their motion along the $\hat{x}$ direction. Assuming that the intensity of the field is the same for all the ions, the interaction Hamiltonian of Eq. (3.13) is generalized to:

$$H_I(t) = \hbar\Omega \cos(\mu t) \sum_{j=1}^{N} \delta k\ \hat{x}_j(t)\ \sigma_\phi^j, \tag{3.14}$$

where, for simplicity, we have ignored the first term in Eq. (3.13) (this term only affects the internal state of each ion individually and does does not contribute to their effective

coupling). The motion of the ions near the equilibrium position can be described in terms of global normal modes. For one dimensional ion strings, the longitudinal and transverse motions decouple, so we are only interested in the N normal modes in which the ions oscillate in the $\bar{x}$ direction. If $\hat{Q}_k(t)$, $k = 1, \cdots, N$, are the amplitudes of each of these normal modes, then we can express the displacement of each ion as $\hat{x}_j(t) = \sum_{k=1}^{N} B_{j,k}\ \hat{Q}_k(t)$, where the orthogonal matrix $B_{j,k}$ indicates what is the amplitude of the motion of the ion j in the normal mode k. Thus, we obtain:

$$H_I(t) = \hbar\Omega \cos(\mu t) \sum_{j,k=1}^{N} \delta k\ B_{j,k}\ \hat{Q}_k(t)\ \sigma_\phi^j \tag{3.15}$$

Obviously, the normal modes amplitudes evolve as $\hat{Q}_k(t) = \sqrt{\hbar/(2m\nu_k)}(a_k e^{-i\nu_k t} + a_k^\dagger e^{i\nu_k t})$, where ν_k is the normal frequency of the corresponding mode.

In general, the interaction Hamiltonian will be time-dependent, oscillating at frequencies $\mu \pm \nu_k$. When μ is close to the frequency ν_k of a given normal mode, the rotating wave approximation can be employed, where only the slow varying terms are conserved. In this case, only the red and blue sidebands of that mode are driven. In general, for arbitrary μ, all the terms must be conserved.

The interaction Hamiltonian of Eq. (3.15) does not directly couple the internal states of each ion. However, the common interaction with the normal modes will induce an effective interaction between internal states. This can be seen by analyzing the dynamics of the system for long times. For that purpose, we will employ the Magnus expansion, that is explained in the following. In the interaction picture, the time evolution of the global state of the ions is given by:

$$i\hbar \frac{d\,|\Psi(t)\rangle}{dt} = H_I(t)\,|\Psi(t)\rangle \tag{3.16}$$

which can be formally integrated as:

$$|\Psi(t)\rangle = \hat{T} e^{\frac{1}{i\hbar}\int_0^t dt' H_I(t')}\ |\Psi(0)\rangle\,, \tag{3.17}$$

where $\hat{T}$ is a time ordering operator. The evolution operator $U(t) = \hat{T} e^{\frac{1}{i\hbar}\int_0^t dt' H_I(t')}$ can be perturbatively expanded as follows:

$$U(t) = \exp\left\{ \frac{1}{i\hbar}\int_0^t dt_1 H_I(t_1)\ +\ \frac{1}{2(i\hbar)^2}\int_0^t dt_1 \int_0^{t_1} dt_2 [H_I(t_1), H_I(t_2)]\ +\ \mathcal{O}(H_I^3) \right\}, \tag{3.18}$$

where we ignored terms of order more than two in $H_I(t)$. In fact, it can be seen that for the Hamiltonian of Eq. (3.15) the Magnus expansion up to second order is exact, i.e, all higher order terms vanish. Since $H_I(t)$ is oscillatory, it is clear that the integral $\int_0^t dt_1 H_I(t_1)$ will have constant and oscillatory contributions. The second order integral, $\int_0^t dt_1 \int_0^{t_1} dt_2 [H_I(t_1), H_I(t_2)]$, in addition to constant and oscillatory contributions, will also have contributions that grow linearly with the time t. Therefore, for long times, these linear contributions will dominate. In this way, the following evolution operator is obtained:

$$U(t) \simeq e^{-\frac{i}{\hbar} H_{\text{eff}}\, t} \qquad \text{with} \qquad H_{\text{eff}} = \sum_{i,j} J_{i,j}\ \sigma_x^i \sigma_x^j. \tag{3.19}$$

The constants $J_{i,j}$ appearing in the effective Hamiltonian H_{eff} are given by:

$$J_{i,j} = -\frac{\hbar^2 (\delta k)^2 \Omega^2}{2m} \sum_{k=1}^{N} \frac{B_{i,k} B_{j,k}}{\mu^2 - \nu_k^2}. \tag{3.20}$$

Two observations are in order. In first place, we see that the effective Hamiltonian H_{eff} that describes the evolution for long times does not depend on the motional state. Only the Pauli operators σ_x^i appear in H_{eff}. However, information about the motional normal modes and frequencies is contained in the interaction constants $J_{i,j}$. Thus, we see that the common interaction of the internal state of each ion with the global motional normal modes of the ion chain induces a Ising-like coupling between the internal states. When the detuning μ is not in resonance with any of the normal modes frequencies ν_k, then the normal modes are only virtually excited, and that is the reason why the Hamiltonian H_{eff} does not involve any motional operator. When the detuning μ is resonant with a particular normal mode (when $\mu \simeq \nu_k$) this description breaks down, as can be seen from the fact that the expression for $J_{i,j}$ diverges. Secondly, it is easy to see that the geometry of the interactions given by the coefficients $J_{i,j}$ is not completely restricted by the geometry of the ion crystal. Although the ion crystal has a one dimensional structure, with Coulomb couplings that as a first approximation can be regarded to be of short range, $J_{i,j}$ does not necessarily decay with the distance $|i-j|$. In particular, if the detuning μ is such that the center of mass normal mode dominates the sum in Eq. (3.20), then the couplings $J_{i,j}$ are approximately independent of $|i-j|$, since in the center of mass mode all the ions oscillate with the same amplitude. In that case, each of the spins encoded in the internal state of each ion will interact with all the others with the same strength. This will be discussed in detail in Chapter 10.

Thus, we have seen that by applying special laser fields to a string of trapped ions it is possible to simulate Ising-like couplings like the ones appearing in the first term of Eq. (3.11). The action of an external transverse magnetic field (second term in Eq. (3.11)) can also be simulated by employing the carrier resonances that were ignored in the previous treatment [23]. The last ingredients needed to run a complete quantum simulation are the initialization and readout of the internal state, which we now discuss.

3.5.4 Initialization and readout of the internal state

In this section we give a very basic description of the most common techniques to initialize and measure the internal state of the trapped ions. They involve a third level, in addition to the two levels used to define each qubit, as shown in Figure 3.5. We assume that this third level, $|r\rangle$, is such that the selection rules forbid the spontaneous decay $|r\rangle \rightarrow |e\rangle$. Then, if the atom is excited with a laser in the $|e\rangle \leftrightarrow |r\rangle$ transition the initial population of the $|e\rangle$ level will be transferred to the $|g\rangle$ level via $|r\rangle \rightarrow |g\rangle$ spontaneous decays. This method is known as 'optical pumping'. The actual implementation of course depends on the ion and the nature of the levels defining the qubit. Experimental details for Calcium atoms and hyperfine qubits can be found in [5]. In this way, the internal state can be prepared in the $|g\rangle$ state with high fidelity.

In order to measure the internal state a similar strategy is employed, known as the 'electron shelving' method. The purpose of the measurement is to determine whether the electron is in the state $|g\rangle$ of $|e\rangle$. For this, the ion is excited with a laser in the $|g\rangle \leftrightarrow |r\rangle$ transition, which generates Rabi oscillations between these two levels, *if the electron is actually in the level* $|g\rangle$. These oscillations are interrupted with spontaneous decays $|r\rangle \rightarrow |g\rangle$, a fluorescence photon is emitted, and the cycle is repeated. If the electron was in the state $|e\rangle$ nothing happens. Thus, the observation of fluorescence light after the excitation of the $|g\rangle \rightarrow |r\rangle$ transition indicates that the electron was in fact in the level $|g\rangle$. The detection efficiencies of this method are near perfection.

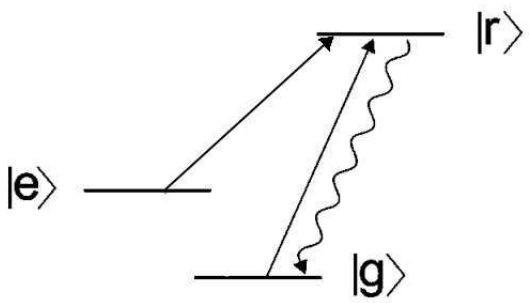

Figure 3.5: An additional level $|r\rangle$ is used to initialize and measure the internal electronic state.

Iones atrapados

En este capítulo se da un descripción básica de sistemas de iones atrapados. Se repasan algunos conceptos básicos sobre la manipulación de estos sistemas, que serán necesarios en la última parte de esta tesis para entender las propuestas experimentales. Principalmente se sigue a [72], [73] y [5]. Las trampas de iones constituyen una plataforma experimental en la cual grados de libertad cuánticos pueden ser controlados con gran precisión. En estos sistemas, iones cargados positivamente son confinados espacialmente mediante campos electromagnéticos dentro de una cámara de vacío. Estos sistemas son buenos candidatos para el procesamiento cuántico de información. Cristales con decenas de iones han sido manipulados para crear estados entrelazados multipartitos, y para implementar versiones reducidas de algoritmos cuánticos [74,75]. Mas recientemente, también han sido utilizados para simular materiales magnéticos frustrados [76], la creación de defectos topológicos en transiciones de fase [77], y la dinámica de teorías de gauge [10]. También ha sido destacado su potencial para simular el flujo de energía a través de redes complejas [78–81]. En la última parte de esta tesis se proponen algunos experimentos para estudiar el transporte de energía en cristales de iones con énfasis en los efectos de la dimensionalidad y el desorden (capítulo 9), y para simular materiales magnéticos con interacciones no triviales (capítulo 10).

Part II

Driven open systems with continuous variables

Chapter 4

An exactly solvable model

In this chapter we define the model which is the main subject of this thesis: a open harmonic network connected to bosonic reservoirs and subjected to parametric driving. As is explained in the following sections this model can be solved exactly. The analysis of the exact solution will shed some light on the limitations of the weak coupling approximation on this and similar models.

Figure 4.1 shows a scheme of the considered model. Each black circle represent a quantum harmonic oscillator, and links between them represent bilinear interactions. The natural frequencies of each oscillator and the interactions between them can be

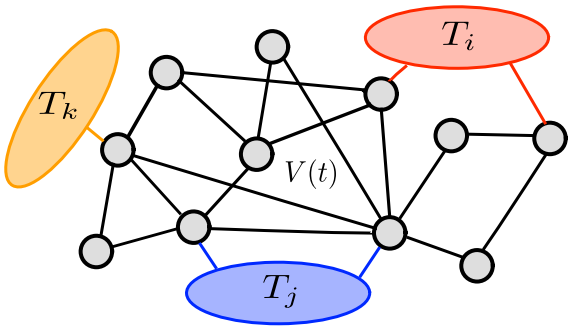

Figure 4.1: A scheme of the model

changed in time. Therefore, the harmonic network is described by the following quadratic Hamiltonian:

$$H_S = \frac{1}{2}P^T M^{-1} P + \frac{1}{2}X^T V(t) X, \tag{4.1}$$

where X and P are vectors whose components are the position and momentum operators of each oscillator, which satisfy the usual commutation relations, $[X_i, X_j] = [P_i, P_j] = 0$ and $[X_i, P_j] = i\hbar\delta_{i,j}$. The matrix M has the masses of each oscillator along the diagonal and zeros elsewhere, while the matrix $V(t)$ encodes the frequencies of each oscillator and the interactions between them. The variation in time of the matrix $V(t)$ allow us to model an external control that can be performed on the system.

Some parts of the network are also connected to independent thermal reservoirs. We will model the reservoirs as collections of harmonic modes which are initially in thermal states. Then, the environmental Hamiltonian is

$$H_E = \sum_\alpha H_{E,\alpha} \qquad H_{E,\alpha} = \sum_{j=1}^{N_\alpha} \frac{\pi_{\alpha,j}^2}{2m} + \frac{m\omega_{\alpha,j}^2}{2} q_{\alpha,j}^2$$

where the operator $q_{\alpha,j}$ is the position operator of the j-th oscillator in the α-th environment, and $\pi_{\alpha,j}$ its associate momentum. We consider a bilinear interaction between system and reservoirs through the position coordinates

$$H_{\text{int}} = \sum_{\alpha} \sum_{j,k} C_{\alpha,jk}\ X_j\ q_{\alpha,k}, \tag{4.2}$$

where $C_{\alpha,jk}$ are time-independent interaction constants. Thus, the full Hamiltonian for system and reservoirs is:

$$H_T = H_S + H_E + H_{\text{int}} \tag{4.3}$$

We are interested in the evolution of the state of the system under the global unitary evolution $U(t)$ given by the above Hamiltonian. If $\rho_T(0) = \rho_S(0) \otimes \rho_E(0)$ is an initial product state for the system and the environment, our main objective is to calculate the subsequent reduced state for the system:

$$\rho_S(t) = Tr_E \left(U(t)\rho_T(0)U^{\dagger}(t) \right) \tag{4.4}$$

We begin by solving the equations of motion for the system's operators in the Heisenberg picture. We will exploit the linearity of these equations (which follows from the quadratic structure of the total Hamiltonian) to exactly integrate them in terms of the Green's function of the system.

4.1 Heisenberg's equations of motion

We now derive, working in the Heisenberg's picture, the equations of motion for all the operators involved in the Hamiltonian of Eq. (4.3). For the system operators the motion equations are

$$\dot{X} = M^{-1}P \tag{4.5a}$$

$$\dot{P} = -V(t)X - \sum_{\alpha} C_{\alpha} q_{\alpha}, \tag{4.5b}$$

where q_α and π_α are vectors formed with the position and momentum operators of the α-th reservoir, respectively. Similarly, the matrix C_α has as elements the interaction constants $C_{\alpha,jk}$. If the system has N degrees of freedom and the α-th reservoir is formed by N_α oscillators, then the matrix C_α has dimensions $N \times N_\alpha$.

Turning to a description in the phase space, we define the $2N$-component vectors $Z = (X, P)^T$ and $z_\alpha = (q_\alpha, \pi_\alpha)^T$. In terms of Z, the Eqs. (4.5a) and (4.5b) can be written as:

$$\dot{Z} + a_s(t)Z = \sum_{\alpha} \mathcal{C}_{\alpha} z_{\alpha}, \tag{4.6}$$

where the matrices $a_s(t)$ and $\mathcal{C}_\alpha$ are defined as

$$a_s(t) = \begin{pmatrix} 0 & -M^{-1} \\ V(t) & 0 \end{pmatrix} \qquad \mathcal{C}_{\alpha} = \begin{pmatrix} 0 & 0 \\ -C_{\alpha} & 0 \end{pmatrix} \tag{4.7}$$

For the operators corresponding to the α-th reservoir the equations of motion in phase space are:

$$\dot{z}_{\alpha} + a_{\alpha} z_{\alpha} = \sum_{\alpha} \bar{\mathcal{C}}_{\alpha} Z \tag{4.8}$$

In this case the matrices a_α and $\bar{\mathcal{C}}_\alpha$ are given by:

$$a_\alpha = \begin{pmatrix} 0 & -\mathbb{1}_{N_\alpha}/m \\ m\Omega_\alpha^2 & 0 \end{pmatrix} \qquad \bar{\mathcal{C}}_\alpha = \begin{pmatrix} 0 & 0 \\ -[C_\alpha]^T & 0 \end{pmatrix} \tag{4.9}$$

where Ω_α^2 is a diagonal matrix containing the squared frequencies of the oscillators of the α-th reservoir.

In summary, if we are interested in the dynamics of the system, the following set of linear coupled differential equations must be solved for Z:

$$\begin{cases} \dot{Z} + a_s(t)Z = \sum_\alpha \mathcal{C}_\alpha z_\alpha, \\ \dot{z}_\alpha + a_\alpha z_\alpha = \bar{\mathcal{C}}_\alpha Z \end{cases} \tag{4.10}$$

with the initial conditions $Z(t=0) = (X(0), P(0))^T$ and $z_\alpha(t=0) = (q_\alpha(0), \pi_\alpha(0))^T$.

4.2 An integro-differential equation for the system's operators

In this section we derive an integro-differential equation describing the dynamics of the system only. We start by considering the Green's function $g_\alpha(t,t')$ for the homogeneous equation of motion of the α-th reservoir. Such function satisfies:

$$\frac{d}{dt}g_\alpha(t,t') + a_\alpha(t)g_\alpha(t,t') = \mathbb{1}_{N_\alpha}\delta(t-t'). \tag{4.11}$$

With initial conditions $g_\alpha(t'^-,t') = 0$, the function $g_\alpha(t,t')$ encodes the response of the α-th reservoir to a delta impulse at time t'. For this simple case it just represents a rotation in phase space: $g_\alpha(t,t') = \theta(t-t')e^{-a_\alpha(t-t')}$ where θ is the Heaviside step function and

$$e^{-a_\alpha t} = \begin{pmatrix} \cos(\Omega_\alpha t) & \sin(\Omega_\alpha t)(m\Omega_\alpha)^{-1} \\ -\sin(\Omega_\alpha t)m\Omega_\alpha & \cos(\Omega_\alpha t) \end{pmatrix} \tag{4.12}$$

The function $g_\alpha(t,t')$ is an homogeneous solution of Eq. (4.8) for $t > t'$. A particular solution is $z_\alpha^p(t) = \int_0^t g_\alpha(t,t')\ \bar{\mathcal{C}}_\alpha z(t')dt'$. Therefore, the complete solution of Eq. (4.8) is

$$z_\alpha(t) = g_\alpha(t,0)\ z_\alpha(0) + \int_0^t g_\alpha(t,t')\ \bar{\mathcal{C}}_\alpha z(t')dt', \tag{4.13}$$

which satisfies the required initial condition. The solution for z_α of Eq. (4.13) can now be inserted in Eq. (4.6), the differential equation for the system coordinates. Doing this we obtain:

$$\dot{Z} + a_s(t)Z - \int_0^t \left[\sum_\alpha \mathcal{C}_\alpha\ g_\alpha(t,t')\ \bar{\mathcal{C}}_\alpha\right] Z(t')dt' = \sum_\alpha \mathcal{C}_\alpha\ g_\alpha(t,0)\ z_\alpha(0) \tag{4.14}$$

This is a non-Markovian equation of motion for the system with a source term depending on the operators of the environment at the initial time. Since the equation is linear a general solution can be obtained in terms of the Green's function of the homogeneous system, as we did before for each reservoir. Before doing that, we define the dissipation kernel.

4.2.1 Dissipation kernel

The quantity multiplying Z in the integrand of Eq. (4.14) is the dissipation kernel, to which we will refer as $\eta(t,t') = \sum_\alpha \eta_\alpha(t,t')$, where $\eta_\alpha(t,t') = \mathcal{C}_\alpha g_\alpha(t,t')\bar{\mathcal{C}}_\alpha$. It can be written in a more convenient way in terms of the spectral densities of the reservoirs, which are defined below. Explicitly, we have:

$$\eta_\alpha(t,t') = \theta(t-t') \begin{pmatrix} 0 & 0 \\ \eta_\alpha^{xx}(t-t') & 0 \end{pmatrix} \tag{4.15}$$

where the matrix η_α^{xx} is defined as:

$$\eta_\alpha^{xx}(t) = \int_0^\infty I_\alpha(\omega)\sin(\omega t)d\omega \tag{4.16}$$

The function $I_\alpha(\omega)$ is the spectral density associated to the α-th reservoir. It is defined as follows:

$$[I_\alpha(\omega)]_{j,k} = \sum_{p=1}^{N_\alpha} \frac{1}{m\omega}[C_\alpha]_{jp}[C_\alpha]_{kp}\delta(\omega-\omega_{\alpha,p}) \tag{4.17}$$

4.2.2 Solution of the equation of motion

Using the previously defined dissipation kernel the equation of motion for the system is:

$$\dot{Z} + a_s(t)Z - \int_0^t \eta(t,t')Z(t')dt' = \sum_\alpha \mathcal{C}_\alpha g_\alpha(t,0)z_\alpha(0) \tag{4.18}$$

We consider the Green function $G(t,t')$ associated with the previous equation. It is such that:

$$\frac{\partial}{\partial t}G(t,t') + a_s(t)G(t,t') - \int_0^t \eta(t,\tau)G(\tau,t')d\tau = \mathbb{1}_{2N}\delta(t-t') \tag{4.19}$$

with initial conditions $G(t'^-,t') = 0$. The function $G(t,t')$ is therefore the response of the system to an impulse at time t'. It fully takes into account the non-Markovian nature of the dynamics and the dissipation induced by the environment. In some cases the function $G(t,t')$ can be computed analytically. In general only a numerical approach is possible. In any case, if $G(t,t')$ is known, the complete solution to Eq. (4.18) can be obtained. In fact, it is easy to verify that the expression

$$Z(t) = G(t,0)Z(0) + \int_0^t G(t,t')\left[\sum_\alpha \mathcal{C}_\alpha g_\alpha(t',0)z_\alpha(0)\right]dt' \tag{4.20}$$

is a solution of Eq. (4.18) and satisfies the required initial condition.

4.2.3 Renormalization and damping kernel

It is useful to rewrite the integro-differential equation in Eq. (4.19) and express the non-Markovian integral term as a functional of the velocity in phase space, $\frac{\partial}{\partial t}G(t,t')$, instead of $G(t,t')$. For that purpose a partial integration must be performed, with the following result:

$$\frac{\partial}{\partial t}G(t,t') + a_R(t)G(t,t') + \int_0^t \gamma(t,\tau)\frac{\partial}{\partial \tau}G(\tau,t')d\tau = \mathbb{1}_{2N}\delta(t-t') \tag{4.21}$$

Note that the matrix $a_s(t)$, that describes the unitary dynamics of the system, has been renormalized to $a_R(t) = a_s(t) - \gamma(0)$. The function $\gamma(t,t')$ is such that $\eta(t,t') = \frac{\partial}{\partial t'}\gamma(t,t')$, and is known as the damping kernel. For $t > t'$ it can be calculated as follows:

$$\gamma_\alpha(t,t') = \begin{pmatrix} 0 & 0 \\ \gamma_\alpha^{xx}(t-t') & 0 \end{pmatrix} \tag{4.22}$$

where the matrix γ_α^{xx} is defined as:

$$\gamma_\alpha^{xx}(t) = \int_0^\infty \frac{I_\alpha(\omega)}{\omega}\cos(\omega t)d\omega \tag{4.23}$$

4.3 Evolution of quantum states

In this section we show that the result obtained in Eq. (4.20) enables the computation of the time evolution of an arbitrary initial state. We begin by obtaining the evolution of the covariance matrix, i.e, the two-point correlations in the system.

4.3.1 Evolution of the covariance matrix

The covariance matrix of the system at time t is defined as

$$C(t) = \mathrm{Re}\left[\langle Z(t)Z(t)^T\rangle\right] - \langle Z(t)\rangle\langle Z(t)^T\rangle \tag{4.24}$$

where $\langle A(t)\rangle = \mathrm{Tr}(\rho^0 A(t))$, and ρ^0 is the initial state of the system and reservoirs.We will consider initial states such that $\langle Z(0)\rangle = \langle z_l(0)\rangle = 0$ and therefore, according to Eq. (4.20), $\langle Z(t)\rangle = 0$ for all t. Inserting Eq. (4.20) in Eq. (4.24) the following expression is obtained:

$$\begin{aligned} C(t) =& G(t,0)C(0)G(t,0)^T + G(t,0)\,\mathrm{Re}\left[\langle Z(0)\beta(t)^T\rangle\right] + \mathrm{Re}\left[\langle\beta(t)Z(0)^T\rangle\right]G(t,0)^T \\ &+ \mathrm{Re}\left[\langle\beta(t)\beta(t)^T\rangle\right] \end{aligned} \tag{4.25}$$

where $\beta(t)$ is the integral term of Eq. (4.20),

$$\beta(t) = \sum_\alpha \beta_\alpha(t) z_\alpha(0) \tag{4.26a}$$

$$\beta_\alpha(t) = \int_0^t G(t,t')\mathcal{C}_\alpha g_\alpha(t',0)dt' \tag{4.26b}$$

The first term in Eq. (4.25) is the deterministic propagation of the initial covariance matrix given by the phase space flow $G(t,0)$. The second and third terms are the propagation of the initial correlations between system and reservoirs. The last term correspond to the noise and diffusion induced by the environment on the system, and in a stable system will dominate the long term behavior. If there are no system-reservoirs correlations in the initial state, i.e, if $\mathrm{Re}\left[\langle Z(0)z_\alpha(0)^T\rangle\right] = 0$ for all α, then the second and third terms of Eq. (4.25) vanish for all t. In that case the evolution of the covariance matrix is just:

$$C(t) = G(t,0)C(0)G(t,0)^T + \mathrm{Re}\left[\langle\beta(t)\beta(t)^T\rangle\right] \tag{4.27}$$

Using Eq. (4.26a) we find the following expression for the diffusive term of the covariance matrix:

$$\mathrm{Re}\left[\langle\beta(t)\beta(t)^T\rangle\right] = \int_0^t\int_0^t G(t,t_1)\left[\sum_{\alpha,\beta}\mathcal{C}_\alpha g_\alpha(t_1,0)\,\mathrm{Re}\left[\langle z_\alpha(0)z_\beta(0)^T\rangle\right]g_\beta(t_2,0)^T\mathcal{C}_\beta^T\right]G(t,t_2)^T dt_1 dt_2 \tag{4.28}$$

Now we introduce the condition that in the initial state the reservoirs are in thermal states and uncorrelated with each other. In that case:

$$\mathrm{Re}\left[\langle z_\alpha(0) z_\beta(0)^T\rangle\right] = \delta_{\alpha,\beta}\frac{\hbar}{2}\begin{pmatrix}(m\Omega_\alpha)^{-1}\coth\left(\frac{\hbar\Omega_\alpha}{2k_BT_\alpha}\right) & 0\\ 0 & (m\Omega_\alpha)\coth\left(\frac{\hbar\Omega_\alpha}{2k_BT_\alpha}\right)\end{pmatrix}, \quad (4.29)$$

Where T_α is the temperature of the α-th reservoir and k_B is the Boltzmann constant. Inserting Eq. (4.29) in Eq. (4.28) the following final expression is obtained:

$$\mathrm{Re}\left[\langle \beta(t)\beta(t)^T\rangle\right] = \frac{\hbar}{2}\int_0^t\int_0^t G(t,t_1)\nu(t_1-t_2)G(t,t_2)^T dt_1 dt_2 \quad (4.30)$$

The matrix function $\nu(t) = \sum_\alpha \nu_\alpha(t)$ is the noise kernel, with

$$\nu_\alpha(t) = \begin{pmatrix}0 & 0\\ 0 & \nu_\alpha^{xx}(t)\end{pmatrix} \quad (4.31)$$

where:

$$\nu_\alpha^{xx}(t) = \int_0^\infty I_\alpha(\omega)\cos(\omega t)\coth\left(\frac{\hbar\omega}{2k_BT_\alpha}\right)d\omega \quad (4.32)$$

4.3.2 Evolution of the Wigner characteristic function

We now show how to obtain the evolution of the Wigner characteristic function of the system in terms of the Green's function $G(t,t')$. The results can be used to evolve an arbitrary initial state. We consider the characteristic function of the system at time t

$$\chi(y,t) = \mathrm{Tr}\left[\rho_s(t)\hat{D}_y\right] \quad (4.33)$$

where y is a column vector and $\hat{D}_y = e^{iZ(0)^T y}$ is the displacement operator in phase space. The operator $\rho_s(t)$ is the density matrix of the system at time t. The trace in Eq. (4.33) can trivially be extended to the Hilbert space of system and reservoirs, i.e, $\chi(y,t) = \mathrm{Tr}\left[\rho(t)\hat{D}_y\right]$, where $\rho(t)$ is the total density matrix at time t. The characteristic function can be written in terms of the initial total density matrix, $\rho(0)$, and a time dependent displacement operator

$$\chi(y,t) = \mathrm{Tr}\left[\rho(0)U(t)^\dagger\hat{D}_y U(t)\right] = \mathrm{Tr}\left[\rho(0)e^{iZ(t)^T y}\right] \quad (4.34)$$

where $U(t)$ is the unitary evolution of system and reservoirs. Now, the operator $Z(t)$ in the previous expression can be substituted using Eq. (4.20). Therefore, we have $e^{iZ(t)^T y} = e^{iZ(0)^T G(t,0)^T y}e^{i\beta(t)^T y}$, where $\beta(t)$ is defined in Eq.(4.26a) (note that $\beta(t)$ only depends on the environmental operators at $t=0$, and therefore commutes with $Z(0)$). Also, we assume that the initial state is separable $\rho(0) = \rho_S(0)\otimes\rho_E(0)$. We obtain

$$\chi(y,t) = \mathrm{Tr}\left[\rho_S(0)e^{iZ(0)^T G(t,0)^T y}\right]\mathrm{Tr}\left[\rho_E(0)e^{i\beta(t)^T y}\right] \quad (4.35)$$

The first factor in the previous expression is the initial characteristic function evaluated at $G(t,0)^T y$. It correspond to the deterministic evolution given by $G(t,0)$. The second factor is a Gaussian function of y and describes the diffusion induced by the reservoirs.

Assuming that the initial state of the environment is separable with respect to each reservoir, i.e., $\rho_E(0) = \bigotimes_\alpha \rho_\alpha(0)$, and using Eq. (4.26a) we find

$$\mathrm{Tr}\left[\rho_E(0)e^{i\beta(t)^T y}\right] = \prod_\alpha \mathrm{Tr}\left[\rho_\alpha(0)e^{iz_\alpha(0)^T\beta_\alpha(t)^T y}\right] = \prod_\alpha \chi_\alpha(\beta_\alpha(t)^T y, 0) \tag{4.36}$$

where $\chi_\alpha(\beta_\alpha(t)^T y, 0)$ is the initial characteristic function of the α-th reservoir evaluated at $\beta_\alpha(t)^T y$ [the function $\beta_\alpha(t)$ is defined in Eq. (4.26b)]. If the initial state of each reservoir is a thermal state at temperature T_α, then its characteristic function is $\chi_\alpha(y) = e^{-\frac{1}{2}y^T\langle z_\alpha(0)z_\alpha(0)^T\rangle y}$, with the matrix $\langle z_\alpha(0)z_\alpha(0)^T\rangle$ given by Eq. (4.29). Therefore the second factor in Eq. (4.35) can be written as

$$\mathrm{Tr}\left[\rho_E(0)e^{i\beta(t)^T y}\right] = e^{-\frac{1}{2}y^t\langle\beta(t)\beta(t)^T\rangle y} \tag{4.37}$$

where $\langle\beta(t)\beta(t)^T\rangle$ is given by Eq. (4.30).

In summary, we obtain the following final expression for the characteristic function at time t

$$\chi(y,t) = \chi(G(t,0)^T y, 0)\; e^{-\frac{1}{2}y^t\langle\beta(t)\beta(t)^T\rangle y} \tag{4.38}$$

4.3.3 Evolution of the Wigner quasiprobability distribution

We now consider the evolution of the Wigner quasiprobability distribution, which can be obtained as a Fourier transform of the Wigner characteristic function in Eq. (4.33),

$$P(z,t) = \frac{1}{(2\pi)^{2N}}\int_{-\infty}^{+\infty}(dy)^{2N}\chi(y,t)e^{-iz^T y}, \tag{4.39}$$

where z is a $2N$-components column vector indicating a point in phase space. Introducing Eq. (4.38) into Eq. (4.39) and invoking the convolution theorem, we obtain:

$$P(z,t) = \frac{1}{\det(G(t,0))}\int (dz')^{2N} P\left((G^{-1}(t,0))^T(z-z'), t=0\right) P_d(z') \tag{4.40}$$

where $P_d(z)$ is a multivariate normal distribution with zero mean and covariance matrix equal to $\langle\beta(t)\beta(t)^T\rangle$,

$$P_d(z) = \frac{1}{(2\pi)^N}\frac{1}{\det(\langle\beta(t)\beta(t)^T\rangle)^{1/2}}e^{\frac{1}{2}z^T\langle\beta(t)\beta(t)^T\rangle^{-1}z} \tag{4.41}$$

Therefore, the Wigner distribution of the state of the system at time t is equal to the convolution of the coherent evolution of the initial Wigner distribution given by $G(t,0)$ with a Gaussian function whose covariance matrix is $\langle\beta(t)\beta(t)^T\rangle$.

Un modelo con solución exacta

En este capítulo se define el modelo principal de esta tesis: una red armónica conectada con entornos bosónicos y sujeta a un forzado paramétrico. Como se explica en las próximas secciones este modelo puede ser resuelto exactamente. El análisis de la solución exacta aclara las limitaciones de la aproximación de acoplamiento débil en este modelo y otros similares.

Chapter 5

Periodic processes

The previous chapter set the basic formalism to calculate the temporal evolution of linear driven open systems with continuous variables. We will now simplify those general results for the particular case in which the driving is periodic and the dynamic is stable. For this we use some ideas of Floquet theory, although we avoid the calculation of Floquet quasienergies and Floquet modes.

5.1 Asymptotic state for stable systems

In this section we characterize the asymptotic state for driven systems that are exponentially stable, i.e., systems with a Green's function $G(t,t')$ decaying exponentially with $t-t'$. The previous condition is not always fulfilled for driven systems, even in the presence of strong dissipation, since it is possible, for example, to induce a divergent dynamics by the phenomenon of parametric resonance.

From Eq. (4.27) it is clear that for stable systems the asymptotic covariance matrix is:

$$C(t) = \mathrm{Re}\left[\langle \beta(t)\beta(t)^T \rangle\right] = \begin{bmatrix} \sigma^{xx}(t) & \sigma^{xp}(t) \\ \sigma^{px}(t) & \sigma^{pp}(t) \end{bmatrix} \tag{5.1}$$

since $G(t,0) \to 0$ for large t. Also, Eq. (4.30) is equivalent to the following expressions for each block of the asymptotic covariance matrix:

$$\sigma^{xx}(t) = \frac{\hbar}{2}\int_0^t \int_0^t g(t,t_1)\ \nu^{xx}(t_1-t_2)\ g(t,t_2)^T\ dt_1 dt_2 \tag{5.2a}$$

$$\sigma^{xp}(t) = \frac{\hbar}{2}\int_0^t \int_0^t g(t,t_1)\ \nu^{xx}(t_1-t_2)\ \frac{\partial}{\partial t} g(t,t_2)^T M\ dt_1 dt_2 \tag{5.2b}$$

$$\sigma^{pp}(t) = \frac{\hbar}{2}\int_0^t \int_0^t M\frac{\partial}{\partial t} g(t,t_1)\ \nu^{xx}(t_1-t_2)\ \frac{\partial}{\partial t} g(t,t_2)^T M\ dt_1 dt_2 \tag{5.2c}$$

In the previous expressions, the function $g(t,t')$ is the Green's function of the system in the configuration space, and satisfies the following second order integro-differential equation for $t > t'$:

$$M\frac{\partial^2}{\partial t^2} g(t,t') + V_R(t) g(t,t') + \int_0^t \gamma^{xx}(t-\tau)\frac{\partial}{\partial \tau} g(\tau,t') d\tau = 0 \tag{5.3}$$

with initial conditions $g(t=t',t')=0$ and $\frac{\partial}{\partial t} g(t=t',t') = M^{-1}$. Also, $V_R(t) = V(t) - \gamma^{xx}(0)$ is the renormalized potential. We now introduce the spectral decomposition of

the noise kernel (see Eq. (4.32)):

$$\nu^{xx}(t_1 - t_2) = \mathrm{Re}\left[\int_0^\infty \tilde{\nu}(\omega) e^{i\omega t_1} e^{-i\omega t_2} d\omega\right] \tag{5.4}$$

where $\tilde{\nu}(\omega)$ is the Fourier transform of $\nu^{xx}(t)$:

$$\tilde{\nu}(\omega) = \sum_\alpha I_\alpha(\omega) \coth\left(\frac{\hbar\omega}{2k_b T_\alpha}\right) \tag{5.5}$$

Introducing Eq. (5.4) into Eqs. (5.2a - 5.2c) we obtain:

$$\sigma^{xx}(t) = \frac{\hbar}{2}\,\mathrm{Re}\left[\int_0^\infty q(t,\omega)\ \tilde{\nu}(\omega)\ q(t,\omega)^\dagger\ d\omega\right] \tag{5.6a}$$

$$\sigma^{xp}(t)M^{-1} = \frac{\hbar}{2}\,\mathrm{Re}\left[\int_0^\infty q(t,\omega)\ \tilde{\nu}(\omega)\ \frac{\partial}{\partial t}q(t,\omega)^\dagger\ d\omega\right] \tag{5.6b}$$

$$M^{-1}\sigma^{pp}(t)M^{-1} = \frac{\hbar}{2}\,\mathrm{Re}\left[\int_0^\infty \frac{\partial}{\partial t}q(t,\omega)\ \tilde{\nu}(\omega)\ \frac{\partial}{\partial t}q(t,\omega)^\dagger\ d\omega\right] \tag{5.6c}$$

where the function $q(t,\omega)$ is defined as:

$$q(t,\omega) = \int_0^t g(t,t')e^{i\omega t'}dt' \tag{5.7}$$

So far we have only given alternatives expressions for the asymptotic covariance matrix valid when the system is stable. We now analyze the asymptotic properties of the function $q(t,\omega)$ for the case in which the driving is periodic.

5.2 Periodic driving

The potential energy matrix $V(t)$ is assumed to be τ-periodic: $V(t+\tau) = V(t)$. From the integro-differential equation defining $g(t,t')$ (Eq. (5.3)) it follows that:

$$g(t+\tau, t'+\tau) = g(t,t'), \tag{5.8}$$

since $g(t+\tau,t'+\tau)$ and $g(t,t')$ are both solution of Eq. (5.3) with the same initial conditions. This observation implies that

$$q(t+\tau,\omega) = \int_0^{t+\tau} g(t+\tau,t')e^{i\omega t'}dt' = \int_{-\tau}^{t} g(t+\tau,t'+\tau)e^{i\omega(t'+\tau)}dt' = \left[\int_{-\tau}^{t} g(t,t')e^{i\omega t'}dt'\right]e^{i\omega\tau}. \tag{5.9}$$

Now, if $g(t,t')$ decays exponentially with $(t-t')$ the following approximation holds for large t:

$$\int_{-\tau}^{t} g(t,t')e^{i\omega t'}dt' \simeq \int_0^t g(t,t')e^{i\omega t'}dt' = q(t,\omega) \tag{5.10}$$

Therefore, in the asymptotic limit, the function $q(t,\omega)$ satisfies:

$$q(t+\tau,\omega) = q(t,\omega)e^{i\omega\tau} \tag{5.11}$$

from which it follows that the function

$$p(t,\omega) = q(t,\omega)e^{-i\omega t} \tag{5.12}$$

is τ-periodic. In summary, the function $q(t,\omega)$, from which the covariance matrix at time t can be obtained, can be expressed for sufficiently long times as $q(t,\omega) = p(t,\omega)e^{i\omega t}$, where $p(t,\omega)$ is τ-periodic. As a consequence, the asymptotic state for long times will also be τ-periodic. To see that, as an example, we rewrite the asymptotic limit of $\sigma^{xx}(t)$ in terms of $p(t,\omega)$:

$$\sigma^{xx}(t) = \frac{\hbar}{2}\,\mathrm{Re}\left[\int_0^\infty p(t,\omega)\;\tilde{\nu}(\omega)\;p(t,\omega)^\dagger\;d\omega\right] \tag{5.13}$$

similar expressions hold for $\sigma^{xp}(t)$ and $\sigma^{pp}(t)$, in which time only enters through $p(t,\omega)$ or its derivative.

To finish this section we note that since the functions $V_R(t)$ and $p(t,\omega)$ are τ-periodic they are determined by their Fourier coefficients V_k and $A_k(\omega,\omega_d)$:

$$V_R(t) = \sum_{k=-\infty}^{+\infty} V_k\; e^{ik\omega_d t} \tag{5.14}$$

$$p(t,\omega) = \sum_{k=-\infty}^{+\infty} A_k(\omega,\omega_d)\; e^{ik\omega_d t} \tag{5.15}$$

where $\omega_d = 2\pi/\tau$ is the fundamental angular frequency of the driving. In the following section we explain how to calculate the coefficients A_k given the driving coefficients V_k. However, if they are known, then the asymptotic correlations can be easily obtained as:

$$\sigma^{xx}(t) = \mathrm{Re}\left[\sum_{j,k}\sigma^{xx}_{j,k}\;e^{i\omega_d(j-k)t}\right] \tag{5.16}$$

where:

$$\sigma^{xx}_{j,k} = \frac{\hbar}{2}\int_0^\infty A_j(\omega,\omega_d)\tilde{\nu}(\omega)A_k^\dagger(\omega,\omega_d)d\omega \tag{5.17}$$

Similar expressions can be found for the correlations $\sigma^{xp}(t)$ and $\sigma^{pp}(t)$.

5.3 Calculation of the function $p(t,\omega)$

An integro-differential equation for $p(t,\omega)$ can be derived from the one defining $g(t,t')$, Eq. (5.3). It reads:

$$\begin{aligned} &M\left[\frac{\partial^2}{\partial t^2}p(t,\omega) + 2(i\omega)\frac{\partial}{\partial t}p(t,\omega) + (i\omega)^2 p(t,\omega)\right] + V_R(t)P(t,\omega) + \\ &+\int_0^t \gamma^{xx}(t-\tau)\left[\frac{\partial}{\partial t}p(\tau,\omega) + (i\omega)p(\tau,\omega)\right]e^{-i\omega(t-\tau)}d\tau = \mathbb{1} \end{aligned} \tag{5.18}$$

Inserting the Fourier decomposition of Eq. (5.15) into the previous equation one obtains the following algebraic relation for the coefficients $A_k(\omega,\omega_d)$:

$$\hat{g}\left(i(\omega+k\omega_d)\right)^{-1}\;A_k(\omega,\omega_d) + \sum_{j\neq k} V_j A_{k-j}(\omega,\omega_d) = \mathbb{1}\delta_{k,0} \tag{5.19}$$

where the matrix function $\hat{g}(s)$ is the Laplace transform of the Green's function of the system without driving, which satisfies:

$$\hat{g}(s)^{-1} = Ms^2 + V_R + s\hat{\gamma}(s) \tag{5.20}$$

In turn, $\hat{\gamma}(s)$ is the Laplace transform of the damping kernel $\gamma^{xx}(t)$:

$$\hat{\gamma}(s) = \int_0^\infty \frac{I(\omega)}{\omega} \frac{s}{\omega^2 + s^2} d\omega \tag{5.21}$$

The infinite set of equations given in Eq. (5.19) can be solved for any given value of ω by standard techniques. For example, a finite linear system can be obtained by only considering coefficients $A_k(\omega, \omega_d)$ with $|k| \leq k_{max}$, which is later solved by a regular matrix inversion. Alternatively, a perturbative approach can be employed. Thus, if the driving is weak (i.e., if $|V_k| \ll |V_0|$ for all $k \neq 0$), then up to second order in V_k we have

$$A_0(\omega, \omega_d) = \hat{g}(i\omega) + \sum_{k \neq 0} g(i\omega)\ V_k\ g(i(\omega - k\omega_d))\ V_{-k}\ g(i\omega) \tag{5.22a}$$

$$A_k(\omega, \omega_d) = -\hat{g}(i(\omega + k\omega_d))\ V_k\ \hat{g}(i\omega) \quad \text{for } k \neq 0 \tag{5.22b}$$

To finish this section, we note that the coefficients $A_k(\omega, \omega_d)$ satisfy certain exact symmetries, which can be obtained by examining the linear system given by Eq. (5.19). Thus, if $\{A_k(\omega, \omega_d)\}$ are the solutions of Eq. (5.19) for a given process $V(t)$, and $\{A^r_k(\omega, \omega_d)\}$ are the solutions corresponding to the time reversed process $V(-t)$, we have:

$$A^r_k(\omega, \omega_d) = A_{-k}(\omega, -\omega_d) \tag{5.23a}$$

$$A^r_k(\omega, \omega_d) = A^T_{-k}(\omega + k\omega_d, \omega_d) \tag{5.23b}$$

$$A^*_k(\omega, \omega_d) = A_{-k}(-\omega, \omega_d) \tag{5.23c}$$

As will be clear in the next sections, if two reservoirs are connected to sites α and β of the network, then the function $|(A_k(\omega, \omega_d))_{\alpha,\beta}|^2$ is related to the rate at which a quantum of energy $\hbar\omega$ is extracted from the reservoir at β while a quantum of energy $\hbar(\omega + \omega_d)$ is dumped into the reservoir at α (via absorption of $k\hbar\omega_d$ energy from the driving, for $k > 0$). Thus, the above relations express fundamental symmetries between energy exchange processes.

Procesos periódicos

El capítulo anterior introdujo el formalismo básico para calcular la evolución temporal de sistemas cuánticos lineales de variable continua que son abiertos y forzados. En este capítulo se simplifican esos resultados generales para el caso particular en que el forzado es periódico y la dinámica es estable. Para esto se utilizan algunas ideas de la teoría de Floquet, aunque se evita el cálculo explicito de las autoenergías y autoestados de Floquet.

Part III

Emergence of thermodynamical laws

Chapter 6

Definitions of work and heat rates

In this chapter we give and justify the basic definitions for heat and work that are later used. This definitions are then expressed in terms of readily computable quantities. Also, physical interpretations of the obtained expressions are discussed. From this interpretations, it follows that a pairs creation mechanism completely analogous to the Dynamical Casismir Effect (DCE) is a fundamental limitation for cooling for the family of thermal machines considered. Finally, a extension of the model is discussed.

6.1 Total work and heat rates

In this section we give microscopic definitions for the work performed on the system by the driving and for the energy exchange with each thermal reservoir, i.e, for the heat rates. We begin by analyzing the variation in time of the system energy. From Eq. (4.1) we have:

$$\langle H_S \rangle(t) = \frac{1}{2}\,\mathrm{Tr}\left[M^{-1}\sigma^{pp}(t)\right] + \frac{1}{2}\,\mathrm{Tr}\left[V(t)\sigma^{xx}(t)\right], \tag{6.1}$$

and therefore,

$$\frac{d}{dt}\langle H_S \rangle(t) = \frac{1}{2}\,\mathrm{Tr}\left[M^{-1}\frac{d}{dt}\sigma^{pp}(t)\right] + \frac{1}{2}\,\mathrm{Tr}\left[V(t)\frac{d}{dt}\sigma^{xx}(t)\right] + \frac{1}{2}\,\mathrm{Tr}\left[\frac{d}{dt}V(t)\sigma^{xx}(t)\right], \tag{6.2}$$

The last term in the previous equation is the rate at which energy is injected into or absorbed from the system by the driving. The remaining terms represent the variation of the system energy due to the interaction with the thermal reservoirs. In order to see that it is useful to rewrite $\frac{d}{dt}\langle H_S \rangle(t)$ as:

$$\frac{d}{dt}\left\langle H_S \right\rangle(t) = \frac{1}{i\hbar}\left\langle [H_S, H] \right\rangle + \left\langle \frac{\partial}{\partial t} H_S \right\rangle = \frac{1}{i\hbar}\left\langle [H_S, H_{int}] \right\rangle + \frac{1}{2}\,\mathrm{Tr}\left[\frac{d}{dt}V(t)\sigma^{xx}(t)\right] \tag{6.3}$$

where H is the total Hamiltonian defined in Eq. (4.3). Comparing Eqs. (6.2) and (6.3) we see that the first two terms in Eq. (6.2) can be interpreted as the energy exchange with the reservoirs. Thus, we arrive at the following definitions for the work rate $\dot{W}$ and total heat rate $\dot{Q}(t)$:

$$\dot{W}(t) = \frac{1}{2}\,\mathrm{Tr}\left[\frac{d}{dt}V(t)\sigma^{xx}(t)\right] \tag{6.4}$$

and,

$$\dot{Q}(t) = \frac{1}{i\hbar}\left\langle [H_S, H_{int}] \right\rangle = \frac{1}{2}\,\mathrm{Tr}\left[M^{-1}\frac{d}{dt}\sigma^{pp}(t)\right] + \frac{1}{2}\,\mathrm{Tr}\left[V(t)\frac{d}{dt}\sigma^{xx}(t)\right] \tag{6.5}$$

6.2 Local heat rates

Equation (6.5) defines the total energy interchange between the system and all the thermal reservoirs. However, the local heat rate corresponding to a particular reservoir is also of interest. A working definition for such local heat rates can be obtained by expanding Eq. (6.5) using Eq. (4.2):

$$\dot{Q} = \frac{1}{i\hbar} \langle [H_S, H_{int}] \rangle = \sum_\alpha \frac{1}{i\hbar} \langle [H_S, H_{int,\alpha}] \rangle \tag{6.6}$$

where $H_{int,\alpha} = \sum_{j,k} C_{\alpha,jk}\ X_j\ q_{\alpha,k} = X^T C_\alpha q_\alpha$ is the Hamiltonian term describing the interaction between the system and the α-th reservoir. We define

$$\dot{Q}_\alpha = \frac{1}{i\hbar} \langle [H_S, H_{int,\alpha}] \rangle \tag{6.7}$$

as the heat rate corresponding to the α-th reservoir. In this way we obtain a set $\{\dot{Q}_\alpha\}$ of local heat rates such that the total heat rate is $\dot{Q} = \sum_\alpha Q_\alpha$. A direct calculation shows that

$$\dot{Q}_\alpha = -\langle P^T M^{-1} C_\alpha q_\alpha \rangle \tag{6.8}$$

We can use the motion equation (4.5b) in order to eliminate the reservoir coordinates from Eq. (6.8). Thus, if P_α is a projector over the sites of the network in contact with the α-th reservoir, then $P_\alpha \dot{P} = -P_\alpha V(t) X - C_\alpha q_\alpha$ (this identity is valid in the case in which different reservoirs are coupled to different sites of the network, i.e., we assume that $P_\alpha P_\beta = \delta_{\alpha,\beta} P_\alpha$ and $P_\alpha C_\beta = \delta_{\alpha,\beta} C_\alpha$). Therefore:

$$\dot{Q}_\alpha = \frac{1}{2} \operatorname{Tr} \left[P_\alpha \frac{d}{dt} \sigma^{pp}(t) M^{-1} \right] + \operatorname{Tr} \left[P_\alpha V(t) \sigma^{xp}(t) M^{-1} \right] \tag{6.9}$$

The previous definition for the local heat rates is not the only possible. Another natural definition for the heat rates is given by the rate of change of the energy of each reservoir:

$$\dot{Q}'_\alpha = \frac{1}{i\hbar} \langle [H_{E,\alpha}, H_{int,\alpha}] \rangle \tag{6.10}$$

If the interactions terms were energy conserving, i.e, if it were $[H_S + H_{E,\alpha}, H_{int,\alpha}] = 0$, then we would have $\dot{Q}'_\alpha + \dot{Q}_\alpha = 0$ and the two definitions of heat rates would be equivalent. Although in our model the energy conserving condition is not fulfilled and in general $\dot{Q}'_\alpha + \dot{Q}_\alpha \neq 0$, it is easy to see that:

$$\dot{Q}'_\alpha + \dot{Q}_\alpha = \frac{d}{dt} \left\langle X^t P_\alpha (\dot{P} + V(t) X) \right\rangle \tag{6.11}$$

Since the asymptotic state is τ-periodic, the right hand side of the last equation is the derivative of a τ-periodic function. This observation implies that the average heat rates per cycle obtained with the two possible definitions are equivalent, as if the interaction terms were energy conserving. This is explained in the next section.

6.3 Work and heat in the asymptotic state

We have seen that if the system is periodically driven and stable the asymptotic state is also periodic, with the same period as the driving. It follows that the function $\langle H_S \rangle(t)$

and its derivative $\frac{d}{dt}\langle H_S\rangle(t)$ are also periodic. Thus, averaging Eq. (6.2) in one period (for long times) we obtain:

$$0 = \dot{\bar{Q}} + \dot{\bar{W}} \tag{6.12}$$

where $\dot{\bar{W}}$ and $\dot{\bar{Q}}$ are the average work and total heat rates per cycle:

$$\dot{\bar{W}} = \frac{1}{\tau}\lim_{n\to\infty}\int_{n\,\tau}^{(n+1)\tau} \dot{W}(t')\,dt' \qquad\qquad \dot{\bar{Q}} = \frac{1}{\tau}\lim_{n\to\infty}\int_{n\tau}^{(n+1)\tau} \dot{Q}(t')\,dt' \tag{6.13}$$

Equation (6.12) is nothing more than the expression of the first law of thermodynamics for cyclic processes. We note that the first term of the right hand side of Eq. (6.5) for $\dot{Q}(t')$ is the derivative of a periodic function and therefore does not contribute to the integral over a period. In the same way we can define the local heat rates per cycle:

$$\dot{\bar{Q}}_\alpha = \frac{1}{\tau}\lim_{k\to\infty}\int_{k\tau}^{(k+1)\tau} \dot{Q}_\alpha(t')dt' = \frac{1}{\tau}\lim_{k\to\infty}\int_{k\tau}^{(k+1)\tau} \mathrm{Tr}\left[P_\alpha V(t')\sigma^{xp}(t')M^{-1}\right]dt' \tag{6.14}$$

This set of heat rates trivially satisfy:

$$\dot{\bar{Q}} = \sum_\alpha \dot{\bar{Q}}_\alpha \tag{6.15}$$

From Eq. (6.11) and the fact that the right hand side is a derivative of τ-periodic function for long times it follows that:

$$\dot{\bar{Q}}'_\alpha + \dot{\bar{Q}}_\alpha = 0 \tag{6.16}$$

Therefore, in a complete cycle the variation of energy of a given reservoir is equal (in absolute value) to the variation of the energy of the system due to the interaction with that reservoir. No energy is stored in the interaction terms. We stress that this is true only for the averaged heat rates.

6.4 Heat transfer matrix

From Eqs. (5.6b), (5.7) and (5.15) it is straightforward to derive the following expression for the correlation between position and momentum in terms of the Fourier coefficients $\{A_k(\omega,\omega_d)\}$:

$$\sigma^{xp}(t) = \mathrm{Im}\left[\sum_{j,k}\sigma^{xp}_{j,k}\; e^{i\omega_d(j-k)t}\right] \tag{6.17}$$

where:

$$\sigma^{xp}_{j,k} = \frac{\hbar}{2}\int_0^\infty (\omega + k\omega_d)A_j(\omega,\omega_d)\tilde{\nu}(\omega)A_k^\dagger(\omega,\omega_d)\;\; d\omega \tag{6.18}$$

Introducing Eq. (6.17) into the expression for the local heat rates of Eq. (6.14), and performing the time integral, the following result is obtained:

$$\dot{\bar{Q}}_\alpha = \frac{\hbar}{2}\int_0^\infty \mathrm{Im}\left\{\sum_{j,k}\mathrm{Tr}\left[P_\alpha V_{k-j}A_j(\omega,\omega_d)\tilde{\nu}(\omega)A_k^\dagger(\omega,\omega_d)\right](\omega+k\omega_d)\right\}d\omega \tag{6.19}$$

Now, expanding the Fourier transform of the noise kernel as in Eq. (5.5), the local heat $\bar{Q}_\alpha$ can be written as:

$$\dot{\bar{Q}}_\alpha = \sum_\beta \int_0^\infty Q_{\alpha,\beta}(\omega) \coth\left(\frac{\hbar\omega}{2k_bT_\beta}\right) d\omega \tag{6.20}$$

where the functions $Q_{\alpha,\beta}(\omega)$ are defined as

$$Q_{\alpha,\beta}(\omega) = \frac{\hbar}{2} \operatorname{Im}\left\{ \sum_{j,k} (\omega + k\omega_d) \operatorname{Tr}\left[P_\alpha V_{k-j} A_j(\omega,\omega_d) I_\beta(\omega) A_k^\dagger(\omega,\omega_d) \right] \right\} \tag{6.21}$$

If the number of reservoirs is L, there are L^2 functions $Q_{\alpha,\beta}(\omega)$, which are considered to be the elements of matrix called the heat transfer matrix. They specify how the heat per cycle corresponding to the α-th reservoir is affected by the temperature of the β-th reservoir. The previous expression for $Q_{\alpha,\beta}(\omega)$ can be simplified. In order to do that we note that one of the sums appearing in Eq. (6.21) can be performed with the aid of the algebraic equation that the coefficients $A_k(\omega,\omega_d)$ satisfy. Indeed, from Eq. (5.19) it follows that

$$\sum_j V_{k-j} A_j(\omega,\omega_d) = \mathbb{1}\delta_{k,0} - \left[\hat{g}\left(i(\omega + k\omega_d)\right)^{-1} - V_0 \right] A_k(\omega,\omega_d) \tag{6.22}$$

Another important relation is:

$$\operatorname{Im}\left\{ \hat{g}\,(i\omega)^{-1} - V_0 \right\} = \omega \operatorname{Re}\left\{\hat{\gamma}(i\omega)\right\} = \frac{\pi}{2} I(\omega) \tag{6.23}$$

where in the last equality the fluctuation-dissipation theorem, $\operatorname{Re}\left\{\hat{\gamma}(i\omega)\right\} = \frac{\pi}{2}\frac{I(|\omega|)}{|\omega|}$, was employed. The last equation is valid if the spectral density $I(\omega)$, originally defined only for positive frequencies, is extended in a odd way for negative frequencies, i.e, such that $I(-\omega) = -I(\omega)$. Taking into account Eqs. (6.22) and (6.23) it is possible to arrive at the following simplified expression for the non-diagonal terms of the heat transfer matrix:

$$Q_{\alpha,\beta}(\omega) = \frac{-\pi\hbar}{4} \sum_k (\omega + k\omega_d) \operatorname{Tr}\left[I_\alpha(\omega + k\omega_d) A_k(\omega,\omega_d) I_\beta(\omega) A_k^\dagger(\omega,\omega_d) \right] \quad (\alpha \neq \beta) \tag{6.24}$$

Also, the sum over the first index can be expressed as:

$$\tilde{Q}_\beta(\omega) = \sum_\alpha Q_{\alpha,\beta}(\omega) = \frac{-\pi\hbar}{4} \sum_k (k\omega_d) \operatorname{Tr}\left[I(\omega + k\omega_d) A_k(\omega,\omega_d) I_\beta(\omega) A_k^\dagger(\omega,\omega_d) \right] \tag{6.25}$$

The last two equations completely determine all the elements of the heat transfer matrix. These expressions can be compared to the ones obtained in [57] for the case without driving.

6.5 Heat rates in terms of elementary processes

Eq. (6.20) is a simple and compact expression for the heat rates. However, as we will see, it condenses in a single formula terms with very different physical origins, and therefore it is not possible to assign a clear physical interpretation to each coefficient $Q_{\alpha,\beta}(\omega)$

of the heat transfer matrix. In this section we analyze Eqs. (6.20), (6.24) and (6.25) and identify different mechanisms of heat generation and energy transport between reservoirs. We begin by using Eq. (6.25) to rewrite Eq. (6.20) as:

$$\begin{aligned}\dot{\tilde{Q}}_\alpha = &\int_0^\infty d\omega\ \tilde{Q}_\alpha(\omega) \coth\left(\frac{\hbar\omega}{2k_bT_\beta}\right) + \\ &+ \sum_{\beta\neq\alpha}\int_0^\infty d\omega\ \left\{Q_{\alpha,\beta}(\omega)\coth\left(\frac{\hbar\omega}{2k_bT_\beta}\right) - Q_{\beta,\alpha}(\omega)\coth\left(\frac{\hbar\omega}{2k_bT_\alpha}\right)\right\}\end{aligned} \tag{6.26}$$

Expanding $\tilde{Q}_\alpha(\omega)$ and $Q_{\alpha,\beta}(\omega)$ using Eqs. (6.24) and (6.25) it is clear that some terms in the previous expression cancel out. Taking that into account, and using the identity $\coth\left(\frac{\hbar\omega}{2k_bT_\alpha}\right) = 2(N_\alpha(\omega)+1/2)$, where $N_\alpha(\omega) = (e^{\hbar\omega/(k_bT_\alpha)}-1)^{-1}$ is the Planck distribution, we find an important exact result: $\dot{\tilde{Q}}_\alpha$ is the sum of three terms

$$\dot{\tilde{Q}}_\alpha = \dot{\tilde{Q}}_\alpha^{\mathrm{RP}} + \dot{\tilde{Q}}_\alpha^{\mathrm{RH}} + \dot{\tilde{Q}}_\alpha^{\mathrm{NRH}}. \tag{6.27}$$

The first term, $\dot{\tilde{Q}}_\alpha^{\mathrm{RP}}$, is responsible for the resonant pumping (RP) of energy from (or into) E_α. It reads:

$$\begin{aligned}\dot{\tilde{Q}}_\alpha^{\mathrm{RP}} = &\sum_{\beta\neq\alpha}\sum_k\int_{0'}^\infty d\omega\ \omega\ p^{(k)}_{\beta,\alpha}(\omega)\ N_\alpha(\omega) - \\ &- \sum_{\beta\neq\alpha}\sum_k\int_{0'}^\infty d\omega\ (\omega+k\omega_d)\ p^k_{\alpha,\beta}(\omega)\ N_\beta(\omega)\end{aligned} \tag{6.28}$$

where $p^{(k)}_{\alpha,\beta}(\omega) = \frac{\pi}{2}\,\mathrm{Tr}[I_\alpha(|\omega+k\omega_d|)A_k(\omega)I_\beta(\omega)A_k^\dagger(\omega)]$ is a positive number, proportional to the probability for the network to couple the mode with frequency ω in E_β with the one with frequency $|\omega+k\omega_d|$ in E_α. The first term in Eq. (6.28) is positive and accounts for energy flowing out of E_α: a quantum of energy ω is lost in E_α and excites the mode $|\omega + k\omega_d|$ in E_β after absorbing energy $k\omega_d$ from the driving. The second term corresponds to the opposite effect: A quantum of energy ω is lost from E_β and dumped into the mode $|\omega + k\omega_d|$ in E_α after absorbing energy $k\omega_d$ from the driving. See figure 6.1.

The second term in Eq. (6.27) is responsible for the resonant heating (RH) of E_α and reads:

$$\dot{\tilde{Q}}_\alpha^{\mathrm{RH}} = -\sum_{\beta\neq\alpha}\sum_k\int_{0'}^\infty d\omega\ k\omega_d\ p^k_{\alpha,\alpha}(\omega)\ N_\alpha(\omega). \tag{6.29}$$

Its interpretation is analogous to the previous one except for the fact that in this case energy is transferred between modes ω and $|\omega+k\omega_d|$ in E_α (see figure 6.1) . Although E_α can gain or loose energy $k\omega_d$ depending on the sign of k, the upwards flow of energy is more probable than the downwards one. This is because $N_\alpha(\omega)$ monotonically decreases with ω. As a consequence, this process always heat up E_α. A subtlety should be noticed: The lower limit of the frequency integral in all the above terms is not $\omega = 0$ but $\omega = 0' = max\{0, -k\omega_d\}$. This is because processes with negative k, which correspond to the emission into the driving, can only take place if $\omega + k\omega_d > 0$. The role of the low frequency modes is crucial, as we now discuss.

Finally, the last term $\dot{\tilde{Q}}_\alpha^{\mathrm{NRH}}$ corresponds to a non resonant heating (NRH) effect and,

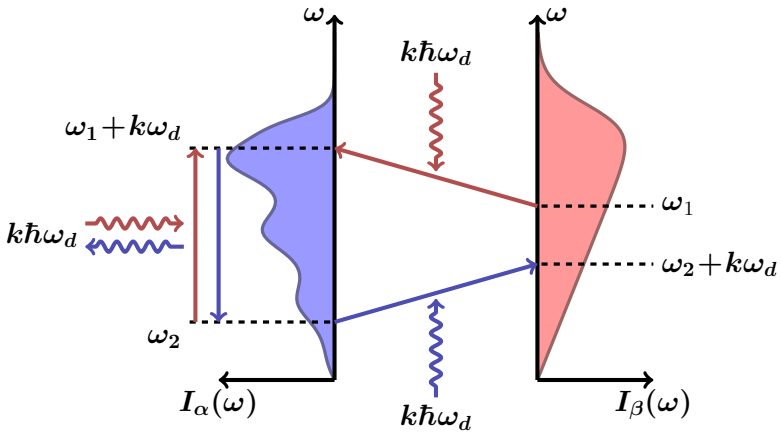

Figure 6.1: Resonant processes. These can take place between modes of different reservoirs (as described by the terms in $\dot{\bar{Q}}_\alpha^{\mathrm{RP}}$), or between modes of the same reservoir (as in $\dot{\bar{Q}}_\alpha^{\mathrm{RH}}$). The total number of excitations in the reservoirs is conserved.

for the case of a time reversal invariant driving, reads:

$$\begin{aligned}\dot{\bar{Q}}_\alpha^{\mathrm{NRH}} = &-\sum_{k>0}\int_0^{k\omega_d} d\omega\; k\omega_d\; p^{-k}_{\alpha,\alpha}(\omega)\;\left(N_\alpha(\omega)+\frac{1}{2}\right) - \\ &-\sum_{\beta\neq\alpha}\sum_{k>0}\int_0^{k\omega_d} d\omega\;(k\omega_d-\omega)\; p^{-k}_{\alpha,\beta}(\omega)\;\left(N_\beta(\omega)+\frac{1}{2}\right) - \\ &-\sum_{\beta\neq\alpha}\sum_{k>0}\int_0^{k\omega_d} d\omega\;\omega\; p^{-k}_{\beta,\alpha}(\omega)\;\left(N_\alpha(\omega)+\frac{1}{2}\right)\end{aligned} \tag{6.30}$$

The physical process that gives rise to $\dot{\bar{Q}}_\alpha^{\mathrm{NRH}}$ is rather different from the resonant ones discussed above. In the non resonant case a pair of excitations is created. One of them has energy ω while the other one has energy $k\omega_d - \omega$ (these values add up to the driving energy $k\omega_d$, notice that only $k > 0$ enters in the above expression). As opposed to the resonant case, in NRH, excitations are not transferred between modes but created in pairs from the driving (see Figure 6.2). The three terms in Eq, (6.30) respectively correspond to the following cases: i) both excitations are created in E_α; ii) mode ω is excited in E_α and mode $k\omega_d - \omega$ in E_β; iii) mode $k\omega_d - \omega$ is excited in E_α while mode ω is excited in E_β. In all cases E_α gains energy: in the first case the net gain is $k\omega_d$ while in the last two E_α gains, respectively, ω and $k\omega_d - \omega$. As $\dot{Q}_\alpha^{\mathrm{NRH}} < 0$, E_α heats up. Noticeably, *the non resonant heating term is the only one surviving when all reservoirs are at zero temperature (in that case both $\dot{\bar{Q}}_\alpha^{RP}$ and $\dot{\bar{Q}}_\alpha^{RH}$ vanish).*

6.6 Dynamical Casimir effect as a fundamental limit for cooling

At zero temperature, the creation of excitation pairs is a purely quantum phenomenon. In fact, it is analogous to the well known dynamical Casimir effect (DCE). This effect was first predicted in the decade of 1970 [88, 89] and it describes the creation of excitations in a quantum field with changing boundary conditions, even if the field starts in its ground state. The creation of photon pairs via the DCE was first observed in 2011, in experiments where the optical length of a superconducting microwave waveguide was

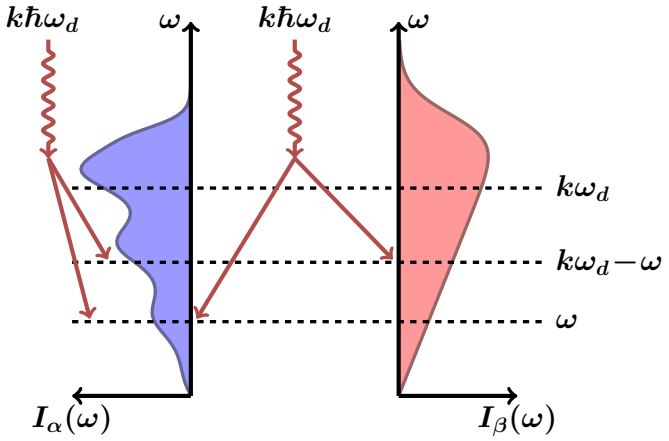

Figure 6.2: Resonant processes. Again, these can take place between modes of different reservoirs, or between modes of the same reservoir. Excitations are created in pairs.

changed in time by coupling it to a Josephson junction [90, 91]. In the context of cyclic thermal machines, the periodic driving of the parameters of the system is seen by the environmental modes as a periodic change in their boundary conditions, thus it is natural to expect creation of excitations in the same way as in the DCE. The same happens in thermodynamical cycles where the interaction between the system and environment is turned on and off in a periodic fashion (Carnot and Otto cycles, for example) [92].

Therefore, we see that at very low temperatures the creation of excitations pairs is a fundamental quantum process that dominate the heat currents. Surprisingly, this fact was not clear in previous discussions of heat transport and refrigeration at very low temperatures [58,69]. The reason is that the pairs creation mechanism is missed in the second order weak coupling approximation. This is because the NRH contribution scales, for weak coupling, as the fourth power of the interaction Hamiltonian H_{int} (or, equivalently, as the second power of the spectral density or the dissipation rate). This is explained in detail in Appendix C but can be understood in the following intuitive way. In the resonant processes excitations are transported between environmental modes *through the system* and this can be described as the following sequence: (i) an excitation is destroyed in a given environmental mode, (ii) it is transported through the system and (iii) an excitation is created in a different environmental mode. The system only couples to single environmental modes at steps (i) and (iii), with an strength proportional to the dissipation rate. In contrast, in the pair creation mechanism of the NRH contribution no excitation is transported through the system, but *the system is coupled simultaneously to two environmental modes*. Therefore, the rate of these processes is proportional to the square of the dissipation rate.

6.7 Time independent systems

In the absence of driving we have $\dot{\bar{Q}}_\alpha^{\text{NRH}} = \dot{\bar{Q}}_\alpha^{\text{RH}} = 0$ and only $\dot{\bar{Q}}_\alpha^{\text{RP}}$ survives. In this case, only $k = 0$ contributes to Eq. (6.28) and the transition probabilities are symmetric (i.e., $p^{(0)}_{\alpha,\beta}(\omega) = p^{(0)}_{\beta,\alpha}(\omega)$, since $A_0 = \hat{g}(i\omega)$ is a symmetric matrix). Therefore, we have:

$$\dot{\bar{Q}}_\alpha = \sum_{\beta\neq\alpha} \int_0^\infty d\omega\ \hbar\omega\ \frac{\pi}{2}\ \text{Tr}[I_\alpha(\omega)\hat{g}(i\omega)I_\beta(\omega)\hat{g}^\dagger(i\omega)]\ \ (N_\alpha(\omega) - N_\beta(\omega)) \tag{6.31}$$

Then, $\dot{Q}_\alpha \geq 0$ when E_α is the hottest reservoir (accordingly, $\dot{Q}_\alpha \leq 0$ for the coldest one). This is nothing but Kelvin's version of the second law (i.e., "heat flows from hot to cold" [57]). In the driven case, it is also possible to derive the most general form of the second law, that reads $\sum_\alpha \dot{\bar{Q}}_\alpha/T_\alpha \leq 0$. This is explained in the next chapter.

6.8 A further extension of the model

The model presented in Chapter 4 can be extended in a simple way: we may allow for the action of time dependent forces $F(t)$. In this case an extra term $H_F(t) = -F(t) \cdot X$ is added to the Hamiltonian of the system, and the motion equations are modified accordingly. Thus, the classical function $F(t)$ enters as a new source in the integro-differential equation of motion for the system operators. Then, the solution to this equation can still be expressed in terms of the same Green's function. It is straightforward to check that the covariance matrix is not affected by the forces $F(t)$. This is because the application of a time dependent force only changes the mean values of the phase space operators, but not their variances and correlations. Therefore, we note that time dependent forces are not an useful resource for the generation of quantum entanglement in this kind of linear systems.

In contrast, the driving of the system by forces do affect the heat currents. This is natural, since the forces can inject energy into the system, which is latter dissipated into the reservoirs. However, it is not clear a priori if the opposite process is possible: can the forces do negative work, in order to extract energy from the system and therefore cool a given reservoir? We will show next that the answer to this question is negative for the steady state and periodic forces. Thus, we conclude that time dependent forces are neither a useful resource for cooling under those conditions.

It is easy to see that in this case an additional term appears in the definition of the averaged local heat rates (Eq. (6.14)). The new expression is:

$$\dot{\bar{Q}}_\alpha = \mathrm{Tr}\left[P_\alpha \overline{V(t)\sigma^{xp}(t)} M^{-1}\right] + \mathrm{Tr}\left[P_\alpha \overline{(V(t)\langle X\rangle(t) - F(t))\ \langle P\rangle^T(t)} M^{-1}\right] \tag{6.32}$$

where the mean values $\langle X\rangle(t)$ and $\langle P\rangle(t)$ are:

$$\begin{aligned} \langle X\rangle(t) &= \int_0^t g(t,t')F(t')dt' = \sum_{j,k} A_j(k\omega_d)F_k e^{i(j+k)\omega_d t} \\ \langle P\rangle(t) &= M\int_0^t \frac{\partial}{\partial t} g(t,t')F(t')dt' = M\sum_{j,k} i(j+k)\omega_d A_j(k\omega_d)F_k e^{i(j+k)\omega_d t} \end{aligned} \tag{6.33}$$

The last equalities in Eq. (6.33) are valid for long times and when the force $F(t)$ is periodic in time with the same period of $V(t)$. We want to show now that the last term in Eq. (6.32) is always negative. For this, we find it convenient to use the motion equation $P_\alpha = V(t)X - F = -P_\alpha \dot{P} - C_\alpha q_\alpha$ (recall that P_α is the projector over the sites of the network in contact with the α reservoir). Then, we have:

$$\mathrm{Tr}\left[P_\alpha \overline{(V(t)\langle X\rangle(t) - F(t))\ \langle P\rangle^T(t)} M^{-1}\right] = -\mathrm{Tr}\left[P_\alpha \overline{\langle \dot{P}\rangle \langle P\rangle^T} M^{-1}\right] - \mathrm{Tr}\left[C_\alpha \overline{\langle q_\alpha\rangle \langle P\rangle^T} M^{-1}\right] \tag{6.34}$$

We see that the first term in the right hand side of the previous equation is the average over a period of the total derivative of a periodic function, and therefore it vanishes. To

evaluate the remaining term we need to to calculate the mean values of the environmental coordinates q_α. we obtain:

$$\langle q_\alpha(t)\rangle = -(m\Omega_\alpha)^{-1}\int_0^t \sin(\Omega_\alpha(t-t'))C_\alpha^T\left\langle X(t')\right\rangle dt' \tag{6.35}$$

which after some algebra can be transformed into:

$$C_\alpha\left\langle q_\alpha\right\rangle(t) = \frac{-1}{2i}\sum_{j,k} I_\alpha((j+k)\omega_d)A_j(k\omega_d)F_k e^{i(j+k)\omega_d t} \tag{6.36}$$

Finally, using Eqs. (6.33) and (6.36) it is easy to see that:

$$\mathrm{Tr}\left[C_\alpha\overline{\langle q_\alpha\rangle\langle P\rangle^T}M^{-1}\right] = \frac{1}{2}\,\mathrm{Tr}\left[\sum_p (p\omega_d)I_\alpha(p\omega_d)r_p r_p^\dagger\right] \geq 0 \tag{6.37}$$

where $r_p = \sum_{j,k/j+k=p} A_j(k\omega_d)F_k$. The previous expression is manifestly positive, since the spectral density $I_\alpha(\omega)$ is negative for negative frequencies. Thus, the additional term for the heat current in Eq. (6.32) is always negative, as we wanted to show. The interpretation of these results is straightforward. The application of time dependent forces only 'shakes' the network, displacing the mean values of the phase space operators. In the presence of dissipation, this shaking can only dissipate energy into the reservoirs, but not absorb it.

Definiciones de calor y trabajo

En este capítulo se dan y justifican las definiciones de calor y trabajo que son empleadas en el resto de la tesis. Estas definiciones son luego expresadas en términos de cantidades fácilmente calculables. Además, se discute una interpretación física de las expresiones obtenidas. A partir de esta interpretación se sigue que un mecanismo de creación de pares de excitaciones enteramente análogo al Efecto Casimir Dinámico (ECD) es una limitación fundamental para el enfriamiento en la familia de máquinas térmicas considerada. Por último, una extensión del modelo es discutida.

Chapter 7

Validity of the second law

Using the definitions for the heat currents obtained in the last chapter, we analyze if they are compatible with the Second Law of Thermodynamics. We first consider the Planck's version of this law. Secondly, we give a general and elegant proof of the Second Law based on the properties of the Von Neumman's entropy for quantum systems.

7.1 The Planck proposition

To investigate the validity of the second law in this context we first consider the Planck proposition: *"It is impossible to construct an engine which will work in a complete cycle, and produce no effect except the raising of a weight and cooling of a heat reservoir"*. Translated to our setting, the previous proposition means that if the temperatures of all the reservoirs are the same, i.e, if $T_\alpha = T_0$ for all α, then the work performed on the system must be positive, that is, $\dot{\bar{W}} \geq 0$. In other words, it must be impossible to extract work from a single thermal reservoir. Thus, considering Eqs. (6.12), (6.15) and (6.25), we should be able to show that:

$$\dot{\bar{W}} = \frac{\pi\hbar}{4}\int_0^\infty \sum_{k=-\infty}^{+\infty} (k\omega_d)\,\mathrm{Tr}\left[I(\omega+k\omega_d)A_k(\omega,\omega_d)I(\omega)A_k^\dagger(\omega,\omega_d)\right]\coth\left(\frac{\hbar\omega}{2k_bT_0}\right)d\omega \;\geq\; 0 \tag{7.1}$$

The main difficulty in assessing the previous inequality is that the integrand in the left hand side has no definite sign. It is thus convenient to write:

$$\dot{\bar{W}} = \frac{\pi\hbar}{4}\sum_{k>0}(k\omega_d)(I_k(\omega_d) - I_{-k}(\omega_d)) \tag{7.2}$$

where the functions $I_k^\pm(\omega_d)$ are defined as:

$$I_k(\omega_d) = \int_0^\infty \mathrm{Tr}\left[I(\omega+k\omega_d)A_k(\omega,\omega_d)I(\omega)A_k^\dagger(\omega,\omega_d)\right]\coth\left(\frac{\hbar\omega}{2k_bT_0}\right)d\omega \tag{7.3}$$

Now, if $I_k^r(\omega_d)$ is the function corresponding to the time reversed process $V(-t)$ it is possible to show that $I_k^r(\omega_d) \geq I_{-k}(\omega_d)$, which we do as follows:

$$I_{-k} = \int_0^\infty \ldots d\omega = \int_0^{k\omega_d} \ldots d\omega + \int_{k\omega_d}^\infty \ldots d\omega \tag{7.4}$$

The first integral in the right hand side is always negative, since $I(\omega - k\omega_d)$ is negative in the interval $(0, k\omega_d)$. The second integral is:

$$\begin{aligned}
&\int_{k\omega_d}^{\infty} \mathrm{Tr}\left[I(\omega - k\omega_d)A_{-k}(\omega,\omega_d)I(\omega)A^{\dagger}_{-k}(\omega,\omega_d)\right]\coth\left(\frac{\hbar\omega}{2k_bT_0}\right)d\omega = \\
&\int_{0}^{\infty} \mathrm{Tr}\left[I(\omega)A_{-k}(\omega + k\omega_d,\omega_d)I(\omega + k\omega_d)A^{\dagger}_{-k}(\omega + k\omega_d,\omega_d)\right]\coth\left(\frac{\hbar(\omega + k\omega_d)}{2k_bT_0}\right)d\omega \leq \\
&\int_{0}^{\infty} \mathrm{Tr}\left[I(\omega + k\omega_d)A^{r\,T}_{k}(\omega,\omega_d)I(\omega)A^{r\,*}_{k}(\omega,\omega_d)\right]\coth\left(\frac{\hbar\omega}{2k_bT_0}\right)d\omega = I^r_k
\end{aligned} \tag{7.5}$$

The first step was a simple change of variable and in the second step we used the identity of Eq. (5.23b) and the fact that $\coth(\omega)$ is a decreasing function of ω. Therefore, we proved that $I_{-k} \leq I^r_k$, as required. Also, $I^r_{-k} \leq I_k$. It follows that $\dot{\bar{W}} + \dot{\bar{W}}^r \geq 0$. Using Eq. (5.23a) it is easy to see that as a function of ω_d we have $\dot{\bar{W}}^r(\omega_d) = \dot{\bar{W}}(-\omega_d)$. In summary, we have shown that

$$\dot{\bar{W}}(\omega_d) + \dot{\bar{W}}(-\omega_d) \geq 0 \tag{7.6}$$

We now note the following three facts: (i) the function $\dot{\bar{W}}(\omega_d)$ is continuous, (ii) the only root of the function $\dot{\bar{W}}(\omega_d)$ is $\omega_d = 0$ and (iii) $\dot{\bar{W}}(\omega_d) = \dot{\bar{W}}(-\omega_d)$ for $\omega_d \to \pm\infty$ (this last fact is physically obvious but can be verified using the approximate solutions of the coefficients $A_k(\omega,\omega_d)$ for large ω_d). It follows that $\dot{\bar{W}}(\omega_d) \geq 0$ for all ω_d.

7.2 Irreversible entropy generation

A general derivation of the second law in our setting can be obtained without using the specific expression for the heat rates. Thus, we would like to show that in a complete cycle of the process the production of entropy is always positive, i.e,

$$\sum_{\alpha} \frac{-\dot{\bar{Q}}_{\alpha}}{T_{\alpha}} \geq 0 \tag{7.7}$$

This statement of the second law is equivalent to the Planck principle only in the adiabatic limit (only in that limit the heat transfer matrix in symmetric), as can be verified by direct calculation in the high temperature regime. Although it must be possible in principle to prove Eq. (7.7) from the general expression for the heat transfer matrix, that is not the more economic or elegant approach. To prove Eq. (7.7) we begin by considering the variations of the Von Neumann entropy of each reservoir and the system. We take $S(t)$ and $S_{\alpha}(t)$ as the entropies of the system and the α-th reservoir at time t. Also, $\Delta S(t) = S(t) - S(0)$. Using that the initial global state is a product state, that the global dynamics is unitary and the subadditivity of the Von Neumann entropy it is easy to see that:

$$\Delta S(t) + \sum_{\alpha} \Delta S_{\alpha}(t) \geq 0 \tag{7.8}$$

We now divide the previous equation by the total time and evaluate in $t = k\tau$. Since the asymptotic state of the system is τ-periodic, its entropy is also a τ-periodic, and since it is continuous, it is also bounded. Therefore $\lim_{k\to\infty} \Delta S(k\tau)/(k\tau) = 0$. On the other hand $\Delta S_{\alpha}(k\tau)/(k\tau)$ converges to $\Delta S^c_{\alpha}/\tau$ for $k \to \infty$, where ΔS^c_{α} is the change in entropy of the α-th reservoir per cycle in the asymptotic state. In this way, we obtain the following

inequality for the variations per cycle of the entropy of the reservoirs in the asymptotic state:

$$\sum_{\alpha} \Delta S_{\alpha}^{c} \geq 0 \tag{7.9}$$

We now take advantage of the fact that the initial state of the α-th reservoir is thermal at temperature T_{α}, and therefore it is the only minimum of the free energy function $F_{\alpha}(\rho) = \mathrm{Tr}(\rho H_{E,\alpha}) - k_b T_{\alpha} S(\rho)$. As a consequence:

$$0 \leq \Delta F_{\alpha}(t) = \Delta E_{\alpha}(t) - k_b T_{\alpha} \Delta S_{\alpha}(t) \tag{7.10}$$

As before, dividing the previous equation by t, evaluating in $t = k\tau$, and taking the limit $k \to \infty$, we obtain:

$$\frac{\Delta E_{\alpha}^{c}}{k_b T_{\alpha}} \geq \Delta S_{\alpha}^{c} \tag{7.11}$$

where ΔE_{α}^{c} is the variation per cycle of the energy of the α-th reservoir in the asymptotic state. It is not immediately obvious how this variation is related to the previously defined heat rates (since in our model the interaction terms are not energy conserving, i.e, $[H_S + H_{E,\alpha}, H_{int,\alpha}] \neq 0$). However, in section 6.3 we show that in the asymptotic state $\Delta E_{\alpha}^{c} = -\tau \dot{\bar{Q}}_{\alpha}$, as expected. Inserting this last identity in Eq. (7.11), summing over all reservoirs, and using Eq. (7.9) we obtain Eq. (7.7).

Validez de la segunda ley

En este capítulo se analiza si las definiciones para las corrientes de calor obtenidas en el capítulo anterior son compatibles con la segunda ley de la termodinámica. En primer lugar se considera la versión de Planck de esta ley. Luego se da una prueba elegante y general de la segunda ley basada en las propiedades de la entropía de Von Neumman para sistemas cuánticos.

Chapter 8

Fundamental limits for cooling processes

In this chapter we analyze the fundamental limits for cooling of the family of thermal machines defined in Chapter 4. The motivation is to study the emergence of the the dynamical version of the Third Law of thermodynamics, or unattainability principle. This principle, first formulated by Nernst [93], states that it is impossible to cool down a system to zero temperature in finite time, or in finite number of steps. This principle has been challenged by recent results on some models of quantum refrigerators. As explained in the following, these results are flawed since they employ the second order weak coupling approximation in the low temperature regime, where the heat currents are dominated by processes that are missed by that approximation. We first discuss the general processes that limit any cooling strategy and then we show how these processes play a role in two relevant examples: (i) the laser cooling of trapped ions, and (ii) an adaptative cooling strategy proposed in [69] that present an apparent challenge to the unattainability principle.

We have shown in the previous chapters that the heat rate entering or leaving reservoir E_α can be written as:

$$\dot{\bar{Q}}_\alpha = \dot{\bar{Q}}_\alpha^{\mathrm{RP}} + \dot{\bar{Q}}_\alpha^{\mathrm{RH}} + \dot{\bar{Q}}_\alpha^{\mathrm{NRH}} \tag{8.1}$$

Therefore, since both $\dot{\bar{Q}}_\alpha^{\mathrm{RH}} \leq 0$ and $\dot{\bar{Q}}_\alpha^{\mathrm{NRH}} \leq 0$, the only way to pump energy out of E_α (and therefore cool it) is to design a process such that $\dot{Q}_\alpha^{\mathrm{RP}} > 0$. In fact, to pump more heat out of E_α than the one flowing into it, requires us to impose spatial (or temporal) asymmetries to the driving or to the coupling with the reservoirs [58, 94, 95]. However, to prove the validity of the third law it is not necessary to go into the details of cooling processes. For this, one should simply notice that both resonant terms vanish at zero temperature while the non resonant heating still survives. This alone is enough to establish the validity of Nernst unattainability principle: heating dominates at sufficiently low temperatures. Moreover, this also implies that for any cooling process there is a minimum achievable temperature which can be estimated as the one for which the cooling term in $\dot{\bar{Q}}_\alpha^{\mathrm{RP}}$ becomes comparable to the $\dot{\bar{Q}}_\alpha^{\mathrm{NRH}}$. The minimal temperature is not universal and depends on the cooling strategy. We first analyze the case of laser cooling of trapped ions, introduced in Chapter 3, and recover well known results. The analysis of laser cooling in terms of our family of thermal machines will also lead us to an interesting prediction about the power spectrum of the radiation emitted by the ions. Then we estimate the minimal temperature that can be achieved by the cooling strategy proposed in [69] to violate the Nernst unattainability principle.

8.1 Laser cooling

We can consider the laser cooling of trapped ions as a thermal cycle in which a system or working medium (the internal electronic state) is driven in time (by the laser light) while it is simultaneously coupled with two thermal reservoirs. One of these reservoirs would be the motional mode of the ion in the trap, which we want cool, while the second one is formed by the modes of the electromagnetic field, to which the energy is dumped. In principle, the developed formalism does not offer a faithful model of the actual situation, due to two main reasons. In first place, the system under consideration is a two level system and therefore the linearity assumption, which is crucial in our treatment, is lost. Secondly, in the usual version of 'resolved-sideband' cooling the laser field actually drives the interaction between the internal electronic state and the motional mode. Thus, if the motional mode is going to be considered as a thermal reservoir we should in principle take into account the periodic modulation of its interaction with the central system, and that feature is not included in our family of thermal machines. However, none of these characteristics (the non-linearity and the modulation of the system-reservoir interaction) is essential to the cooling mechanism. Cooling could also be achieved if the internal state corresponded to a harmonic vibrational mode, with infinite equispaced levels. Also, instead of driving the interaction with the reservoir to be cooled (the motional mode), it is enough to drive the energy difference between the internal levels, as we will see.

With the previous considerations in mind, we develop the following analogy to laser cooling. The internal state of the ion is represented by a harmonic mode of frequency ω_e and mass m_e. The internal mode is driven by periodically modulating its frequency around ω_e, with frequency ω_d. Thus, the Hamiltonian of the system is:

$$H_S(t) = \frac{p^2}{2m_e} + \frac{m_e\omega^2(t)}{2}x^2 \tag{8.2}$$

with $\omega^2(t) = \omega_e^2 + \delta\omega^2\cos(\omega_d t)$. The internal mode is simultaneously connected to two reservoirs. One of the reservoirs has a single mode, the motional mode of the ion at frequency ω_m, and therefore its spectral density is $I_A(\omega) = C^2/(m\omega_m)\ \delta(\omega-\omega_m)$, where C is a coupling constant. The other reservoir is the electromagnetic field with spectral density $I_B(\omega)$. The permanent coupling of the internal mode to the continuous environment B will induce dissipation, that is characterized by the dissipation rate Γ. This parameter enters in two places: in the spectral density, which scales as $I_B(\omega) \propto \Gamma$, and in the Laplace's transform of the Green's function, that reads:

$$\hat{g}(i\omega) = \frac{m_e^{-1}}{\omega_e^2 - (\omega - i\Gamma)^2} \tag{8.3}$$

We will consider that the driving is weak (i.e, that $\delta\omega \ll \omega_e$) in order to use the expressions of Eqs. (5.22b) for the coefficients $A_k(\omega)$. We are interested in the heat current extracted from the reservoir A. The form of the spectral density $I_A(\omega)$ makes the evaluation of the frequency integrals in Eqs. (6.28), (6.29) and (6.30) trivial. For $\omega_d > \omega_m$ (that is the case for laser cooling), and when the reservoir B is at zero temperature (which is the most favorable case and an excellent approximation for optical frequencies) the only relevant processes contributing to the heat current of reservoir A are shown in Figure 8.1. Thus, the resonant pumping of energy out of A (blue arrow in Figure 8.1) is:

$$\dot{\bar{Q}}^{\mathrm{RP}} = \hbar\omega_m\frac{\pi}{2}\frac{C^2}{m\omega_m}I_B(\omega_d+\omega_m)|A_1(\omega_m)|^2N_A(\omega_m) \tag{8.4}$$

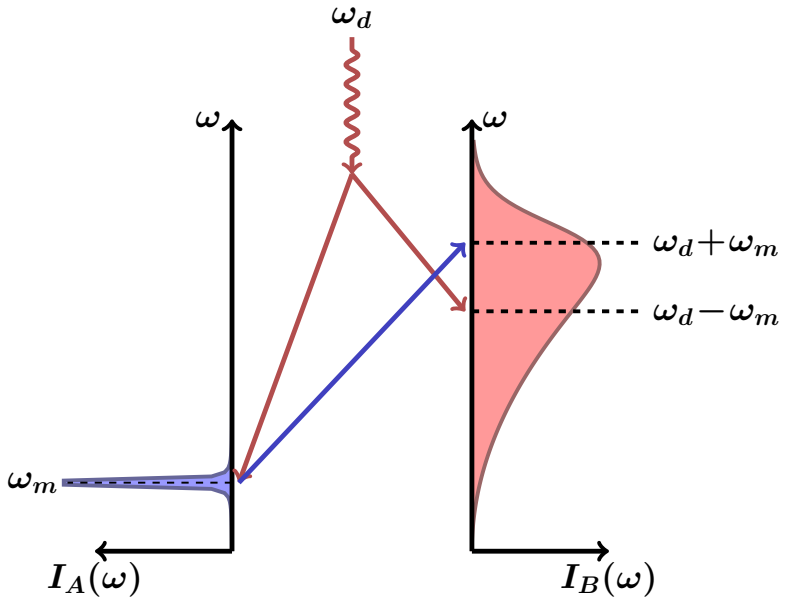

Figure 8.1: Relevant processes contributing to the heat current of reservoir A when $\omega_d > \omega_m$ and $T_B \simeq 0$.

while the non-resonant heating is:

$$\dot{\bar{Q}}^{\text{NRH}} = -\hbar\omega_m \frac{\pi}{2}\frac{C^2}{m\omega_m} I_B(\omega_d - \omega_m)|A_{-1}(\omega_m)|^2(N_A(\omega_m)+1) \tag{8.5}$$

Thus, the motional mode is cooled whenever $|\dot{\bar{Q}}^{\text{RP}}/\dot{\bar{Q}}^{\text{NRH}}| > 1$, which is equivalent to:

$$\frac{\bar{n}}{\bar{n}+1} > \frac{|\hat{g}(i(\omega_m-\omega_d))|^2}{|\hat{g}(i(\omega_m+\omega_d))|^2}\frac{I_B(\omega_d-\omega_m)}{I_B(\omega_d+\omega_m)} \tag{8.6}$$

where $\bar{n} = N_A(\omega_d)$ and it was used that $A_k(\omega) = -\hat{g}(i(\omega+k\omega_d))V_k\hat{g}(i\omega)$ (for $k \neq 0$ and weak driving). For simplicity we assume that $I_B(\omega_d+\omega_m) \simeq I_B(\omega_d-\omega_m)$, which is almost exact in optical settings since $\omega_m \lll \omega_d$. Then, the minimum possible value of $\bar{n}$ (such that the previous condition is saturated for fixed parameters) is given by:

$$\bar{n}_{\text{min}} = \frac{\left[\omega_e^2 - (\omega_m+\omega_d)^2\right]^2 + 2\Gamma^2(\omega_e^2+(\omega_m+\omega_d)^2)+\Gamma^4}{8\omega_d\omega_m(\omega_e^2-\omega_d^2-\omega_m^2-\Gamma^2)} \tag{8.7}$$

Of course, to optimize the cooling strategy we should choose the value of ω_d, the driving frequency, in order to minimize $\bar{n}_{\text{min}}$. There are two relevant regimes of operation, already discussed in Chapter 3. In the 'resolved-sideband' regime where $\omega_m \gg \Gamma$ the optimal driving frequency is $\omega_d = \omega_e - \omega_m$, exactly on resonance with the red sideband. In this case $\bar{n}_{\text{min}} \simeq (1/4)(\Gamma/\omega_m)^2$. In the opposite regime where $\Gamma \gg \omega_m$ the optimal driving frequency is $\omega_d = \omega_e - \Gamma/2$ and $\bar{n}_{\text{min}} \simeq (5/8)(\Gamma/\omega_m)$. Apart from constant prefactors, these results are equivalent to the minimum occupation numbers obtained for the usual Sideband and Doppler cooling schemes.

8.1.1 Power spectrum of the radiation emitted into the EM field

In the usual discussions and explanations of laser cooling the heating mechanisms preventing the perfect preparation of the motional ground state are understood as inelastic scattering events involving transitions to virtual electronic levels followed by

spontaneous emissions. When one of these processes take place, the overall effect is the creation of a motional excitation and the emission of a photon with the frequency reduced by ω_m with respect to the incident radiation. From our point of view, this process can also be understood as a particular case of the pairs creation mechanism, or dynamical Casimir effect (DCE), which is the fundamental limitation for cooling in our family of linear quantum refrigerators. Thus, the motional excitation and the photon emitted at frequency $\omega_d - \omega_m$ can be considered as a Casimir pair. However, there is another aspect of the cooling process in which the DCE plays a role, as can be seen by analyzing the heat current entering the reservoir B, which represent the electromagnetic field. In addition to the pair creation in Figure 8.1, which produces photons of frequency $\omega_d - \omega_m$, pairs of photons can be created directly in the EM field, as shown in Figure 8.2. The power

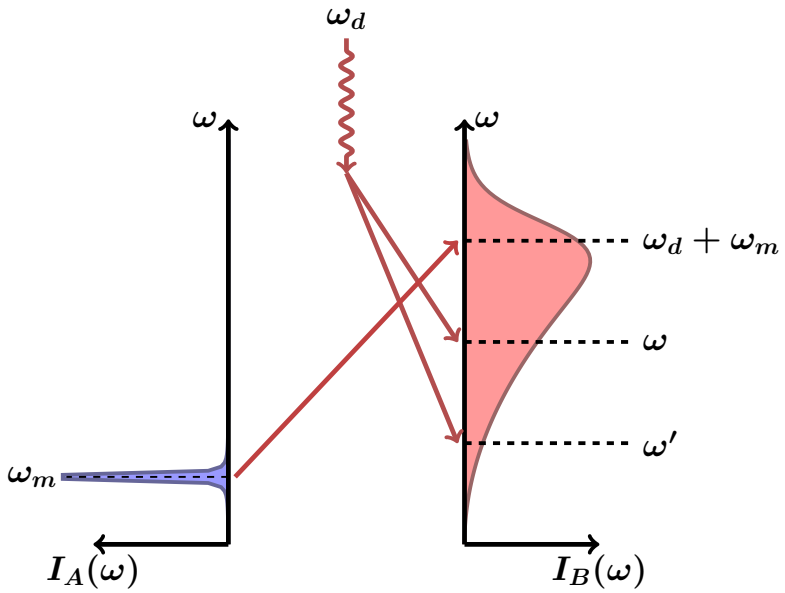

Figure 8.2: Relevant processes contributing to the heat current of reservoir B when $\omega_d > \omega_m$ and $T_B \simeq 0$. Pairs of photons are created at frequencies ω and ω' such that $\omega + \omega' = \omega_d$.

spectrum of the emission of energy into the EM field can be read from the integrand of Eqs. (6.28), (6.29) and (6.30). It has three contributions. The first one comes from the resonant pumping (RP) of energy from reservoir A to B, which creates photons at frequency $\omega_d + \omega_m$. Thus, if $f_{\text{RP}}(\omega)$ is the number of photons per unit of time created at frequency ω by this process, we have:

$$f_{\text{RP}}(\omega) = \frac{\pi}{2}\frac{C^2}{m\omega_m} I_B(\omega_d + \omega_m)|A_1(\omega_m)|^2 N_A(\omega_m)\delta(\omega - \omega_d - \omega_m) \tag{8.8}$$

In the same way, the number of photons per unit of time created at frequency ω by the pair creation of Figure 8.1 is:

$$f_{\text{NRH}}(\omega) = \frac{\pi}{2}\frac{C^2}{m\omega_m} I_B(\omega_d - \omega_m)|A_{-1}(\omega_m)|^2 \left[N_A(\omega_m) + 1\right] \delta(\omega_d - \omega - \omega_m) \tag{8.9}$$

Finally, for the pair creation of Figure 8.2 we have:

$$f'_{\text{NRH}}(\omega) = \frac{\pi}{4} I_B(\omega) I_B(\omega_d - \omega)|A_{-1}(\omega)|^2 \tag{8.10}$$

This last contribution, in contrast with the other two, is not spectrally narrow. These created photons are symmetrically distributed with respect to $\omega_d/2$. The total power spectrum if plotted in Figure 8.3 for the parameters $\omega_m/\omega_e = .1$, $\Gamma/\omega_m = 10^{-2}$, and $\omega_d = \omega_e - \omega_m$ (since this is optimal for $\Gamma/\omega_m \ll 1$). The temperature of the reservoir A is the minimum temperature, for which the heights of the peaks at $\omega_d \pm \omega_m$ is the same. This is only an illustrative example an does not correspond to a physical situation. Also, for plotting, the Dirac delta in Eqs. (8.8) and (8.9) was replaced by a Lorentzian function $(\Gamma'/2)^2/(\omega^2+(\Gamma'/2)^2)$ with $\Gamma' = \Gamma$. We see the two expected peaks at frequencies $\omega_d \pm \omega_m$,

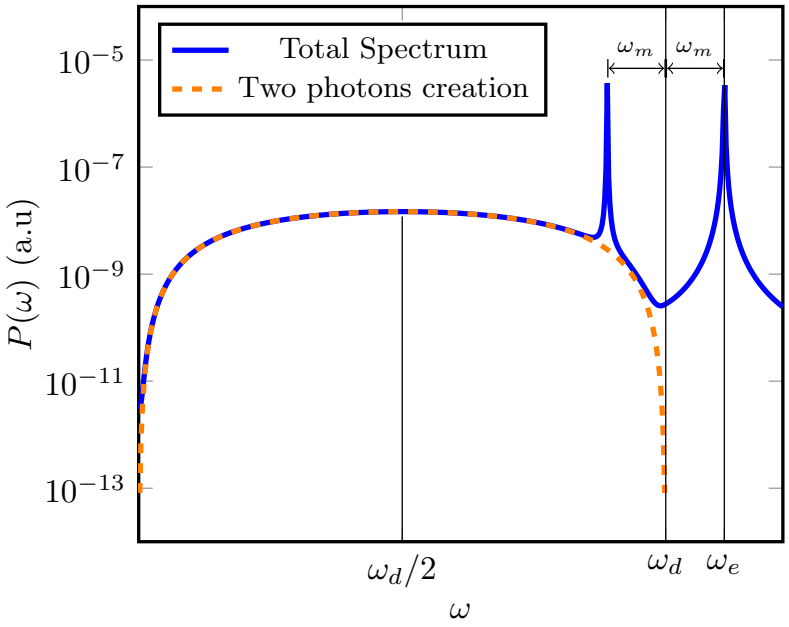

Figure 8.3: Number of photons per unit of time emitted at a particular frequency into the EM field. For this figure, it was considered that $I_B(\omega) \propto \omega^3$.

which result from the interaction of the system with the motional mode, but also a broad spectrum for $\omega < \omega_d$, which correspond to the creation of pairs of photons. Of course, the two peaks could not be resolved if $\Gamma \gg \omega_m$.

The DCE was first experimentally observed in 2011, in experiments using superconducting microwave cavities. So far, it was never observed at optical frequencies. Therefore, it is interesting the question of whether the photon pairs created during the laser cooling of ions could be observed. To answer this question a careful analysis of a more realistic model is needed. The generalization of the results obtained by Mollow in [96] to second order in the decay rate would be a first step. However, it is possible to perform some preliminar estimations based on the model of laser cooling presented here. For this, we will compute the following quantity: the ratio R between the photons emitted in a frequency band of width $\Delta\omega$ centered at $\omega_d/2$ (per unit of time), and the total number of photons emitted in the peaks around ω_d (the scattered photons). From Eqs. (8.9) and (8.10), we obtain:

$$R = \frac{1}{2}\frac{I_B^2(\omega_d/2)}{I_B(\omega_d-\omega_m)}\frac{m\omega_m}{C^2}\frac{|A_{-1}(\omega_d/2)|^2}{|A_{-1}(\omega_m)|}\frac{\Delta\omega}{N_A(\omega_m)+1} \tag{8.11}$$

At this point it is necessary to have some information about the spectral density of the reservoir B. For the electromagnetic field in open space the spectral density goes like ω^3,

and it can be seen that for a fixed dissipation rate Γ it should be $I_B(\omega) = \frac{6}{\pi}(\frac{\omega}{\omega_e})^3 m_e \omega_e \Gamma$. Also, by comparison with the interaction Hamiltonian between the internal levels and the motion in the Lamb-Dicke regime, presented in Chapter 3, it can be seen that the coupling constant C in our model should be such that $C^2/(m\omega_m) = \Omega^2 \eta^2 m_e \omega_e$, where Ω is the Rabi frequency and η the Lamb-Dicke parameter. Using this expressions, the fact that for trapped ions $\omega_e \gg \omega_m, \gamma$, and the approximations of $A_{\pm 1}(\omega)$ for weak driving, it is possible to show that:

$$R \simeq \frac{3}{2} \frac{\Gamma \omega_e}{\Omega^2 \eta^2} \left(\frac{\omega_t}{\omega_e} \right)^2 \frac{\delta}{N_A(\omega_m) + 1} \tag{8.12}$$

where $\delta = \Delta\omega/(\omega_d/2)$ is the relative width of the selected band. We see that R grows with Γ, which is natural since Γ is a measure of the coupling of the atom to the EM field. We take the following parameters compatible with the experiments performed by the group of Rainer Blatt at Innsbruck [97]:

- $\omega_t/(2\pi) \simeq 5$ Mhz
- $\omega_e/(2\pi) \simeq 755$ Thz and $\Gamma/(2\pi) \simeq 20$ Mhz (for the 397 nm $S_{1/2} \to P_{1/2}$ transition of a calcium atom)
- $\Omega/(2\pi) \simeq 1$ Mhz
- $\eta \simeq 0.078$

For these parameters we found that the value of R for the steady state of Doppler cooling is:

$$R \simeq (5 \times 10^{-5})\, \delta, \tag{8.13}$$

and, using the Eq. (3.9), we can estimate the number of scattered photons per unit time around $\dot{N} \simeq 7500$ hz. Thus, for $\delta = 1/100$ we expect only $R\dot{N} \simeq 4 \times 10^{-3}$ photon pairs per second at $\omega_d/2$. This quantity is exceedingly small, which explains why this effect, if existent, was not yet observed. A possibility to improve this rate in order to observe the effect is to simultaneously cool many ions. If one thousand ions are simultaneously trapped and cooled, the expected rate of created pairs is similar to the dark count rates of the best single photon detectors available today, so the signal might be detected for long integration times. Of course, these are only preliminary estimations, but they suggest that the analysis of a more realistic model could yield interesting results.

8.2 An adaptative cooling strategy

In this section we will analyze a strategy proposed in [69] that was claimed to challenge the Third Law of thermodynamics. The proposed strategy involves a two-level system that is simultaneously connected to two reservoirs with different spectral densities. We will consider a similar situation in which the two level system is replaced by a harmonic oscillator. We will see that if the contribution of the pair creation mechanism to the heat currents is not taken into account, our results are completely equivalent to those obtained in [69], and under certain conditions allow for the cooling of one reservoir to zero temperature in finite time, thus violating the dynamical version of the Third Law of thermodynamics. Of course, if the pair creation mechanism is considered, then we see that it is not possible to reach zero temperature even for infinite time. We conclude then that the problem of the results presented in [69] is that they are based on a master

equation that is only valid to the second order in the interaction between the system and the environments, or equivalently, to first order in the dissipation rate.

We will compute the heat rates using the following simplifying assumptions: a) We assume that the driving is weak (i.e. if $|V_k|/|V_0| \ll 1$). Then, using perturbation theory we find that $A_k(\omega) = -\hat{g}(i(\omega + k\omega_d))V_k\hat{g}(i\omega)$, for $k \neq 0$. b) We assume that the coupling with the environments is also weak. Then, $\hat{g}(s)$ (the Green function of the undriven network) can be expressed as a sum over the normal modes of the isolated network, whose eigenfrequencies we denote as Ω_a. Using this, the frequency integrals in Eqs. (6.28) and (6.29) can be performed since the integrand is strongly peaked around the eigenfrequencies and their sidebands $\Omega_a \pm k\omega_d$ (the peaks in $p^k_{\alpha,\beta}(\omega)$ arise because of their dependence on $A_k(\omega)$). In this way, as shown in SM IV the resonant heat rates can be expressed as a sum over all normal modes and sidebands. Finally, in the low temperature limit, this sum is dominated by the term with the lowest frequency (Ω_0) because the Planck distribution enforces a natural cutoff. c) To further simplify the analysis we will consider all reservoirs at the same temperature T_0 (the most favorable condition for cooling), and use the harmonic driving $V(t) = V_0 + 2V_1\cos(\omega_d t)$ (for which only $k = \pm 1$ appear in the weak driving limit). In this case we obtain

$$\begin{aligned}\dot{\bar{Q}}^{\mathrm{RP}}_\alpha =& \frac{e^{-\frac{\Omega_0-\omega_d}{T_0}}|V_1^0|^2(\pi^2/8)}{\Omega_0^2(\Omega_0^2-(\Omega_0-\omega_d)^2)^2}\sum_{\beta\neq\alpha}\frac{I^0_\beta(\Omega_0)}{\Gamma_0}I^0_\alpha(\Omega_0-\omega_d)\\ &\times\left\{(\Omega_0-\omega_d)-\Omega_0\frac{I^0_\alpha(\Omega_0)I^0_\beta(\Omega_0-\omega_d)}{I^0_\beta(\Omega_0)I^0_\alpha(\Omega_0-\omega_d)}\right\}\end{aligned} \tag{8.14}$$

where Γ_0 is the decay width of the mode Ω_0 (see below) and M^0 denotes the matrix element of M in the normal mode with frequency Ω_0. The above equation is revealing: when the spectral densities are identical the heat rate is negative and E_α absorbs energy. However, if the condition $I^0_\alpha(\Omega_0) \ll I^0_\beta(\Omega_0)$ is satisfied $\dot{\bar{Q}}^{\mathrm{RP}}_\alpha > 0$ and the reservoir loses energy. This cooling condition simply states that the cooling process (i.e., extracting energy $\Omega_0 - \omega_d$ from E_α and dumping it in the mode Ω_0 of E_β) has a higher rate than the heating process (taking energy $\Omega_0 - \omega_d$ from E_β and dumpling it in mode Ω_0 in E_α). The reduction in the heating rate arises because the density of final states is small. As explained in SM IV, the same condition implies that $\dot{\bar{Q}}^{\mathrm{RP}}_\alpha \gg \dot{\bar{Q}}^{\mathrm{RH}}_\alpha$.

Even if the cooling condition is satisfied, the heat rate rapidly decreases with the temperature. This is because the thermal factor appearing Eq. (8.14) decreases with temperature faster than any power law. However, there is an interesting strategy that we could use to maximize the heat rate. For this, as suggested in [69], we can slowly adjust the driving frequency ω_d in such a way that $\Omega_0 - \omega_d = T_\alpha$. Using this adaptive method, for $T_\alpha \ll \Omega_0$, the heat rate is

$$\dot{\bar{Q}}^{\mathrm{RP}}_\alpha = \frac{\pi^2}{8e}\frac{|V_1^0|^2}{\Omega_0^6}T_0 I^0_\alpha(T_0)\sum_{\beta\neq\alpha}\frac{I^0_\beta(\Omega_0)}{\Gamma_0} \tag{8.15}$$

It is clear that the ratio $\sum_\beta I_\beta(\Omega_0)/\Gamma_0$ is of zero-th order in the coupling strength between the system and the environment. Therefore, the above identity shows that $\dot{\bar{Q}}^{\mathrm{RP}}_\alpha$ is of first order in the coupling strength. In contrast, it can be seen from Eq. (6.30) that $\dot{\bar{Q}}^{\mathrm{NRH}}_\alpha$ is of second order in the coupling strength for $\omega_d < \Omega_0$ (since in that case the integration domain does not include any resonance peak). We will use these results to estimate the

minimal temperature that can be achieved by this cooling protocol. For this, we must study cooling as a dynamical process.

Only a finite reservoir can be cooled. Thus, we assume that the E_α has a finite heat capacity C_v. As discussed in [69], C_v depends on the dimensionality (d) of the reservoir and scales with temperature as $C_v \propto T_\alpha^d$. If the rate at which energy flows away from E_α is sufficiently small, one can think that the environment has a time dependent temperature $T_\alpha(t)$ that satisfies the equation $\dot{T}_\alpha = -\dot{\bar{Q}}_\alpha/C_v$. To solve this equation we need an expression for the heat rate. We could use Eq. (8.15) provided that the rate of change of T_α is smaller than the driving frequency (since in that case we can instantaneously satisfy the adaptive condition $\omega_d = \Omega_0 - T_\alpha$). In this way, we obtain that $T_\alpha(t)$ satisfies

$$\frac{dT_\alpha}{dt} = -\frac{1}{C_v}\dot{Q}_\alpha \;\propto\; -\gamma_0 \eta\, T_\alpha^{1+\lambda_\alpha - d} \tag{8.16}$$

where we used that for low frequencies the spectral density $I_\alpha^0(\omega) \propto \gamma_0 \omega^{\lambda_\alpha}$ (where γ_0 is a relaxation rate scaling quadratically with the coupling constants between the system and the environment while the exponent λ_α characterizes the environment, being $\lambda_\alpha = 1$ the one corresponding to a Ohmic reservoir). Above, η is a constant depending on Ω_0 and V_1. The solutions of this equation approach $T_\alpha = 0$ in finite time when $1 + \lambda_\alpha - d < 1$, which leads us to the surprising conclusion that the unattainability principle could be violated. However, this argument, presented in [69], is not correct, because the above equation for T_α stops being valid at sufficiently low temperatures. In that case, $\dot{Q}_\alpha^{\text{NRH}}$, which was not taken into account so far, becomes dominant.

The non resonant heating cannot be neglected in spite of the fact that (for $\omega_d \leq \Omega_0$) it is proportional to γ_0^2. This scaling with γ_0 makes this term invisible to any treatment based on the weak coupling limit (such as the master equation used in [69], which is valid to first order in γ_0). On the contrary, the weak coupling limit captures the resonant term given in Eq. (8.15), which is first order in γ_0 (in fact, such expression is equivalent to the heat rate used in [69]).

Our analysis, which is non perturbative, shows that the non resonant term given in Eq. (6.30) will end up stopping any cooling. Moreover, it enables us to estimate the minimum achievable temperature by estimating when resonant and non resonant contributions become comparable. $\dot{\bar{Q}}_\alpha^{\text{NRH}} \propto \gamma_0^2$ (and is roughly independent of T_α for sufficiently low temperatures) and Eq. (8.15) shows that the cooling term scales as $\dot{\bar{Q}}_\alpha^{\text{RP}} \propto \gamma_0 T_\alpha^{1+\lambda_\alpha}$. Therefore, both terms become comparable for temperatures scaling as $T_\alpha \propto \gamma_0^{1/(1+\lambda_\alpha)}$. In Figure 8.4 we see that this naive scaling argument is confirmed by a detailed numerical evaluation of both resonant and non resonant heat rates (the minimal temperature is estimated for various reservoirs characterized by different values of λ_α and plotted as a function of γ_0).

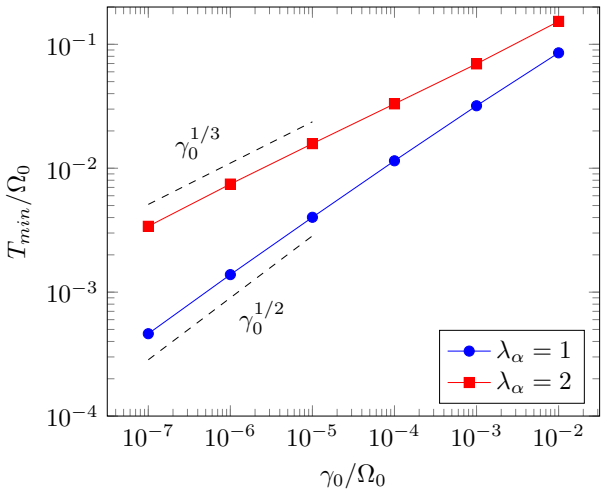

Figure 8.4: Minimum temperature T_{min} as a function of the coupling strength γ_0. T_{min} is numerically obtained as the lowest temperature for which $\dot{Q}_\alpha^{RP} > |\dot{Q}_\alpha^{NRH}|$. Results are shown for the adaptative cooling strategy considered in [69]. The system consists of a single harmonic oscillator of frequency Ω_0 in contact with two reservoirs whose spectral densities satisfy the cooling condition $I_\alpha(\Omega_0) \ll I_\beta(\Omega_0)$. Heat rates are obtained through an exact numerical evaluation (see details in SM IV).

Límites fundamentales para procesos de enfriamiento

En este capítulo se analizan los límites fundamentales para el enfriamiento de la familia de máquinas térmicas definidas en el capítulo 4. La motivación es estudiar el origen de la versión dinámica de la tercera ley de la termodinámica. Esta ley, formulada originalmente por Nernst [93], establece que es imposible enfriar un sistema a temperatura cero en un tiempo finito, o en una cantidad finita de pasos. Resultados recientes en algunos modelos de refrigeradores cuánticos desafían esta ley. Como se explica en este capítulo, estos resultados son incorrectos ya que están basados en la aproximación de acoplamiento débil, la cuál no captura los procesos responsables del calentamiento a bajas temperaturas. En primer lugar se discuten los procesos generales que limitan cualquier esquema de enfriamiento y luego se muestra cuál es el papel que juegan estos procesos en dos ejemplos relevantes: (i) el enfriamiento láser de iones atrapados, y (ii) una estrategia adaptativa de enfriamiento que fue propuesta en [69] y presenta un aparente desafío a la tercera ley.

Part IV

Experimental proposals

Chapter 9

Heat transport through ion crystals

In this chapter we study the thermodynamical properties of crystals of trapped ions which are laser cooled to two different temperatures in two separate regions. We show that these properties strongly depend on the structure of the ion crystal. As explained in chapter 3, such structure can be changed by varying the trap parameters and undergoes a series of phase transitions from linear to zig-zag or helicoidal configurations. Thus, we show that these systems are ideal candidates to observe and control the transition from anomalous to normal heat transport. We find that all structures behave as 'heat superconductors', with a thermal conductivity increasing linearly with system size and a vanishing thermal gradient inside the system. However, zig-zag and helicoidal crystals turn out to be hyper sensitive to disorder having a linear temperature profile and a length independent conductivity. Interestingly, disordered 2D ion crystals are heat insulators. Sensitivity to disorder is much smaller in the 1D case.

9.1 Anomalous transport and the failure of the Fourier's Law

The Fourier's Law for heat transport is a two centuries old phenomenological theory describing the flux of heat through a material [98]. It relates in a linear way the flux with the temperature gradient, adopting the following differential form:

$$\bar{j} = -\kappa \nabla T \tag{9.1}$$

where $\bar{j}$ the heat current per unit of time and area, and κ is the thermal conductivity of the material, independent of the system size. The Fourier's law is identical to the Ohm's Law for electric conduction. It has been highly successful in describing heat conduction in macroscopic systems. Two general conclusions can be derived from it: if a system of length L is connected to two thermal reservoirs at different temperatures, the heat current should be proportional to the temperature difference ΔT, and inversely proportional to the system length L. Also, for homogeneous systems, the inner temperature profile should be a linear interpolation between the fixed temperatures of the reservoirs (in the steady state). However, in a seminal work by Rieder, Lebowitz and Lieb [99], where a one-dimensional microscopic model of heat conduction was considered, the authors found that: 1) the heat current is independent of the system length[1] for fixed ΔT, and 2) the thermal gradient vanish inside the system. This was called

[1] This behavior, in terms of the Fourier's Law, amounts to a thermal conductivity increasing linearly with length.

'anomalous' or 'ballistic' (in contrast to 'diffusive') heat transport. Since then, many researchers tried to understand under which conditions the Fourier's Law emerge from a given microscopic substrate. The original model of Rieder, Lebowitz and Lieb was linear, one-dimensional and homogeneous, so initial efforts were devoted to investigate the effects of non-linearity, dimensionality and disorder. Some modern approaches to this problem can be found in [100–104]. In the following we investigate theoretically the possibility of experimentally studying the emergence of Fourier's Law and the transition between diffusive and ballistic transport with trapped ions.

9.2 The model

We consider N ions in a Paul trap with harmonic trapping potentials both in the axial and transverse directions. We have seen in chapter 3 that the interplay between Coulomb repulsion and the trapping potentials forms crystals with variable geometries. For strong transverse confinement, the crystal is linear (1D). As the transverse potential is relaxed or the number of ions is increased the crystal undergoes a series of phase transitions. First, there is a second order phase transition from linear (1D) to a zig-zag (2D) configuration which is followed by a transition to a helicoid (3D) and a variety of other shapes. Fully taking into account trapping potentials and Coulomb repulsion we use an evolutionary algorithm to obtain the equilibrium state of the crystal (in a regular desktop computer we can find the equilibrium state of crystals with hundreds of ions, see Appendix A). In Figure 9.1 we show three different structures. Zig-zag and helicoidal structures develop at the center of the crystal and are characterized by two order parameters: the mean distance to the axis and the average azimuthal angle between ions. As shown in Figure 9.1-b, structures with similar order parameters are obtained by appropriately scaling the trap aspect ratio (i.e., the ratio between transverse and longitudinal trapping frequencies: $\alpha = \omega_t/\omega_z$) and the number of ions N (this is explained in detail in Appendix A). Once the equilibrium structure is obtained, we quantize the oscillations of the ions around equilibrium, whose dynamics are described by the Hamiltonian

$$H_S = \frac{1}{2m} P^T P + \frac{1}{2} X^T V X, \tag{9.2}$$

where the column vector $X = (x_1, \ldots, x_K)^T$ stores all coordinates (P stores all the momenta; m is the mass of the ions; $K = 3N$ is the number of degrees of freedom and the superscript T denotes the transpose). The coupling matrix V arises from the second order expansion of the full Hamiltonian. Thus, the coupling strengths depend non-trivially on the structure.

We consider that each transverse coordinate is laser cooled to two different temperatures in the left (L) and right (R) regions of the crystal, in order to induce an energy current through the crystal. In addition to these engineered reservoirs, other sources of heat could be considered. Trapped ion strings are subject to heating arising from black body radiation and RF noise, among other factors. Such mechanisms can be modeled by adding an additional thermal reservoir in contact with the whole ion string. However, for state-of-the-art traps external heating can be reduced to less than a couple of phonons per second [105, 106]. Moreover, most noise sources only contribute to heating of the center-of-mass motional modes, since typical wavelengths (larger than 1 cm for frequencies less than 30 GHz) are several orders of magnitude higher than typical ion string lengths (not more than ≈ 100 μm). Therefore, we will neglect external heating

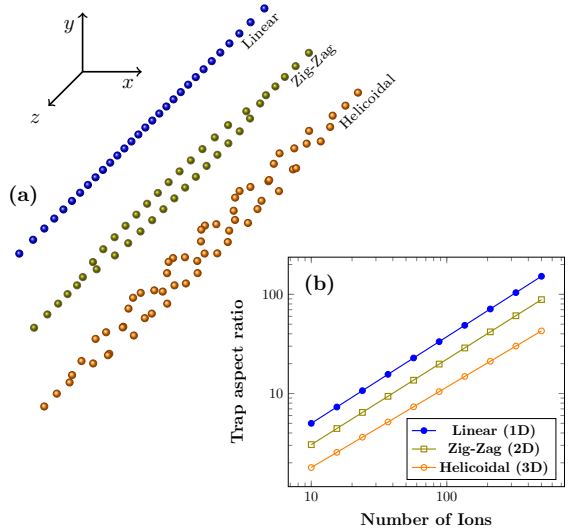

Figure 9.1: (a) Typical crystals with 30, 40 and 60 ions with one, two and three dimensional structures, respectively. (b) Paths in parameter space corresponding to structures with the same order parameters (average distance to the trap axis and mean azimuthal angle between neighboring ions).

of the ion string in this work. Additionally, off-axis ions will be subject to micromotion coming from the trap RF fields. For the present treatment, we will assume that the heating due to micromotion does not affect the transport properties of the crystals.

The evolution of the motional state of a laser cooled ion in a harmonic trap satisfies a master equation which is analogous to that of a damped harmonic oscillator coupled to a finite-temperature heat bath [107]. Therefore, to model the cooling process, we couple each of the quantized transverse coordinates in the left and right regions of the crystal to two bosonic thermal baths (at temperatures T_L and T_R). In order to describe the viscous force experienced by the ion, which is proportional to the instantaneous velocity, we choose an Ohmic spectral density for each thermal bath. Thus, our simplified model consists of a complex network of harmonic degrees of freedom coupled to two bosonic thermal baths at different temperatures. We can therefore apply the formalism developed in chapters 4, 5 and 6 to calculate the heat current established through the ion crystal. Thus, evaluating Eq. (6.31) for the particular case in which there are only two thermal reservoirs, we obtain:

$$\dot{\bar{Q}}_L = -\dot{\bar{Q}}_R = \int_0^\infty d\omega\, \hbar\omega\, \frac{\pi}{2}\, \mathrm{Tr}[I_L(\omega)\hat{g}(i\omega)I_R(\omega)\hat{g}^\dagger(i\omega)]\ (N_L(\omega) - N_R(\omega)) \tag{9.3}$$

where, as before, $\hat{g}(s) = (s^2 mI + V_R + s\gamma(s))^{-1}$ and $N_\alpha = (e^{\hbar\omega/(k_b T_\alpha)} - 1)^{-1}$. We have chosen Ohmic spectral densities in order to model viscous forces proportional to the velocity of the ions:

$$I_{L/R}(\omega) = \frac{2}{\pi}\gamma_0 P_{L/R}\frac{\omega\Lambda^2}{\Lambda^2 + \omega^2} \tag{9.4}$$

where Λ is a high frequency cutoff, γ_0 fixes the relaxation rate and $P_{L/R}$ is the projector onto the coordinates in contact with the left (L) or right (R) environment.

Also, since in this case the system is not driven, the asymptotic covariance matrix is time independent. Thus, for $t \to \infty$ equations (5.6a)-(5.6c) take the following simpler

form:

$$\sigma^{(j,k)} = \mathrm{Re}\left[\int_0^\infty d\omega (i)^{k-j} (m\omega)^{j+k} \hat{g}(i\omega)\hat{\nu}(\omega)\hat{g}(-i\omega)\right] \tag{9.5}$$

where we have denoted $\sigma^{(0,0)} = \sigma^{xx}$, $\sigma^{(0,1)} = \sigma^{xp}$ and $\sigma^{(1,1)} = \sigma^{pp}$.

The main ingredient to calculate the two-point correlations and the heat current in the stationary state is $\hat{g}(s)$, the Laplace transform of the Green's function. To compute the integrals in Eqs. 9.5 and 9.3 several approximations and techniques are used in the literature [108]. For example, an infinite frequency cut-off is often assumed (which corresponds to a Markovian approximation, since the dissipation and noise kernels become local in time). Also, the integrals are usually evaluated numerically, which requires the inversion of $-m\omega^2 + V_R + 2i\omega\hat{\gamma}(i\omega)$ for each evaluation point, and therefore those methods are not efficient (nor accurate) for systems with complex interactions like ion crystals, where the matrix V_R is in general hard to invert.

We have developed and implemented a drastically different approach based on an analytic formula for $\hat{g}(s)$, which can be used to analytically evaluate the frequency integrals. The method is described in detail in Appendix B. However, we explain here the main ideas of it. We consider for simplicity the high-cutoff limit (i.e, $\Lambda \to \infty$), although the method is also valid for an arbitrary cutoff. In that limit $\hat{g}(s)^{-1} = ms^2 + V_R + s\gamma_0 P_T$ is a quadratic polynomial in s with matrix coefficients. Therefore, to find $\hat{g}(s)$ it is required to invert a quadratic matrix polynomial. In analogy with the case of a regular matrix, the inverse of a quadratic matrix polynomial can be related to the eigenvalues and eigenvectors of the generalized eigenvalue problem defined by that polynomial. Explicitly, it is possible to show that $\hat{g}(s)$ can be written as [109]:

$$\hat{g}(s) = \sum_{\alpha=1}^{2K} \frac{s_\alpha}{s - s_\alpha} r_\alpha r_\alpha^T, \tag{9.6}$$

where $\{s_\alpha\}$ and $\{r_\alpha\}$ are generalized eigenvalues and eigenvectors satisfying:

$$\hat{g}^{-1}(s_\alpha) r_\alpha = 0, \tag{9.7}$$

which implies $\det(\hat{g}^{-1}(s_\alpha)) = 0$. Since $\det(\hat{g}^{-1}(s))$ is a $2K$ degree polynomial in s, there are $2K$ eigenvalues $\{s_\alpha\}$. Furthermore, since the matrix coefficients of $\hat{g}^{-1}(s)$ are real, the eigenvalues and eigenvectors come in complex conjugate pairs. The Laplace transform of the Green's function $\hat{g}(s)$ is then expressed in terms of its poles, which are $\{s_\alpha\}$. In this way the integrals appearing in Eqs. 9.5 and 9.3 can be evaluated using the residue theorem. The following result is obtained for the asymptotic covariance matrix:

$$\sigma^{(j,k)} = 2\gamma_0 Re\left[\frac{m^{j+k}}{i^{k-j+1}} \sum_{\alpha,\beta=1}^{2K} \omega_\alpha^{j+k+1} \omega_\beta \frac{r_\alpha^T A r_\beta}{\omega_\alpha + \omega_\beta} r_\alpha r_\beta^T\right], \tag{9.8}$$

where $A = 2k_B \sum_l T_l P_l$, and $\omega_\alpha = -is_\alpha$ are the complex normal frequencies. For the heat current the result is:

$$\dot{Q} = 4\gamma_0^2 \Delta \sum_{\alpha,\beta=1}^{2K} \frac{\omega_\alpha^3 \omega_\beta}{\omega_\alpha + \omega_\beta} (r_\alpha^T P_l r_\beta)(r_\beta^T P_{l'} r_\alpha), \tag{9.9}$$

with $\Delta = -2ik_B(T_L - T_R)$. Equations 9.8 and 9.9 are valid for high temperatures. Exact expressions for arbitrary temperature involving the digamma function can be found in

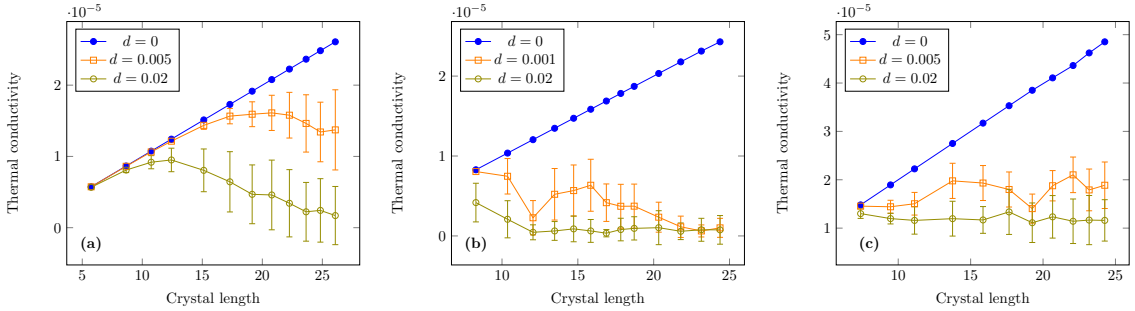

Figure 9.2: (Color online) Thermal conductivity (in units of $k_B l \omega_z$) as a function of crystal length and disorder for 1D lineal (a), 2D zig-zag (b) and 3D helicoidal (c) structures. In all cases we considered between 20 and 200 ions. Points and error bars correspond to mean values and dispersions over several realizations of disorder.

Appendix B. Using Eqs. 9.8 and 9.9, the asymptotic state and heat currents can be evaluated by simply solving a quadratic eigenvalue problem. In turn, the quadratic eigenvalue problem can be mapped to a regular (i.e., linear) eigenvalue problem by standard techniques [109] (at the price of doubling the dimension of the problem).

Surprisingly, this method has never been used to study transport in harmonic networks. In simple terms, the method provides the solution to a system of K differential equations $m\ddot{X} + \Gamma\dot{X} + CX = 0$ for arbitrary non-commuting coupling and damping matrices C and Γ. In the case of spectral densities with finite frequency cutoff expressions similar to Eqs. 9.8 and 9.9 can be derived, this time in terms of the eigenvalues and eigenvectors of a cubic eigenvalue problem (see Appendix B). The method can be used to study transport phenomena in arbitrary harmonic networks, and it is thus suitable for non-trivial coupling matrices as the ones describing ion crystals, that include long-range Coulomb interactions.

9.3 Results

We now present results for ion crystal with up to $N = 200$ ions with various structures. We use m, the mass of the ions, as the unit of mass, and $2\pi\omega_z^{-1}$ as the unit of time. The length unit we use is given by $l = (Q^2/(m\omega_z^2))^{1/3}$ where Q is the electric charge of the ions (see Appendix A).

We analyzed the energy flow for the transverse motion and considered cases where the environment couples with single sites or with extended regions containing up to 10 percent of the crystal (no significant differences were found, in accordance with the results in [[110]] for the weak coupling regime). We computed the thermal conductivity κ, which is such that $\dot{Q}_L = \kappa\Delta T/L$ where $\Delta T = T_R - T_L$ and L is the length of the crystal. Fourier's law for macroscopic heat flow implies that κ is L independent and also temperature independent. We find that fixing ΔT, κ rapidly becomes independent of the average $\bar{T}$. Also, κ becomes independent of ΔT for moderately high values of $\bar{T}$ (this behavior is observed for temperatures of the order of the frequencies in V_R/m). Thus, these aspects of Fourier's law are valid. All the following results correspond to a regime in which the heat current is proportional to ΔT, i.e, we consider that all the normal modes are thermally excited.

However, for all structures κ depends linearly on the length, as shown in Figure 2. This anomalous behavior is a well known property of harmonic chains [108, 111, 112]

that has not yet been experimentally tested. If that behavior is extrapolated to the thermodynamic limit an infinite thermal conductivity would be obtained. Therefore, heat could be transported with the application of a vanishingly small temperature gradient. This fact, and the absence of an internal temperature gradient, which is discussed later, are reminiscent of the behavior of the electric current in superconducting materials. In Appendix B it is shown that in the weak coupling limit any system which is symmetric with respect to the interchange of the reservoirs (condition that is fulfilled in our model) will display a thermal conductivity increasing linearly with the size of the system. That general scaling law is not longer valid if the coupling between system and reservoirs is not small with respect to the internal couplings in the system (even if the symmetry condition still holds). Since our main interest is to study the effect of disorder on structures of different dimensionality, we restrict ourselves to the weak coupling regime (we set $\gamma_0 = 10^{-6}$ for the numerical computations), although the method we use is valid for arbitrary coupling strength.

We show that ion crystals are ideal candidates to measure and control anomalous transport by changing the crystal structure or by adding disorder. Experimentally, disorder can be implemented in different ways. One possible approach would be to locally modify the confining potentials. However, if the potentials are to be tuned using variations in the RF confinement voltages, the electrodes have to be small enough to allow control of individual ions. The electrode size is limited by the ion-electrode spacing, and the actual state-of-the-art allows for ion-electrode spacings of $\sim$30-40 μm [[113, 114]] which is larger than typical ion-ion distances of $\sim$10 μm. Improvements in trap miniaturization might render this approach feasible in the near future. However, disorder can be implemented with the present technology using site-specific optical dipole forces. Individual ions in the ion string can be addressed with lasers to create an optical lattice with a confinement that can be tuned from site to site [80, 115].

In order to study the effects of disorder in a simple way, we numerically introduced disorder by modifying the coupling matrix V corresponding to a particular equilibrium structure. Specifically, we changed the pinning potential of $N/2$ randomly selected ions according to the rule $V_{ii} \to (1 \pm d)V_{ii}$, where d is a measure of disorder. This is expected to be a qualitatively good model of particular physical realizations of disorder only for small values of d. However, values of d as small as 0.005 are enough to control the transition from anomalous to diffusive heat transport. As shown in Figure 2, linear, zig-zag and helicoidal crystals display drastically different behavior as a function of disorder. Thus, zig-zag and helicoidal crystals are highly sensitive to disorder. In fact, a small d turns the zig-zag crystal into a heat insulator with κ rapidly approaching a vanishingly small value. The thermal conductivity of helicoidal crystals approaches a nonzero value for long crystals. Hypersensitivity to disorder is evident in the dependence of κ on d for a fixed length L. This is shown in Figure 3-(a) where we see that κ rapidly decays with d for 2D and 3D crystals. Decay for 1D crystals is clearly much slower.

We also studied the local temperature of the transverse motion. As seen in Figure 9.4-a the temperature profile strongly deviates from the linear behavior predicted by the classical Fourier's law (we only show the profile for a 3D crystal but no substantial differences are seen in 1D or 2D). Without disorder the profile is almost planar except for the ions in contact with the reservoirs. As disorder is introduced, a central temperature gradient develops. Thus, deviation from Fourier's law can be measured by the central slope of the temperature profile, which is shown in Figure 9.4-b. The central derivative strongly depends on the dimensionality: again, the zig-zag and helicoidal crystals are hyper sensitive to disorder. For small values of d the central derivative saturates to a

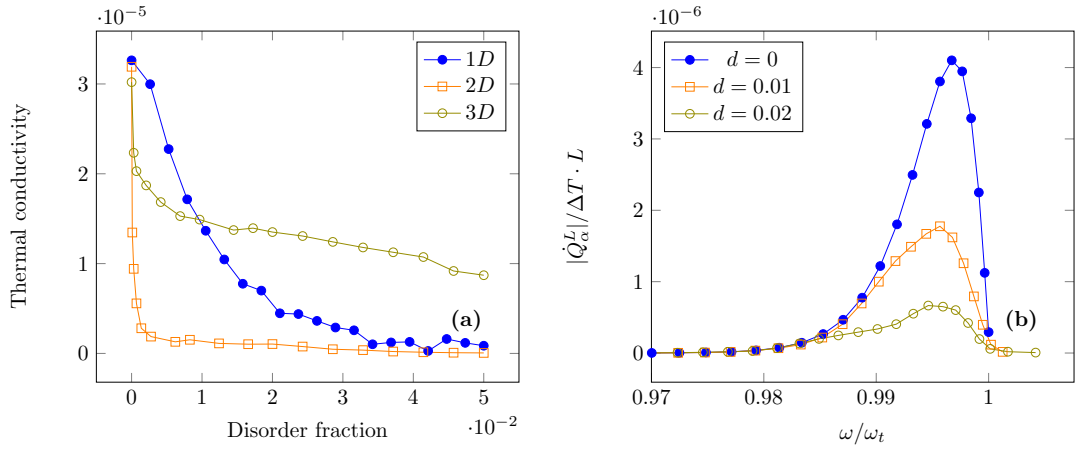

Figure 9.3: (Color online) (a) Thermal conductivity versus disorder for crystals of 120 ions with different structures. (b) Contribution of each normal mode to the thermal conductivity in a 1D crystal of 100 ions.

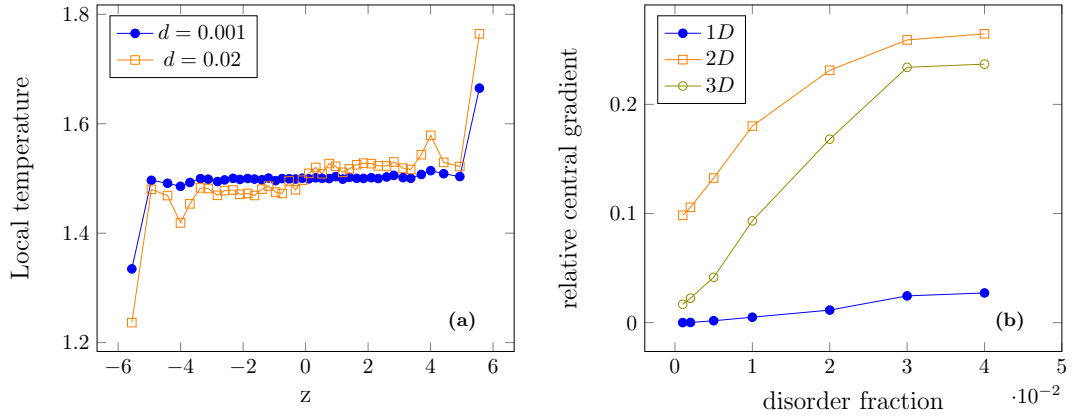

Figure 9.4: (Color online) (a) Temperature profiles for a helicoidal chain of 40 ions with increasing disorder. (b) Central gradient of the temperature profile (in units of $\Delta T/L$) as a function of the disorder fraction.

value which is a significant fraction of the one that correspond to a linear interpolation between the temperatures of both reservoirs.

Equations 9.8 and 9.9 enable us to estimate the contribution of each mode to thermal conductivity and temperatures. For example, the contribution of the normal mode at frequency $\omega = Re(\omega_\alpha)$ to the heat current is:

$$\dot{Q}_\alpha = 4\gamma_0^2\ \Delta\ \omega_\alpha^3 \sum_{\beta=1}^{2K} \frac{\omega_\beta}{\omega_\alpha + \omega_\beta} (r_\alpha^T P_l r_\beta)(r_\beta^T P_{l'} r_\alpha). \tag{9.10}$$

The behavior of $\dot{Q}_\alpha$ as a function of the mode frequency is shown in Figure 3-(b) for different levels of disorder. The figure shows that the largest contributions come from the modes with higher frequencies. This is expected since those are the normal modes with greater amplitude in the ends of the crystals, and therefore are the ones most coupled to the reservoirs.

In summary, we showed that ion crystals are excellent candidates to observe and control the transition from anomalous to normal transport. Thus, by changing the trap

parameters we induce structural phase transitions which may drive the crystal to a heat insulating phase (with a zig-zag shape), which is a rather remarkable effect (evidence of the insulating properties of some idealized 2D models was presented in [108]). The toolbox presented in [80] can be used not only to measure the heat flow and local temperature but also to artificially simulate disorder. In this way, the strong dependence of thermodynamical quantities on the structure of the crystal could be observed with current technologies. To study this, we implemented a new method providing exact formulas for heat currents and temperature profiles. All these analytic (exact) results depend on generalized eigenvalues and eigenvectors of a quadratic problem (which can be easily linearized).

Transporte de calor a través de cristales de iones

En este capítulo se estudian las propiedades termodinámicas de cristales de iones atrapados que son enfriados por medio de láseres en dos regiones distintas a diferentes temperatura. Se muestra que estas propiedades dependen fuertemente de la estructura del cristal. Como se explica en el capítulo 3, esta estructura puede ser modificada variando los parámetros de la trampa y sufre una serie de transiciones desde configuraciones lineales a configuraciones planas (zig-zag) y helicoidales. Los resultados indican que estos sistemas son candidatos ideales para observar y controlar la transición entre el transporte de calor difusivo y balístico. Se observa que todas las estructuras se comportan como superconductoras de calor, con una conductividad térmica que crece linealmente con el tamaño del sistema y sin presentar un gradiente térmico en su interior. Sin embargo, las estructuras zig-zag y helicoidales son muy sensitivas al desorden, mostrando una perfil de temperatura lineal y una conductividad térmica independiente del tamaño. Notablemente, las estructuras zig-zag desordenadas son aislantes de calor. La sensitividad al desorden es mucho menor para las estructuras unidimensionales.

Chapter 10

Simulation of the ANNNI model with trapped ions

In this chapter we discuss the simulation of a non-trivial model of magnetic materials known as the ANNNI model (for Anisotropic Next to Nearest Neighbor Interaction). We will consider the one-dimensional version, in which ferromagnetic nearest neighbor (NN) interactions compete with anti-ferromagnetic next to nearest neighbor (NNN) ones. First, we review recent experiments involving the quantum simulation of simpler models of magnetic materials, and then we show how they could be extended in order to simulate the ANNNI model.

10.1 Adiabatic quantum simulations with trapped ions

In the Chapter 3 we have seen that an effective two-level or spin-1/2 system can be encoded in the internal electronic state of trapped ions, and that it is possible to induce Ising-like couplings among these effective spins by employing suitable laser fields. Thus, it is possible to impose on the spins a time evolution corresponding to the following Hamiltonian (for long times):

$$H = \sum_{i,j} J_{i,j}\sigma_x^i\sigma_x^j - \sum_i B_y\sigma_y^i, \tag{10.1}$$

where the constants $J_{i,j}$ and B_y can be controlled by modifying experimental parameters like the intensity and phases of the laser fields, or the trapping frequencies of the trap. For example, when the laser fields (or their interference signal) have two spectral components with the same amplitude and symmetrically detuned with respect to the electronic transition, the interaction constants $J_{i,j}$ are given by:

$$J_{i,j} = -\frac{\hbar^2(\delta k)^2\Omega^2}{2m}\sum_{k=1}^{N}\frac{B_{i,k}B_{j,k}}{\mu^2-\nu_k^2}. \tag{10.2}$$

In the following we will denote the eigenstates of σ_x for each ion as $|\uparrow\rangle = (|e\rangle + |g\rangle)/\sqrt{2}$ and $|\downarrow\rangle = (|e\rangle - |g\rangle)/\sqrt{2}$, to further advance the analogy with spin systems.

We are interested in the physical preparation of the ground state of the Ising Hamiltonian $H = \sum_{i,j} J_{i,j}\sigma_x^i\sigma_x^j$, given the interaction constants $J_{i,j}$. This problem is important from a computational point of view since the determination of the ground state for general Ising models is a NP-hard problem. This means that the answer to other

problems with no known efficient solution can be encoded in the ground state of an Ising-like system by appropriately choosing the interaction constants $J_{i,j}$ (this is explicitly done in [116] for many well known problems like the Traveling Salesman and Exact Cover problems). In fact, the only claimed 'quantum processor' commercially available so far, the D-Wave computer [24], supposedly implements an quantum annealing algorithm [117] in order to find the ground state of an Ising system with programmable interactions.

The determination of the ground state of the Ising part of the Hamiltonian is also interesting from a physical point of view, since its features can change abruptly when one of the parameters in the Hamiltonian is varied, resulting in what is known as Quantum Phase Transitions [118], that share many properties with the usual thermal phase transitions. Also, the simulation of systems that display frustration as a result of non-trivial interactions is relevant in the study of magnetic materials and condensed mater models like spin glasses.

One approach to prepare the ground state of a Hamiltonian like $H = \sum_{i,j} J_{i,j}\sigma_x^i\sigma_x^j$ is to employ what is known as an adiabatic evolution. In this approach the Hamiltonian $H(t)$ of a controllable system is varied in time, and is such that the ground state of the initial Hamiltonian $H(0)$ is known and can be easily prepared. Then, the Hamiltonian is slowly changed from the 'easy' one, $H(0)$, to a difficult, target, Hamiltonian $H(T)$, where T is the total time of evolution. During the evolution the state $|\Psi(t)\rangle$ of the system evolves according to the Schrodinger's equation $i\hbar d\left|\Psi(t)\right\rangle/dt = H(t)\left|\Psi(t)\right\rangle$. The adiabatic theorem states that if the initial state $|\Psi(0)\rangle$ is the ground state of $H(0)$ and the evolution is slow enough, then the state evolution will follow the instantaneous ground state of $H(t)$. In this way, it is possible to prepare the ground state of $H(T)$. Actually, the adiabatic theorem is valid if there is a finite energy gap at all times between the ground state and excited states. Otherwise, it is impossible to avoid creating low energy excitations, or defects, as the Hamiltonian is varied. This is in fact a limitation for the adiabatic algorithm, since for models displaying quantum phase transitions, in the vicinity of the critical point, the energy gap becomes exponentially small with the system size. Hence, for this kind of systems, in order to remain close to the ground state when crossing a critical point, the total evolution time T must increase exponentially with the system size [119].

Leaving these details aside for the moment, we can describe the implementation of the adiabatic evolution algorithm with trapped ions as the application of the following steps:

- Initially, parameters B_y and $J_{i,j}$ in the Hamiltonian of Eq. (10.1) are selected in such a way that $B_y \gg |J_{i,j}|$. Each spin is prepared in the state $|\uparrow_y\rangle = (|\uparrow\rangle + |\downarrow\rangle)/\sqrt{2}$, and therefore the global state is a good approximation of the ground state of the Hamiltonian for the chosen parameters.
- The parameter B_y is decreased from its initial value to $B_y = 0$.
- The final state of the system is probed by measuring each spin in the $\{|\uparrow\rangle, |\downarrow\rangle\}$ basis.

10.1.1 Controlling the range and sign of the Ising interactions

We now analyze what kind of interactions $J_{i,j}$ we can simulate employing a single pair of spectral components symmetrically detuned with respect to the electronic transition. In this case the interaction constants are given by Eq. (10.2), so the relevant control

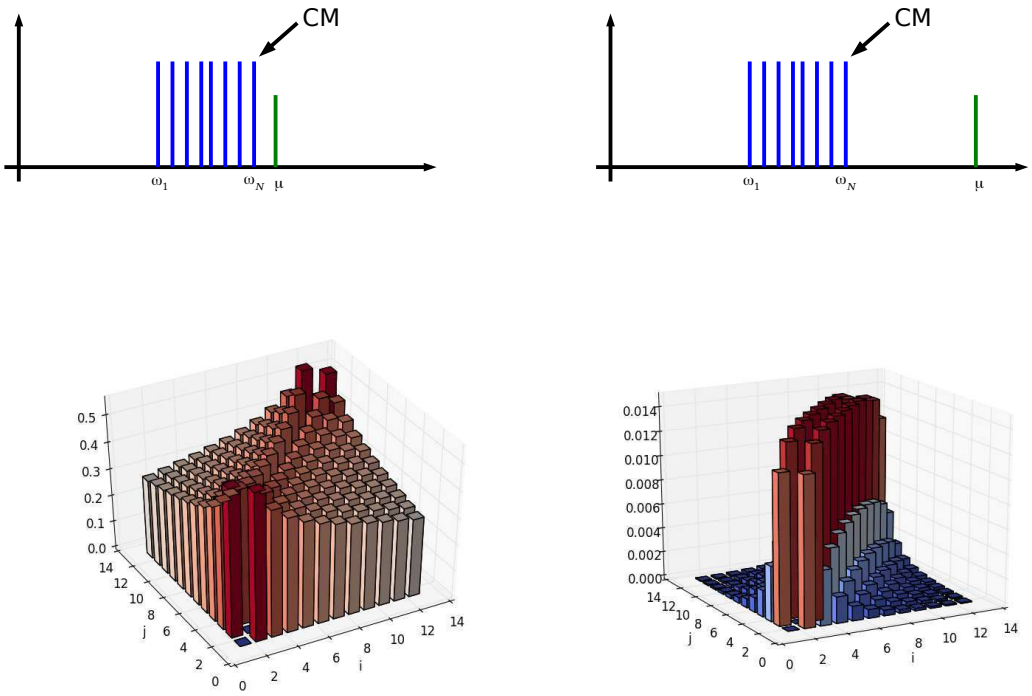

(a) Long range interactions. The center of mass mode gives the dominant contribution.

(b) Short range interactions. All normal modes contribute equally.

Figure 10.1: Examples of induced Ising couplings $J_{i,j}$ for two different choices of detuning μ in a linear chain of 12 ions.

parameters are the detuning μ and the Rabi frequency Ω (for a given equilibrium structure the transverse normal modes contained in the matrix $B_{i,j}$ and the normal frequencies Ω_k are fixed). The spatial structure of the interactions $J_{i,j}$ will of course be ultimately determined by the spatial structure of the transverse normal modes. We consider a 1D ion crystal along the longitudinal axis of the trap, which is the equilibrium structure when the trap frequencies along the longitudinal (ω_z) and transverse directions (ω_x and ω_y) are such that $\omega_z \gg \omega_x, \omega_y$. In such situation the center of mass mode, in which all the ions oscillate in the transverse direction with the same amplitude, has the highest frequency, and this is obviously $\Omega_{CM} = \omega_x$. Therefore, it is clear from Eq. (10.2) that when the detuning μ is close to Ω_{CM} the dominant contribution is given by the center of mass mode, and since in this mode all the ions oscillate with the same amplitude, the induced interactions $J_{i,j}$ are almost the same for any pair of spins. In this case the range of the interactions is large. An example of this situation for a chain of 12 spins is shown in Figure 10.1a. When the detuning μ is increased away from Ω_{CM}, all the normal modes contribute with approximately the same strength in Eq. 10.2. In this case, contributions of different modes interfere destructively and the long range couplings vanish, as is shown in Figure 10.1a. Hence, it is clear that by interpolating between these two situations it is possible to control the range of the induced spin interactions.

The sign of the interactions constants $J_{i,j}$ can also be controlled, although not individually[1]. For example, if a detuning μ close to Ω_{CM} is selected, in order to induce

[1] As we will see, some form of single ion addressing is needed for complete controllability of the Ising

long range interactions like in Figure 10.1, it still possible to choose whether $\mu \gg \Omega_{\text{CM}}$ or $\mu \ll \Omega_{\text{CM}}$. The difference between these two choices is a global sign change of $J_{i,j}$. More generally, another possibility is to adiabatically follow the *higher energy state* of the system instead of the ground state. This is equivalent to a global sign change in the simulated Hamiltonian. Of course, by choosing a detuning μ between different normal modes (i.e., such that $\Omega_j < \mu < \Omega_k$), more complicated interactions can be induced, where not all the constants $J_{i,j}$ have the same sign. This will be discussed in the next section.

10.2 Many spectral pairs and approximation of target interactions

We now consider the more general case in which the laser light that drives the ions have many, instead of only one, pairs of symmetrically detuned spectral components. In this case the induced interactions are simply given by the sum of an expression like Eq. (10.2) for each spectral pair. Thus, if we note in addition that the sum $\hat{G}(\mu)_{i,j} = \sum_{k=1}^{N} \frac{B_{i,k}B_{j,k}}{\nu_k^2-\mu^2}$ is nothing more that the Laplace transform of the Green's function for the transverse harmonic motion, we have:

$$J = \hbar R \sum_{m=1}^{M} \Omega_m^2 \hat{G}(\mu_m) \tag{10.3}$$

where μ_m and Ω_m are the detuning and Rabi frequency of the m-th spectral pair, respectively, and the 'recoil frequency' $R = \hbar(\delta k)^2/(2m)$ was defined. In this way, the spin-spin interaction matrix is only a weighted sum of the vibrational Green's function evaluated at the detunings μ_m, and the weights are the squared Rabi frequencies.

We now analyze what kind of interactions is possible to generate by adjusting the control parameters given by the M detunings $\{\mu_m\}$ and their associated intensities $\{\Omega_m\}$. As a first observation, we note that *the set of eigenvectors of the coupling matrix $J_{i,j}$ is the set of motional normal modes*. For any choice of detunings and Rabi frequencies, the eigenvectors are always the same, and the only properties of the matrix $J_{i,j}$ that are sensitive to control are the eigenvalues associated to each eigenvector, which are:

$$a_k = R \sum_{m=1}^{M} \frac{\Omega_m^2}{\nu_k^2 - \mu^2} \tag{10.4}$$

Since the matrix $J_{i,j}$ has only N eigenvalues, it turns out that it is only necessary to have N independent control parameters. There is no advantage in increasing the number of control parameters beyond N. To achieve maximum control over the matrix J, one possible scheme in to consider $M = N$ spectral components at some fixed detunings $\{\mu_m\}$, and only control the Rabi frequencies $\{\Omega_m\}$. This is a convenient approach, since the squared Rabi frequencies enter linearly in the expression for $J_{i,j}$. Consequently, it is very simple to find the optimal Rabi frequencies given a target matrix, as is explained next. As a last observation, we note that the eigenvectors of $\hat{G}(\mu)$ are nothing more that the normal modes of a linear chain of ions with dipolar ($\propto 1/r^3$) interactions. Therefore, they form a one-dimensional backbone for any matrix $J_{i,j}$ that is possible to simulate without single ion addressing. The fact that it is not possible to change the eigenvectors

interactions

of $J_{i,j}$ means that it won't be possible to simulate coupling matrices corresponding to two- or three-dimensional systems, because their eigenvectors won't be compatible with the normal modes of the underlying one-dimensional ion crystal. Only with some form of single ion addressing it is possible to overcome this limitation.

Although it is clear from the previous considerations that it is not possible to simulate a general coupling matrix, one can ask, given a target matrix J_T, which are the parameters $\{\Omega_m^2\}$ that minimize the distance $\delta = |J(\Omega_m^2) - J_T|$. If the distance considered is the element-wise euclidean distance, then the minimization of δ^2 over the parameters $\{\Omega_m^2\}$ can be done analytically, since J is a linear function of them. Fixed the detunings, the matrices $\{\hat{G}(\mu_m)\}$ can be calculated in advance (see Eq. 9). Then $J(\Omega_m^2)$ is simply a linear combination of known matrices. A simple calculation shows that the minimum value of δ^2 (which is a quadratic form on $\{\Omega_m^2\}$) correspond to the values of Ω_m^2 that satisfy the following linear system:

$$\mathrm{Tr}(J_T G_n) = \sum_m \mathrm{Tr}(G_n G_m)\Omega_m^2 \tag{10.5}$$

Where $G_m = G(\mu_m)$. We set $R = 1$ for convenience. Therefore, the optimal values for the squared Rabi frequencies $\{\Omega_n^2\}$ are given by the solution x of the linear system $Ax = b$ with $A_{n,m} = \mathrm{Tr}(G_n G_m)$ and $b_n = \mathrm{Tr}(J_T G_n)$. We have considered that there are N different spectral components, but the results are the same for any number of them. It is never necessary to use more than N, but the desired result might be attained at reasonable accuracy with less spectral components. One issue with this approach is that the optimal squared Rabi frequencies $\{\Omega_n^2\}$ given by the solution of the previous linear system might be negative, which is a non-physical situation. However, it can be seen that it is always possible, in principle, to choose the detunings $\{\mu_n\}$ so that all the optimal squared Rabi frequencies are positive.

10.3 The ANNNI model

This model is an Ising model with ferromagnetic nearest-neighbor and anti-ferromagnetic next-nearest- neighbor interactions. It was studied in one, two and three dimensions. I will consider only the one-dimensional model, for simplicity, and also because is the only one that is possible to simulate without single ion addressing. For an infinite one-dimensional chain, the Hamiltonian is:

$$H = -J_1 \sum_i \sigma_x^i \sigma_x^{i+1} + J_2 \sum_i \sigma_x^i \sigma_x^{i+2} + B \sum_i \sigma_z^i \tag{10.6}$$

with J_1, $J_2 > 0$. A transverse magnetic field was added in order to drive quantum phase transitions at zero temperature. Obviously, the properties of the system only depend on the ratios $\kappa = J_2/J_1$ and $h = B/J_1$. The ANNNI model received much attention in the past. It was mainly used to explain the observation of periodic magnetic structures, and the dependence of the period of these structures on the temperature and other parameters. A good introduction to the model can be found in [120–122]. A modern review of the main results and recent work can be found in [123].

The zero temperature one-dimensional ANNNI model in a transverse field, which is the one that can be simulated in current ion trap experiments, has many interesting features. There is no exact solution and the most reliable source of information about the model are numerical simulations of finite chains. It can be mapped to other interesting models like the two-dimensional ANNNI model at finite temperature and the

zero-temperature XY model with a in-plane external field. It can also be mapped to a chain of fermions with two and three-body interactions (through the Wigner-Jordan transformation).

It is very simple to understand the behavior of the ground state for different values of κ (and $B = 0$). If the ferromagnetic interaction dominates ($\kappa \ll 1$) then in the ground state all the spins will point in the same direction ($\cdots \uparrow\uparrow\uparrow \cdots$). This is the ferromagnetic phase. In the opposite limit ($\kappa \gg 1$), the anti-ferromagnetic next-nearest-neighbor interaction will force the spins that are two sites apart to point in opposite directions and the ground state will be $\cdots \uparrow\uparrow\downarrow\downarrow\uparrow\uparrow\downarrow\downarrow\uparrow\uparrow \cdots$. This ground state is called 'anti-phase'. The transition between these two ground states is a quantum phase transition that occurs at $\kappa = 1/2$, a point where the system is highly degenerated.

Figure 10.2 shows the different phases observed in the ANNNI model (figure obtained from [124], where the model was investigated using the DMRG algorithm). For

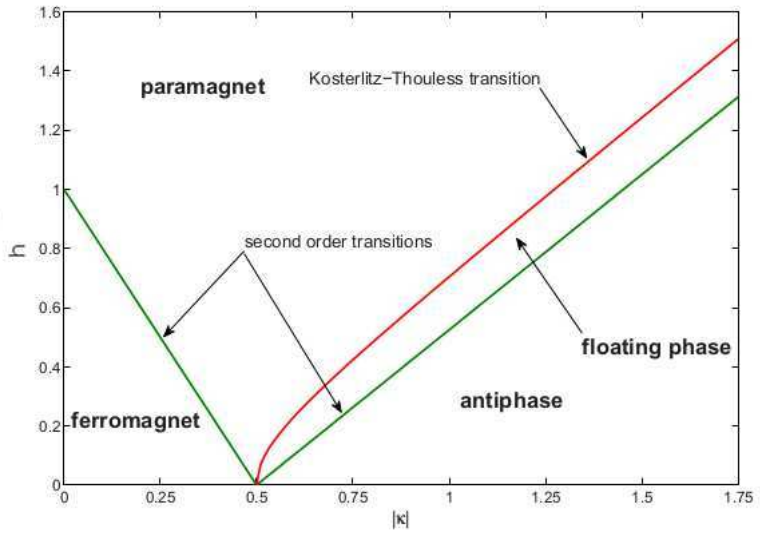

Figure 10.2: Phase diagram of the 1D ANNNI model in the h-κ plane.

$\kappa = 0$ the typical ferro to paramagnetic transition of the regular Ising model is present. The critical value of h at which this transition occurs decreases with increasing κ (increasing frustration). Beyond the critical point $\kappa = 1/2$ (high frustration) and for low values of h the 'anti-phase' phase is observed, while for moderate values of h a 'floating' phase emerges, before entering the paramagnetic phase. One interesting aspect of this quantum phase transition is that it is of the Kosterlitz-Thouless type. This is a phase transition of infinite order typically observed in the two-dimensional XY model. It is also related to the 2D superconductor-insulator transition [125, 126]. It was experimentally investigated using a trapped gas of rubidium atoms [127] and also in a simulation of a XXZ chain with four spins in a NMR setup [128].

10.4 Approximating the ideal ANNNI model

In this section we consider the simulations of the ANNNI model at the critical point $\kappa = 1/2$ with a chain of 16 ions. One possible approach to the problem is to use the method described in section 10.2 to approximate the ideal coupling matrix J_T , which is shown in Figure 10.3. The first step is to choose and fix the detunings μ_n. To have maxi-

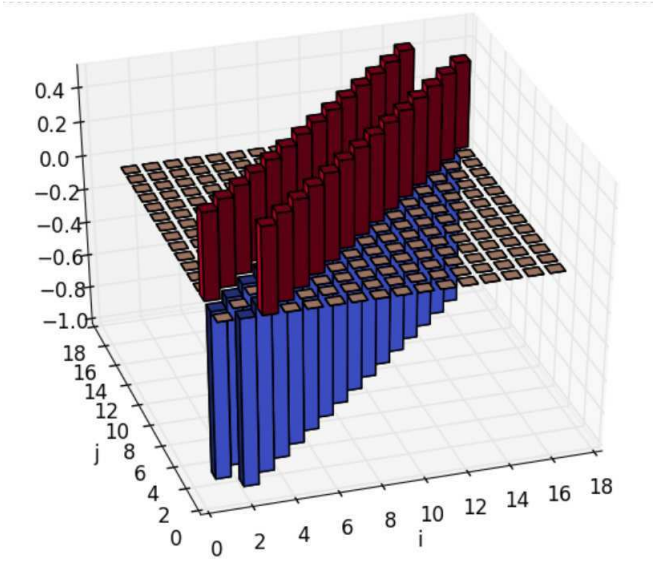

Figure 10.3: Couplings of the ideal 1D ANNNI model with 16 sites

mum control over the spin-spin interaction matrix we will user N spectral components, one per normal mode. These spectral components will be located between successive normal mode frequencies, i.e, $\mu_n = \nu_n + d(\nu_{n+1} - \nu_n)$, with $-1 < d < 1$, $d \neq 0$. For example, when d = 1/2 the spectral components are right in the middle of the successive normal mode frequencies. The value of d is adjusted in order for the optimal squared Rabi frequencies to be all positive. For this example I considered a ion crystal which is the equilibrium configuration of 16 ions in a linear Paul trap whit an aspect ratio of 100. Figure 10.4a show the 16 optimal Rabi frequencies for $d = .6$. The corresponding interaction matrix J is shown in Figure 10.4b. The matrix J captures some of the features of the target matrix J_T, while it fails to represent other aspects. For example, the n.n couplings are ferromagnetic and the n.n.n are anti-ferromagnetic (at least in the center of the chain, see Figure 10.5). On the other hand the following differences with the target matrix are evident: i) The n.n and n.n.n couplings are not uniform along the chain, as shown in Figure 5 more detail, and ii) the long range couplings are not zero. In the following I show that the points i) and ii) can be corrected by an iterative procedure. In contrast, the non-uniformity of the couplings is a direct consequence of the non-uniformity of the motional normal modes, and can only be corrected by changing the structure of the ion-crystal.

10.4.1 An iterative procedure

The following iterative procedure is proposed to correct the relative strength of the ferromagnetic and anti-ferromagnetic couplings in the optimal solution, and the non-vanishing long range interactions. Each iteration is as follows:

1. Build a target ANNNI matrix J_T with some parameter κ_T, as the one in Figure 10.3.

2. Apply the approximation method of section 10.2, and find the optimal Rabi frequencies $\Omega_1^2, \Omega_2^2, \cdots \Omega_N^2$ and the corresponding coupling matrix J.

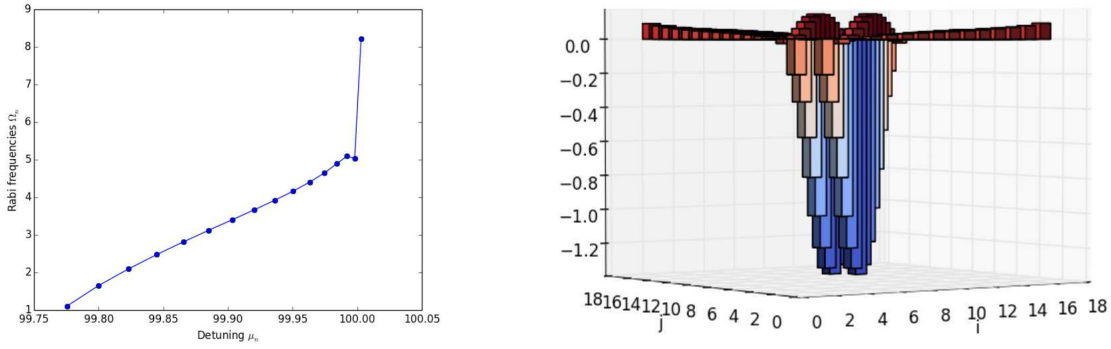

(a) (b)

Figure 10.4: Results obtained from a first approximation of the ideal ANNNI couplings using Eq. 10.5: (a) Optimal Rabi frequencies for the target matrix of Figure 10.3 and $d = .6$, (b) Approximated couplings

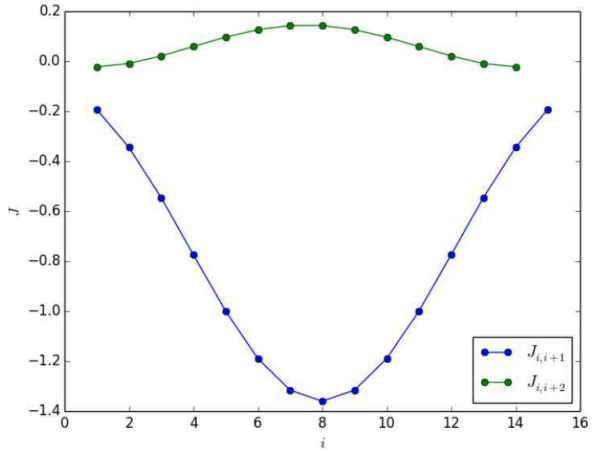

Figure 10.5: Detail of the n.n and n.n.n couplings shown in Figure 10.4b

3. Build the interaction matrix J' as follows:
   - Set $J' = J$
   - Eliminate long range interactions: set $J_{i,i+k} = 0$ for all i and for $k > 2$
   - Appropriately scale n.n and n.n.n interactions, in such a way that $\frac{|J_{i,i+2}|}{|J_{i,i+1}|} = \kappa_T$.
4. Repeat the iteration with J' as a target matrix

The iteration continues until some convergence criteria is fulfilled. The result of this algorithm for the same initial target matrix as the previous section is shown in Figure 10.6b. It is evident from Figure 10.6b that the iterative procedure was able to eliminate the long range couplings. Also, the ratio between the n.n and n.n.n interactions is similar to the one of the initial target matrix. The dependence of the couplings on the position along the chain is shown in Figure 10.7. The non-uniformity of the couplings can only be improved by changing the trap fields in order for the ions in the equilibrium configuration to be more equidistant. Figure 10.6a shows the Rabi frequencies corresponding to the solution of Figure 10.6b. In this case the detuning parameter is $d = -.1$.

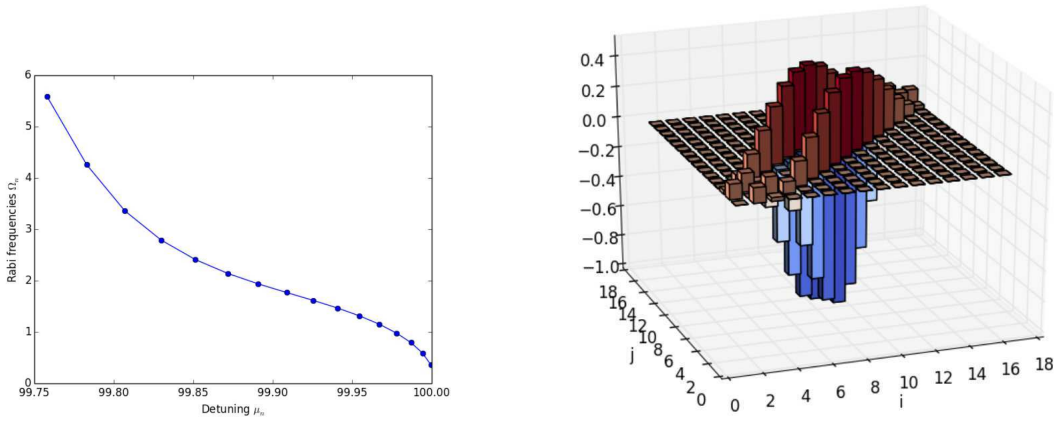

(a) (b)

Figure 10.6: Results obtained from the iterative approximation: (a) Optimal Rabi frequencies, (b) Approximated couplings

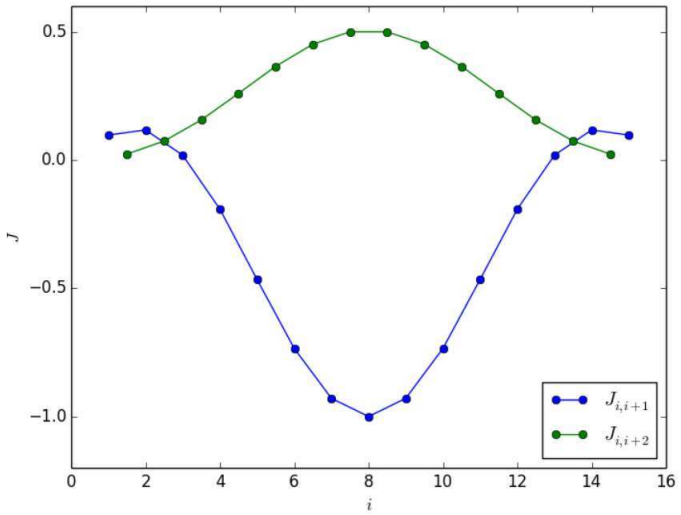

Figure 10.7: n.n and n.n.n of the iterative result

10.4.2 Phase transitions at zero temperature

We know that for the ideal ANNNI model there is a phase transition at $\kappa = 1/2$, in which the ground state of the system changes between $\cdots \uparrow\uparrow\uparrow \cdots$ and $\cdots \uparrow\uparrow\downarrow\uparrow\uparrow\downarrow\uparrow\uparrow \cdots$. In the following the zero temperature phase transitions occurring for the approximated couplings of the previous section are investigated. For the moment, we take the number of clusters as a simple characterization of the ground state. This number, denoted as C, is calculated as the number of contiguous blocks of the chain with the same spin value. Figure 10.8a shows the clustering of the ground state as a function of κ for the ideal ANNNI model. We see the expected sharp transition at $\kappa = 1/2$ between the single cluster of the ferromagnetic ground state and the 8 clusters of size 2 of the anti-phase ground state. On the other hand, for the approximated model there is no a single transition between the anti-phase and ferromagnetic ground states, but many. The clustering for large values of κ is larger than in the ideal case. Table 10.8b shows

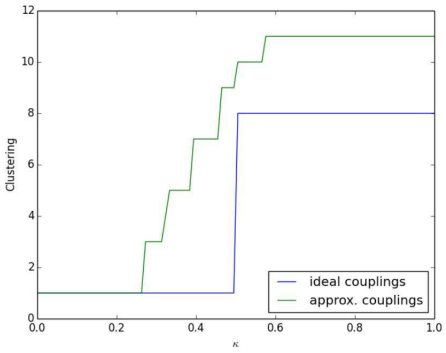

(a)

κ	state	C
0.2626	↓↓↓↓↓↓↓↓↓↓↓↓↓↓↓	1
0.3131	↓↑↑↑↑↑↑↑↑↑↑↑↑↑↓	3
0.3232	↓↑↓↓↓↓↓↓↓↓↓↓↑↑	4
0.3434	↓↑↓↓↓↓↓↓↓↓↓↓↑↓	5
0.3838	↓↑↑↓↓↓↓↓↓↓↓↑↑↓	5
0.4545	↓↑↓↓↑↑↑↑↑↑↑↓↓↑↓	7
0.4949	↓↑↓↓↑↑↓↓↓↓↑↑↓↓↑↓	9
0.5657	↓↑↓↓↑↑↓↓↑↑↓↓↑↑↓↑	10
1.0000	↓↑↓↑↑↓↓↑↑↓↓↑↑↓↑↓	11

(b)

Figure 10.8: (a) Clustering vs κ for the ideal and approximated models. (b) Ground states for the approximated model

the exact sequence of ground states as the value of κ increases. The first column of the table indicates the value of κ at which the transition to the next ground state happens. Because of the non-uniformity of the crystal magnetic domains begin to form in the ends of the chain and propagates to the center. The high clustering in the ground state for high values of κ comes from the ends of the chain, because there the n.n interactions are anti-ferromagnetic and therefore successive spins have opposite values.

Simulación del modelo ANNNI con iones atrapados

En este capítulo se discute la simulación cuántica de un modelo no trivial de materiales magnéticos conocido como modelo ANNNI (ANNNI son las siglas en inglés para Interacciones Anisotrópicas a Segundos Vecinos). Se considera la versión unidimensional del modelo, en la cual interacciones ferromagnéticas a primeros vecinos compiten con interacciones anti-ferromagnéticas a segundos vecinos. En primer lugar se describen experimentos recientes sobre la simulación cuántica de modelos mas sencillos de materiales magnéticos, y luego se muestra como estos podrían extenderse para simular el modelo ANNNI.

Part V

Conclusions

The central subject of the work presented in this thesis is the analysis of a family of linear and driven quantum thermal machines. This family is composed of arbitrary networks of harmonic oscillators that are connected to bosonic thermal environments at arbitrary temperatures. The parameters of the network can be modulated periodically in time. It was shown how this model can be solved exactly and how the usual laws of macroscopic thermodynamics emerge for long times. Regarding the validity of the dynamical third law of thermodynamics, or unattainability principle, the fundamental limits for cooling for this family of machines were identified and related to the Dynamical Casimir Effect (DCE). Thus, it was shown that at ultra low temperatures the energy interchange between the system and the reservoirs (heat currents) is dominated by a pairs creation process that always heat up the reservoirs. Importantly, this effect cannot be captured by treatments based on the weak coupling approximation. Since our treatment is exact, it offers a clean physical interpretation of the processes contributing to the heat currents, and that is informative for other models where an exact solution is not yet available. In particular, these results indicate that to analyze the ultimate limits for cooling in non-linear models (like quantum absorption refrigerators or driven two-level systems) it is necessary to rely in treatments valid (at least) up to fourth order in the interaction between the central system and the reservoirs, and not only to second order like is usual. Also, these findings could enable the proposal of new experiments to observe the creation of optical photons by the DCE, which so far was only measured with superconducting cavities at microwave frequencies.

Two experimental proposals were also presented. The first one propose the utilization of crystals of trapped ions to study heat transport across structures with different dimensionality, with emphasis in the study of the emergence of the Fourier law in this setting. It was shown that systems of trapped ions are a promising platform to control and observe the transition from ballistic to diffusive heat transport, as the interplay between the dimensionality and the disorder of the crystal is varied. New semi-analytical techniques were developed for the efficient calculation of the heat currents across non-periodic structures with complex interactions. Finally, the last proposal studies how current state of the art experiments on the quantum simulation of magnetic materials could be extended to simulate more complex models. In particular we consider the ANNNI model, that is a Ising-like model with no analytical solution and displaying a number of interesting phase transitions. A numerical algorithm was developed to select the best experimental parameters corresponding to a particular instance of the one-dimensional ANNNI model.

Conclusiones

El tema central del trabajo presentado en esta tesis es el análisis de una familia de máquinas térmicas lineales. Esta familia esta compuesta por redes arbitrarias de osciladores armónicos conectadas a entornos térmicos bosónicos a temperaturas arbitrarias. Los parámetros de la red pueden ser modulados externamente de forma periódica. Se mostró como este modelo puede ser resuelto de forma exacta, y como las leyes usuales de la termodinámica emergen a tiempos largos. Con respecto a la validez de la versión dinámica de la tercera ley de la termodinámica, los límites fundamentales para el enfriamiento fueron identificados y relacionados con el Efecto Casimir Dinámico (ECD). Así, se demostró que a temperaturas ultra bajas el intercambio de energía entre el sistema central y los entornos térmicos (corrientes de calor), está dominado por un proceso de creación de pares de excitaciones que siempre genera calentamiento de los entornos. Este efecto no puede ser capturado por tratamientos basados en la aproximación de acoplamiento débil. Debido a que nuestro tratamiento es exacto, este ofrece una clara interpretación física de los procesos que contribuyen a las corrientes de calor, lo que es de utilidad en otros modelos que no disponen de una solución exacta. En particular, esta solución indica que para analizar los límites fundamentales para el enfriamiento en modelos no lineales (como los refrigeradores de absorción cuánticos, o sistemas de dos niveles dependientes del tiempo), es necesario recurrir a tratamientos válidos, al menos, hasta cuarto orden en la interacción entre el sistema central y los entornos. Además, estos resultados podrían permitir el diseño de nuevos experimentos para observar la creación de fotones a frecuencias ópticas mediante el ECD, que hasta el momento solo ha sido observado con cavidades superconductoras de microondas.

Dos propuestas experimentales fueron presentadas. La primera propone la utilización de cristales de iones atrapados para estudiar el transporte de calor a través de estructuras con distinta dimensionalidad, con énfasis en el estudio del origen de la ley de Fourier. Se demostró que los iones atrapados son una plataforma promisoria para controlar y observar la transición entre transporte de calor difusivo y transporte anómalo, a medida que se modifica tanto la dimensionalidad como el desorden en el cristal. Nuevos técnicas semi-analíticos tuvieron que ser desarrolladas para el cálculo eficiente de las corrientes de calor a través de estructuras sin periodicidad y con interacciones complejas. Finalmente, la última propuesta estudia cómo pueden ser modificados experimentos modernos donde se simulan materiales magnéticos utilizado iones atrapados de forma de poder simular modelos más complejos. En particular, se considera el modelo ANNNI, que es un modelo tipo Ising sin una solución analítica conocida y que muestra varias transiciones de fase interesantes. Un algoritmo numérico fue desarrollado para seleccionar los mejores parámetros experimentales correspondientes a una instancia particular del modelo ANNNI.

Part VI

Supplementary Material

Appendix A

Structural phases in ion crystals

In this appendix we explain how the structural phases corresponding to 1D, 2D and 3D structures employed in Chapter 9 were defined. First we present details about the method used to find the equilibrium configuration of the ion crystals. We show how structural phase transitions can be determined and use them to define which are the trap parameters and number of ions needed to obtain the different structures.

We consider a linear Paul trap with an effective potential that is harmonic in all directions. The potential energy including Coulomb repulsion and the effective trap potential for a system of N ions with mass m and charge Q is:

$$V = \frac{m}{2}\sum_{i=1}^{N}\omega_x^2 x_i^2 + \omega_y^2 y_i^2 + \omega_z^2 z_i^2 + \frac{1}{2}\sum_{i=1}^{N}\sum_{j\neq i}\frac{Q^2}{|\bar{r}_i - \bar{r}_j|}, \tag{A.1}$$

where $\bar{r}_i = (x_i, y_i, z_i)$ is the position of the ion i measured from the minimum of the trap potential. The angular frequencies of the harmonic potential are ω_x, ω_y and ω_z. We rewrite the energy in terms of the parameters $\alpha_x = \omega_x/\omega_z$, $\alpha_y = \omega_y/\omega_z$ and $q^2 = Q^2/(m\omega_z^2)$:

$$V = \frac{m\omega_z^2}{2}\sum_{i=1}^{N}\left(\alpha_x^2 x_i^2 + \alpha_y^2 y_i^2 + z_i^2 + \sum_{j\neq i}^{N}\frac{q^2}{|\bar{r}_i - \bar{r}_j|}\right). \tag{A.2}$$

It is clear from this expression that the equilibrium configuration of the N ions will only depend on the parameters N, α_x, α_y and q. We will only consider the case of a trap with cylindrical symmetry, i.e, $\alpha_x = \alpha_y = \alpha$. A length scale is fixed by setting $q^2 = 1$. Thus, the equilibrium structure is completely determined by N and α, apart from a scaling in the position of all the ions (this scaling can be performed by varying ω_z while keeping α to a constant value).

The determination of $3N$ coordinates $\{(x_i, y_i, z_i)\}$ that correspond to a global minimum of the energy is a hard problem that even for small values of N can only be treated numerically. A typical approach to find a global minimum would be to use some gradient-descent algorithm combined with some strategy to avoid local minima. We decided to use a simpler solution based on the differential evolution algorithm [129]. This algorithm does not use gradient information, although it can be taken into account in a very simple way to improve both convergence and the quality of the solution. This method enable us to determine equilibrium configurations of crystals with more than 200 ions (600 degrees of freedom) in a modest personal computer.

As is well known, the ion crystals studied here present structural phase transitions as the trap parameters or the number of ions are changed [82]. We will use these phase

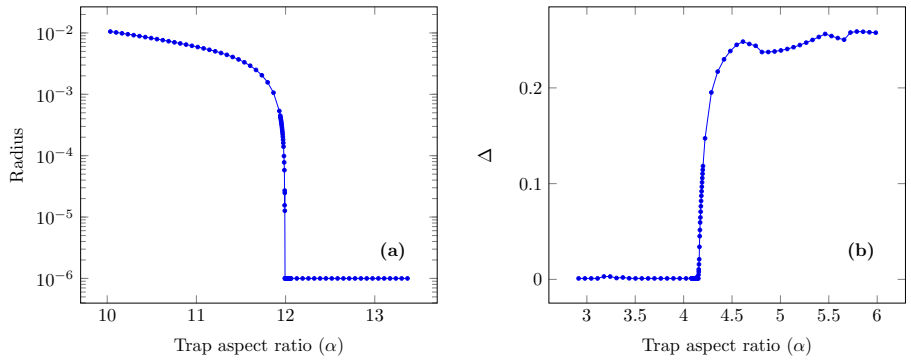

Figure A.1: (a)Radius of a chain of 30 ions as the trap aspect ratio is decreased. Transition from 1D to 2D structures. (b)Minimum longitudinal separations of the ions (Δ) as the aspect ratio is decreased.

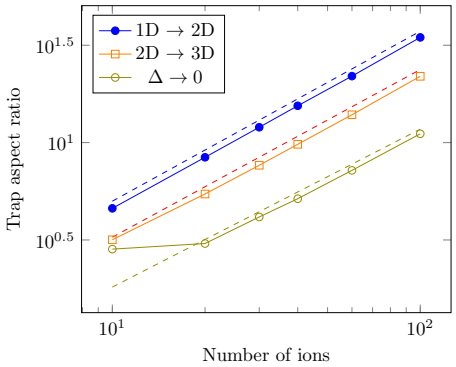

Figure A.2: Transition points for several numbers of ions.

transitions to define 'structural phases' in the parameter space spawned by α and N. As an example, Figure A.1-a shows the transition from a 1D linear configuration to a 2D zig-zag configuration in a chain of 30 ions as the transverse trapping potential is relaxed (α is decreased). In this case the order parameter is the chain radius defined as $R = \max_{1\leq i\leq N}\{\sqrt{x_i^2 + y_i^2}\}$. In a similar way it is possible to measure the transition from 2D configurations to 3D helical configurations [82]. Another phase transition occurs if the trap aspect ratio continues to decrease: beyond some point, the ions in the equilibrium configuration can no longer be ordered according to their z coordinate, i.e, $z_i \simeq z_j$ for one or more pairs of ions. It is possible to detect this phase transition by measuring the order parameter $\Delta = \min_{1\leq i,j\leq N(i\neq j)}\{|z_i - z_j|\}$, as shown in Figure A.1-b.

The transition points for chains with different numbers of ions are shown in Figure A.2. As noted in [82], the relation of the critical values of α with the number of ions is well approximated (for $N > 20$) by a simple power law: $\alpha_c \propto N^{\beta}$. We estimated the exponent β for each transition. Therefore, we can define power laws $\alpha = cN^{\beta}$ with the same exponent β but choosing c so that the power laws are sub-critical. The resulting power laws are shown with dashed lines in Figure A.2. These paths in parameter space define 'structural phases', in the sense that they determine a family of crystals with similar structural properties. In table A.1 we give the values of c and β we used to generate 1D, 2D and 3D structures with different number of ions.

	c	β
1D	0.67	0.873
2D	0.44	0.861
3D	0.28	0.811

Table A.1: Coefficients of the power laws used to generate crystal structures of different dimensionality.

Appendix B

Integration techniques for undriven systems

B.1 Green's function and the cubic eigenvalue problem

In this appendix we present a semi-analytical technique to perform the frequency integrals that give the covariance matrix and the heat currents in the asymptotic state for the case of undriven systems connected to ohmic thermal reservoirs.

We consider the particular case in which all the environments are Ohmic and have the same cutoff, i.e, when all the spectral densities are $I_l(\omega) = \frac{2}{\pi}\gamma_0 P_l \omega \Lambda^2/(\Lambda^2+\omega^2)$. In this case, the Laplace transform of the dissipation kernel is $\hat{\gamma}(s) = \gamma_0 \frac{\Lambda}{s+\Lambda}\sum_l P_l$. Then, it is straightforawrd to see that the Laplace transform of the Green's function can be expressed as

$$\hat{g}(s) = (s+\Lambda)\, h(s)^{-1}, \tag{B.1}$$

where $h(s)$ is an $K \times K$ matrix (K is the number of oscillators in the system) which depends polynomically on s and satisfies

$$h(s) = s^3 M + s^2 \Lambda M + s(V + \Delta V) + \Lambda(V - \Delta V). \tag{B.2}$$

where $\Delta V = \gamma_0 \Lambda \sum_l P_l$. Therefore, to compute $\hat{G}(s)$ one needs to obtain $h(s)^{-1}$ and for this purpose we need to invert the cubic matrix polynomial that defines $h(s)$. The inversion of such matrix is related to the solution of the cubic eigenvalue problem defined by $h(s)$. The cubic eigenvalue problem consists in finding the generalized eigenvalues $\{s_\alpha\}$ and eigenvectors $\{r_\alpha\}$ that satisfy the equations:

$$\det(h(s_\alpha)) = 0 \quad \text{and} \quad h(s_\alpha) r_\alpha = 0. \tag{B.3}$$

As $\det(h(s))$ is a $3K$ degree polynomial in s, it has $3K$ complex roots $\{s_\alpha\}$. Moreover, as the matrix coefficients appearing in $h(s)$ are real, the eigenvalues $\{s_\alpha\}$ come in complex conjugate pairs. We now show that $h(s)^{-1}$ can be expressed in a simple way in terms of the eigenvalues and eigenvectors $\{s_\alpha\}$ and $\{r_\alpha\}$.

The first step in our derivation is to show that the previous cubic eigenvalue problem can be cast as a linear one. For this we generalize the technique used in [109] to linearize the quadratic eigenvalue problem. First, we note that Eq. (B.3) can be rewritten as:

$$(s_\alpha B - A) \begin{bmatrix} r_\alpha \\ s_\alpha r_\alpha \\ s_\alpha^2 r_\alpha \end{bmatrix} = 0 \tag{B.4}$$

where the $3K \times 3K$ matrices A and B are :

$$A = \begin{bmatrix} 0 & C_1 & 0 \\ 0 & 0 & C_2 \\ -\Lambda V_- & -V_+ & -\Lambda M \end{bmatrix} \quad B = \begin{bmatrix} C_1 & 0 & 0 \\ 0 & C_2 & 0 \\ 0 & 0 & M \end{bmatrix} \tag{B.5}$$

Here, $V_\pm = V \pm \Delta V$ while C_1 and C_2 are arbitrary invertible matrices. Below, we will choose $C_1 = C_2 = \mathbb{1}$, a choice that ensures that B is positive definite.

The equivalence between Eq. (B.3) and Eq. (B.4) can be verified by a direct calculation. Other choices for A and B are possible. In summary, so far we proved that the generalized eigenvalues s_α are simply the eigenvalues of the linear problem defined by A and B while the generalized eigenvectors r_α can be obtained as the first K components of the eigenvectors of the same linear problem.

The relation between the cubic and linear problems becomes more transparent by noticing the following identity:

$$\begin{bmatrix} h(s) & & \\ & \mathbb{1} & \\ & & \mathbb{1} \end{bmatrix} = E(s)(sB - A)F(s) \tag{B.6}$$

where $E(s)$ and $F(s)$ are:

$$\begin{aligned} E(s) &= \begin{bmatrix} V_+ + s(\Lambda + s)M & (\Lambda + s)M & \mathbb{1} \\ -\mathbb{1} & 0 & 0 \\ 0 & -\mathbb{1} & 0 \end{bmatrix} \\ F(s) &= \begin{bmatrix} \mathbb{1} & 0 & 0 \\ s\mathbb{1} & \mathbb{1} & 0 \\ s^2\mathbb{1} & s\mathbb{1} & \mathbb{1} \end{bmatrix} \end{aligned} \tag{B.7}$$

Note that $E(s)$ and $F(s)$ are polynomial matrices on s but nevertheless their determinant is constant and equal to 1. Therefore $\det(h(s)) = \det(sB - A)$, i.e, the characteristic polynomials of the cubic and linear problems are the same and consequently their eigenvalues match.

The inversion of Eq. (B.6) leads to the following expression for $h(s)^{-1}$:

$$h(s)^{-1} = \begin{bmatrix} \mathbb{1} & 0 & 0 \end{bmatrix} F(s)^{-1}(sB - A)^{-1}E(s)^{-1} \begin{bmatrix} \mathbb{1} \\ 0 \\ 0 \end{bmatrix} \tag{B.8}$$

Since $E(s)^{-1}$ and $F(s)^{-1}$ can be readily calculated from Eq. (B.7) it is easy to see that Eq. (B.8) can be transformed into:

$$h(s)^{-1} = \begin{bmatrix} \mathbb{1} & 0 & 0 \end{bmatrix} (sB - A)^{-1} \begin{bmatrix} 0 \\ 0 \\ \mathbb{1} \end{bmatrix} \tag{B.9}$$

We assume that the matrix $M = sB - A$ is indeed invertible and that we can find matrices L and R such that $L^\dagger BR = \mathbb{1}$ and $L^\dagger AR = S$, where $S_{\alpha,\beta} = s_\alpha \delta_{\alpha,\beta}$. As A is not symmetric, this assumption is not trivial (when A is not diagonalizable, S has a Jordan normal form, a case that will not be treated here as all physically relevant situations can be studied under the above assumption). For simplicity, we also assume that all eigenvalues are non-degenerate (this can be easily relaxed). Then, we can write

$$(sB - A)^{-1} = R(s\mathbb{1} - S)L^\dagger \tag{B.10}$$

and consequently:

$$h(s)^{-1} = \begin{bmatrix} \mathbb{1} & 0 & 0 \end{bmatrix} R(s\mathbb{1} - S)^{-1} L^{\dagger} \begin{bmatrix} 0 \\ 0 \\ \mathbb{1} \end{bmatrix} = \sum_{\alpha=1}^{3K} \frac{r_\alpha l_\alpha^{\dagger}}{s - s_\alpha} \tag{B.11}$$

The last identity contains the important result. In such equation, the K component vector r_α is obtained by the first K components of the α-th column of R. Similarly, the K component vector l_α is formed with the last K components of the α–th column of L. The columns of R and L are just the right and left eigenvectors of A. In this way we have expressed the Laplace transform of the non-equilibrium Green's function of a system with K degrees of freedom in terms of the eigenvalues and eigenvectors of a linear problem of size $3K \times 3K$.

B.2 Frequency integrals for the covariance matrix and heat currents

The result we obtained above is useful to compute the covariance matrix and, in this way, fully determine the stationary state of the network. However, for this purpose we still need to perform the frequency integrals appearing in Eq. 9.5. First, it is useful to notice that for Ohmic environments with the same cutoff Λ, we can write $\hat{g}(i\omega)\hat{\nu}(w)\hat{g}(-i\omega) = \frac{2}{\pi}\gamma_0\Lambda^2 h(i\omega)^{-1}A(\omega)h(-i\omega)^{-1}$ with $A(\omega) = \omega\sum_l P_l \coth(\frac{\omega}{2T_l})$. Therefore Eq. (9.5) can be rewritten as :

$$\sigma^{(n,m)} = \frac{2}{\pi}\gamma_0\Lambda^2 \int_0^{\infty} Re\left[\omega^{n+m} i^{n-m} h(i\omega)^{-1} A(\omega) h(-i\omega)^{-1}\right] d\omega \tag{B.12}$$

Let us now analyze the properties of the function $f_{n,m}(\omega) = Re\left[\omega^{n+m} i^{n-m} h(i\omega)^{-1} A(\omega) h(-i\omega)^{-1}\right]$ (where $m, n = 0, 1$). This function is such that:

- $f_{n,m}(\omega)$ is an even function of ω.
- $\omega f_{n,m}(\omega) \to 0$ for $|\omega| \to \infty$
- $f_{n,m}(\omega)$ is analytic in all the complex plane with the exception of the poles of $\hat{h}^{-1}(i\omega)$, $\hat{h}^{-1}(-i\omega)$, and $A(\omega)$.

Since the integrand is an even function of ω we can extend the integral appearing in Eq. (B.12) to negative values of ω:

$$\sigma^{(n,m)} = \frac{\gamma_0\Lambda^2}{\pi} \int_{-\infty}^{\infty} f_{n,m}(\omega) d\omega \tag{B.13}$$

The integrand has simple poles at the points $\omega_\alpha = -is_\alpha$ and $\omega_\alpha = is_\alpha$ (poles of $h(i\omega)$ and $h(-i\omega)$, respectively). The poles of $h(i\omega)$ are always in the upper half-plane. Also, the integrand has infinite simple poles at the points $\{\pm i\omega_{n,l}, n \in \mathbb{N}\}$, where $\omega_{n,l} = n\pi 2T_l$ are the Matsubara frequencies corresponding to the temperature T_l. As explained in [130], the proper way to deal with the poles at the points $\{i\omega_{n,l}\}$ is to use the following indentity:

$$\coth\left(\frac{\omega}{2T}\right) = \frac{2T}{\omega} - \frac{1}{i\pi}\psi\left(1 - \frac{i\omega}{2\pi T}\right) + \frac{1}{i\pi}\psi\left(1 + \frac{i\omega}{2\pi T}\right), \tag{B.14}$$

where ψ is the digamma function. Using Eq. B.14 the function $A(\omega)$ can be written as:

$$A(\omega) = A_H(\omega) - A_L(\omega) - A_L(-\omega), \tag{B.15}$$

where:

$$\begin{aligned} A_H(\omega) &= \sum_l 2T_l P_l \\ A_L(\omega) &= \frac{\omega}{i\pi} \sum_l P_l \psi\left(1 - \frac{i\omega}{2\pi T_l}\right). \end{aligned} \tag{B.16}$$

The decomposition of Eq. (B.15) is useful because $A_H(\omega)$ (which correspond to the high temperature approximation) is only a constant and $A_L(\omega)$ is analytic in the upper half-plane. Inserting Eq. (B.15) into the integral of Eq. (B.13) the following expression is obtained:

$$\sigma^{(n,m)} = \sigma_H^{(n,m)} - \left(\sigma_L^{(n,m)} + (-1)^{n+m}\left[\sigma_L^{(n,m)}\right]^T\right), \tag{B.17}$$

where

$$\sigma_{H/L}^{(n,m)} = \frac{\gamma_0\Lambda^2}{\pi} Re\left[\int_{-\infty}^{\infty} (i\omega)^n(-i\omega)^m h(i\omega)^{-1} A_{H/L}(\omega) h(-i\omega)^{-1}\right] \tag{B.18}$$

Now, the integrand of the previous expression is analytic in the complex plane with the only exception of the poles of $h^{-1}(i\omega)$. Since $h^{-1}(\omega) \propto \omega^{-3}$ for $|\omega| \to \infty$ it is possible to choose a closed integration path in the complex plane such that the contribution at inifinity vanishes, and that only encloses the poles of $h(i\omega)^{-1}$. This is depicted in Fig. B.1. It is thus possible to evaluate the integral of Eq. B.18 using the residue theorem. The residue of $h(i\omega)^{-1}$ at the pole $\omega_\alpha = -is_\alpha$ is $-ir_\alpha l_\alpha^\dagger$, therefore:

$$\frac{\pi}{\gamma_0\Lambda^2}\sigma_{H/L}^{(n,m)} = Re\left[\sum_{\alpha=1}^{3K} (i\omega_\alpha)^n(-i\omega_\alpha)^m(-ir_\alpha l_\alpha^\dagger) A_{H/L}(\omega_\alpha) h^{-1}(-i\omega_\alpha)\right] \tag{B.19}$$

At this point the spectral decomposition of Eq. B.11 can be used to expand $h^{-1}(-i\omega)$. In this way we arrive at our final result:

$$\sigma_{H,L}^{(n,m)} = 2\gamma_0\Lambda^2 Re\left[i^{n-m+1}\sum_{\alpha,\beta=1}^{3K} \omega_\alpha^{n+m} \frac{l_\alpha^\dagger A_{H,L}(\omega_\alpha) r_\beta}{\omega_\alpha + \omega_\beta} r_\alpha l_\beta^\dagger\right]. \tag{B.20}$$

Therefore, we have expressed the asymptotic covariance matrix of the system (which fully characterize the asymptotic state) in terms of the complex eigenvalues and eigenvectors of a linear problem.

One possible way to obtain the heat currents is to use the position-momentum covariance matrix $\sigma^{(0,1)}$ and then evaluate the heat current of the l-th reservoir as $\dot{Q}_l = Tr(P_l V_R \sigma^{(0,1)})$. Another possibility is to solve the integral in Eq. (9.3) using the same ideas as before. We find that $\dot{Q}_l = \sum_{l' \neq l} \dot{q}_{l,l'}$, with:

$$\dot{q}_{l,l'} = \left[2\gamma_0\Lambda^2\right]^2 \sum_{\substack{\alpha,\beta=1 \\ \omega_\alpha \neq i\Lambda}}^{3K} \frac{\omega_\alpha^3 \Delta_{l,l'}(\omega_\alpha)}{\omega_\alpha^2 + \Lambda^2} \frac{(l_\beta^\dagger P_l r_\alpha)(l_\alpha^\dagger P_{l'} r_\beta)}{\omega_\alpha + \omega_\beta}, . \tag{B.21}$$

where:

$$\Delta_{l,l'}(\omega) = i\frac{2(T_l - T_{l'})}{\omega} - -\frac{2}{\pi}\left[\psi\left(1 - \frac{i\omega}{2\pi T_l}\right) - \psi\left(1 - \frac{i\omega}{2\pi T_{l'}}\right)\right] \tag{B.22}$$

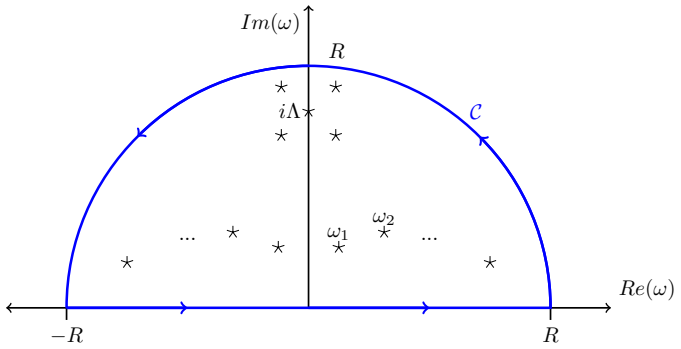

Figure B.1: Integration path and poles of $h(i\omega)$.

Note that in Eq. (B.21) the index α does not run over the poles equal to $i\Lambda$. The contribution of these poles vanishes if there are no environments in contact with the same sites of the network, i.e, if $P_l P_l' = 0$ for $l \neq l'$. This was assumed in the derivation of Eq. B.21. Another assumption of the previous results is that there are no poles $\omega_\alpha = -is_\alpha$ with null imaginary part. This is equivalent to assume that all the normal modes of the system suffer dissipation. If some normal models are not in effective contact with the environments and do not suffer dissipation then they can be treated independently as free oscillators. In that case the asymptotic state will be time dependent, and will conserve information about the initial state of the system.

To finish this section we discuss the typical distribution of poles. It is easy to see that if $rank(\sum_l P_l) < K$ then $i\Lambda$ will be a pole of $h(i\omega)$. This is because $h(-\Lambda) = -2\gamma_0\Lambda^2 \sum_l P_l$ and if $\sum_l P_l$ is not full-rank then $\det(h(-\Lambda)) = 0$. Furthermore, the multiplicity of this root will be $K - rank(\sum_l P_L)$. For moderate coupling γ_0 there are another $rank(\sum_l P_l)$ poles close to $i\Lambda$ but with nonzero real part. A typical distribution of poles is depicted in Fig. B.1.

Appendix C

Weak coupling approximation, minimum cooling temperature, and numerical evaluation of the heat rates

C.1 Weak coupling approximation

In the weak coupling regime the frequency integrals in Eq. (6.26) involving the heat transfer matrix can be approximated by sums over the normal modes of the closed system. To see that we need an analytic expression for the coefficients $A_k(\omega, \omega_d)$. Thus, we employ the weak driving approximation of Eq. (5.22b), which gives the solution for those coefficients in terms of the Laplace's transform of the Green's function $\hat{g}(i\omega)$. As explained in [131], in the weak coupling limit $\hat{g}(i\omega)$ can be approximated as

$$\hat{g}(i\omega) = \sum_a \frac{q_a q_a^T}{\Omega_a^2 - (w - i\Gamma_a)^2} \tag{C.1}$$

where $\{\Omega_a\}$ and $\{q_a\}$ are the normal frequencies and modes of the closed system and Γ_a is the dissipation rate of each normal mode. We assume for simplicity that the system is not degenerated. As an example, we write the expression for $p^{(k)}_{\alpha,\beta}(\omega)$ using the previous approximations (for $k \neq 0$):

$$p^{(k)}_{\alpha,\beta}(\omega) = \frac{\pi}{2} \sum_{a,b,c,d} \frac{(q_a^T V_k q_b)(q_d^T V_k^\dagger q_c)(q_c^T I_\alpha(|\omega + k\omega_d|) q_a)(q_b^T I_\beta(\omega) q_c)}{(\Omega_a^2 - (\omega + k\omega_d - i\Gamma_a)^2)(\Omega_b^2 - (\omega - i\Gamma_b)^2)(\Omega_c^2 - (\omega + k\omega_d + i\Gamma_c)^2)(\Omega_d^2 - (\omega + i\Gamma_d)^2)} \tag{C.2}$$

In the weak coupling limit where $\Gamma_a \ll \Omega_a, \omega_d$ and under the condition $\omega_d < \min_{\Omega_a \neq \Omega_b}\{|\Omega_a - \Omega_b|/2\}$ the typical shape of the functions $p^{(k)}_{\alpha,\beta}(\omega)$ is like the one depicted in figure C.1. We see the expected resonances at frequencies $\{\Omega_a\}$ and $\{\Omega_a - k\omega_d\}$, which for the mentioned conditions are well defined and do not overlay. Therefore, an approximate solution for integrals of the form $\int_0^\infty p^{(k)}_{\alpha,\beta}(\omega) N(\omega)$ can be obtained by dealing separately with each resonance peak, evaluating the remaining factors at the center of the peak. It is clear that the dominant terms are those with $\Omega_c = \Omega_a$ and $\Omega_d = \Omega_b$. Also, for low temperatures the Planck distribution $N(\omega)$ exponentially supresses high frequencies, and therefore the dominant contribution to the integral is given by the peak at $\omega = \Omega_0 - k\omega_d$, where Ω_0 is

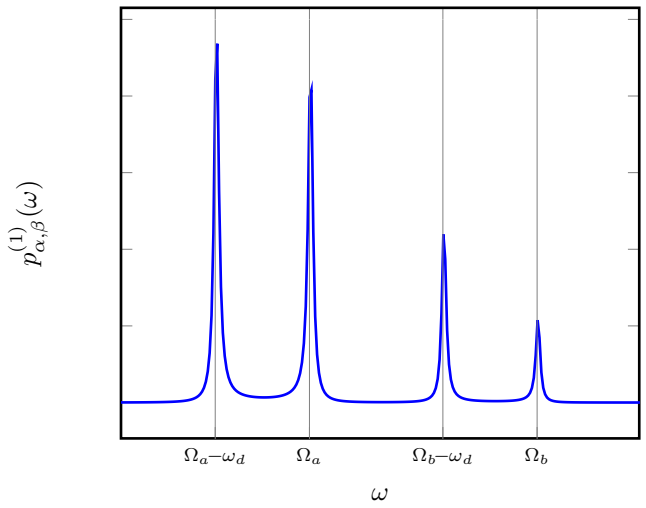

Figure C.1: Typical shape of the function $p^{(1)}_{\alpha,\beta}(\omega)$ in the weak coupling limit

the smallest normal frequency of the system. Using this method the following expression is found:

$$\int_0^\infty d\omega\; p^{(k)}_{\alpha,\beta}(\omega)N(\omega) \simeq \frac{\pi^2}{8}\frac{N(\Omega_0-k\omega_d)}{\Omega_0^2\Gamma_0}\sum_{b,c}\frac{(q_0^tV_kq_b)(q_b^tV_k^\dagger q_c)(q_b^tI_\beta(\Omega_a-k\omega_d)q_c)(q_0^tI_\alpha(\Omega_a)q_0)}{(\Omega_b^2-(\Omega_0-k\omega_d)^2)(\Omega_c^2-(\Omega_0-k\omega_d)^2)} \tag{C.3}$$

Note that this expression is invariant upon time inversion of the process (i.e, invariant under complex conjugation of the Fourier coefficients V_k). We now use the previous result to calculate the resonant contributions to the heat rates for the simple driving protocol $V(t) = V_0 + 2V_1\cos(\omega_d t)$ in a system connected to only two reservoirs, E_α and E_β, which are at the same temperature T_0. Considering, for simplicity, only the contribution of the Ω_0 normal mode, we have:

$$\begin{aligned}\dot{\bar{Q}}^R_\alpha = \dot{\bar{Q}}^{RP}_\alpha + \dot{\bar{Q}}^{RH}_\alpha = \frac{\pi^2}{8}\frac{N(\Omega_0-\omega_d)}{\Omega_0^2\Gamma_0}\frac{|V_1^0|^2}{(\Omega_0^2-(\Omega_0-\omega_d)^2)^2}\\ \times\left\{(\Omega_0-\omega_d)I^0_\beta(\Omega_0)I^0_\alpha(\Omega_0-\omega_d) - \Omega_0 I^0_\alpha(\Omega_0)I^0_\beta(\Omega_0-\omega_d) - k\omega_d I^0_\alpha(\Omega_0)I^0_\alpha(\Omega_0-\omega_d)\right\},\end{aligned} \tag{C.4}$$

where we have defined $M^0 = q_0^tMq_0$ for any matrix M. It is easy to see that if the two reservoirs are spectrally equivalent (if $I_\alpha(\omega) = I_\beta(\omega)$), then the previous expression is always negative and therefore both reservoirs are heated. However, if the spectral densities satisfy $I_\alpha(\Omega_0) \ll I_\beta(\Omega_0)$ then the last two terms between brackets in the previous expression can be neglected with respect to the first, and $\dot{\bar{Q}}^R$ becomes positive. Therefore, the condition $I_\alpha(\Omega_0) \ll I_\beta(\Omega_0)$ allows cooling of the reservoir E_α.

C.2 Minimum temperature

For low temperatures the Planck distribution in Eq. (C.4) can be approximated by $N(\Omega_0-\omega_d) \simeq e^{-(\Omega_0-\omega_d)/T_0}$, which vanishes faster than any power law as $T_0 \to 0$. This strong dependence for low temperatures makes it imposible to reach zero temperature in finite time. However, as explained in the main text, this effect can be avoided by

instantaneously adjusting the driving frequency ω_d as T_0 decreases, in such a way that $\Omega_0 - \omega_d \simeq T_0$. If we assume that $I_\alpha(\omega) \propto \gamma_0 \omega^{\lambda_\alpha}$ for low frequencies, then it is clear that the resonant heat rate in Eq. (C.4) scales as $\dot{Q}_\alpha^R \propto \gamma_0(\Omega_0 - \omega_d)^{1+\lambda_\alpha}$ (the factor $I_\beta(\Omega_0)/\Gamma_0$ is independent of the coupling constant between the system and reservoir E_β). Thus, for the mentioned adaptative strategy, we have $\dot{Q}_\alpha^{\mathrm{R}} \propto \gamma_0 T_0^{1+\lambda_\alpha}$. On the other hand, it can be seen from Eq. (6.30) that for $\omega_d < \Omega_0$ the non resonant heating $\dot{Q}_\alpha^{\mathrm{NRH}}$ is proportional to γ_0^2 (since the integration domain does not include any resonance peak of the function $p_{\alpha,\beta}^{-1}(\omega)$). Also, for low driving frequency ω_d it scales as $\omega_d^{2+2\lambda_\alpha}$. Thus, for the adaptative strategy, we obtain $\dot{Q}_\alpha^{\mathrm{NRH}} \propto \gamma_0^2(\Omega_0 - T_0)^{2+2\lambda_\alpha}$.

Therefore, we see that there always exists a temperature T_{min} below which $|\dot{Q}_\alpha^{\mathrm{NRH}}| > \dot{Q}_\alpha^{\mathrm{R}}$ and the net effect is to heat up the reservoir E_α. Also, this minimum temperature scales as $T_{min} \propto \gamma_0^{1/(1+\lambda_\alpha)}$ (for $T_{min} \ll \Omega_0$).

C.3 Numerical evaluation of the heat rates for a simple case

In order to test the last result we evaluated numerically the heat rates in a particular case. We consider a system composed of a single harmonic oscillator of bare frequency Ω_0 coupled to two reservoirs, E_α and E_β, with spectral densities given by:

$$\begin{aligned} I_\alpha(\omega) &= \gamma_\alpha\, \omega^{\lambda_\alpha}\, (\Omega_0 - \omega)\, \theta((\omega - \Lambda_\alpha)/r_\alpha) \qquad\qquad (\omega < \Omega_0) \\ I_\beta(\omega) &= \gamma_\beta\, \omega^{\lambda_\beta}\, \theta((\omega - \Lambda_\beta)/r_\beta) \end{aligned} \tag{C.5}$$

where $\theta(x) = e^{-x}/(1+e^{-x})$ is an exponential cutoff. Note that $I_\alpha(\omega)$ vanishes at $\omega = \Omega_0$. In this way, the cooling condition $I_\alpha(\Omega_0) \ll I_\beta(\Omega_0)$ is exact. In particular, we choose the parameters $\gamma_\beta = \gamma_0$, $\gamma_\alpha = 0.7\gamma_0$ (where γ_0 is a coupling constant that will be varied), $\Lambda_\alpha = 0.9$, $\Lambda_\beta = 1.2$,$r_\alpha = 0.04$, $r_\beta = 0.1$ (all this parameters are in units of Ω_0). In figure C.2 we show the spectral densities for the case in which both are ohmic ($\lambda_\alpha = \lambda_\beta = 1$).

For these spectral densities, the contributions $\dot{Q}_\alpha^{\mathrm{NRH}}$ and $\dot{Q}_\alpha^{\mathrm{R}} = \dot{Q}_\alpha^{\mathrm{RP}} + \dot{Q}_\alpha^{\mathrm{RH}}$ to the heat rates are calculated by numerical integration of the expressions given in Eqs. (4), (5), and (6) in the main text (under the weak driving approximation). As an example, we plot in Figure C.3 these resonant and non-resonant contributions (in absolute value) versus the common temperature T_0, for two different values of the coupling constant γ_0. These results corresponds to the adaptative strategy for which the driving frequency is selected as $\omega_d = \Omega_0 - T_0$. We see that $\dot{Q}_\alpha^{\mathrm{NRH}}$ scales as γ_0^2 while $\dot{Q}_\alpha^{\mathrm{R}}$ scales as γ_0. The temperature for which $\dot{Q}_\alpha^{\mathrm{NRH}}$ and $\dot{Q}_\alpha^{\mathrm{R}}$ become equal is the minimum temperature T_{min} for which the adaptative strategy supports cooling of reservoir E_α. The dependence of T_{min} with the coupling constant γ_0 is shown in Figure 1 in the main text for $\lambda_\alpha = 1$ and $\lambda_\alpha = 2$ and is found to be well described by the power law discussed above.

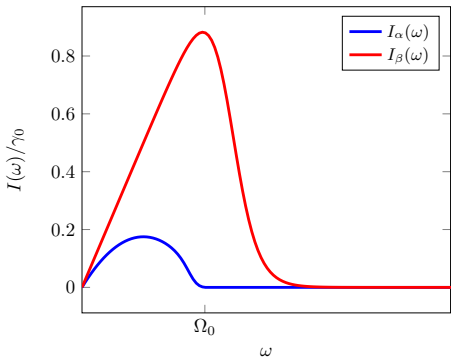

Figure C.2: Spectral densities used for the numerical evalution of the heat rates ($\lambda_\alpha = \lambda_\beta = 1$). They exactly satisfy the cooling condition $I_\alpha(\Omega_0) \ll I_\beta(\Omega_0)$.

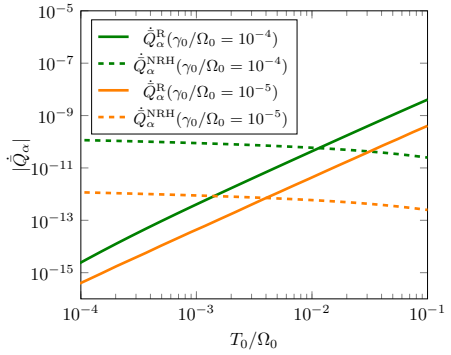

Figure C.3: Resonant and non-resonant contributions to the total heat rate $\dot{\bar{Q}}_\alpha$. The driving frequency is $\omega_d = \Omega_0 - T_0$ and $\lambda_\alpha = 1$.

Bibliography

[1] Michael A Nielsen and Isaac Chuang. Quantum computation and quantum information, 2002.

[2] Richard P Feynman. Simulating physics with computers. *International journal of theoretical physics*, 21(6):467–488, 1982.

[3] Charles H Bennett and Gilles Brassard. Quantum cryptography: Public key distribution and coin tossing. *Theoretical computer science*, 560:7–11, 2014.

[4] Peter W Shor. Algorithms for quantum computation: Discrete logarithms and factoring. In *Foundations of Computer Science, 1994 Proceedings., 35th Annual Symposium on*, pages 124–134. IEEE, 1994.

[5] Hartmut Häffner, Christian F Roos, and Rainer Blatt. Quantum computing with trapped ions. *Physics reports*, 469(4):155–203, 2008.

[6] Rainer Blatt and CF Roos. Quantum simulations with trapped ions. *Nature Physics*, 8(4):277–284, 2012.

[7] Stephan Gulde, Mark Riebe, Gavin PT Lancaster, Christoph Becher, Jürgen Eschner, Hartmut Häffner, Ferdinand Schmidt-Kaler, Isaac L Chuang, and Rainer Blatt. Implementation of the deutsch–jozsa algorithm on an ion-trap quantum computer. *Nature*, 421(6918):48–50, 2003.

[8] Philipp Schindler, Julio T Barreiro, Thomas Monz, Volckmar Nebendahl, Daniel Nigg, Michael Chwalla, Markus Hennrich, and Rainer Blatt. Experimental repetitive quantum error correction. *Science*, 332(6033):1059–1061, 2011.

[9] Thomas Monz, Daniel Nigg, Esteban A Martinez, Matthias F Brandl, Philipp Schindler, Richard Rines, Shannon X Wang, Isaac L Chuang, and Rainer Blatt. Realization of a scalable shor algorithm. *Science*, 351(6277):1068–1070, 2016.

[10] Esteban A Martinez, Christine A Muschik, Philipp Schindler, Daniel Nigg, Alexander Erhard, Markus Heyl, Philipp Hauke, Marcello Dalmonte, Thomas Monz, Peter Zoller, et al. Real-time dynamics of lattice gauge theories with a few-qubit quantum computer. *Nature*, 534(7608):516–519, 2016.

[11] Thomas Jennewein, Christoph Simon, Gregor Weihs, Harald Weinfurter, and Anton Zeilinger. Quantum cryptography with entangled photons. *Physical Review Letters*, 84(20):4729, 2000.

[12] Stefano Pirandola, Jens Eisert, Christian Weedbrook, Akira Furusawa, and Samuel L Braunstein. Advances in quantum teleportation. *Nature photonics*, 9(10):641–652, 2015.

[13] Marcelo Alejandro Luda, Miguel Antonio Larotonda, Juan Pablo Paz, and Christian Tomás Schmiegelow. Manipulating transverse modes of photons for quantum cryptography. *Physical Review A*, 89(4):042325, 2014.

[14] Laura T Knoll, Christian T Schmiegelow, and Miguel A Larotonda. Noisy quantum teleportation: An experimental study on the influence of local environments. *Physical Review A*, 90(4):042332, 2014.

[15] Wikipedia. Quantum key distribution — Wikipedia, the free encyclopedia, 2004. [Online; accessed 29-January-2017].

[16] Elizabeth Gibney. Chinese satellite is one giant step for the quantum internet. *Nature*, 535(7613):478–479, 2016.

[17] Rami Barends, Alireza Shabani, Lucas Lamata, Julian Kelly, Antonio Mezzacapo, Urtzi Las Heras, Ryan Babbush, AG Fowler, Brooks Campbell, Yu Chen, et al. Digitized adiabatic quantum computing with a superconducting circuit. *Nature*, 534(7606):222–226, 2016.

[18] Andrew A Houck, Hakan E Türeci, and Jens Koch. On-chip quantum simulation with superconducting circuits. *Nature Physics*, 8(4):292–299, 2012.

[19] Michel H Devoret and Robert J Schoelkopf. Superconducting circuits for quantum information: an outlook. *Science*, 339(6124):1169–1174, 2013.

[20] IBM. The ibm quantum experience. [Online; accessed 29-January-2017].

[21] IM Georgescu, S Ashhab, and Franco Nori. Quantum simulation. *Reviews of Modern Physics*, 86(1):153, 2014.

[22] Kihwan Kim, M-S Chang, S Korenblit, R Islam, EE Edwards, JK Freericks, G-D Lin, L-M Duan, and C Monroe. Quantum simulation of frustrated ising spins with trapped ions. *Nature*, 465(7298):590–593, 2010.

[23] K Kim, S Korenblit, R Islam, EE Edwards, MS Chang, C Noh, H Carmichael, GD Lin, LM Duan, CC Joseph Wang, et al. Quantum simulation of the transverse ising model with trapped ions. *New Journal of Physics*, 13(10):105003, 2011.

[24] Troels F Rønnow, Zhihui Wang, Joshua Job, Sergio Boixo, Sergei V Isakov, David Wecker, John M Martinis, Daniel A Lidar, and Matthias Troyer. Defining and detecting quantum speedup. *Science*, 345(6195):420–424, 2014.

[25] Cecilia Cormick and Juan Pablo Paz. Observing different phases for the dynamics of entanglement in an ion trap. *Physical Review A*, 81(2):022306, 2010.

[26] D Marcos, P Rabl, E Rico, and P Zoller. Superconducting circuits for quantum simulation of dynamical gauge fields. *Physical review letters*, 111(11):110504, 2013.

[27] Jonathan Simon, Waseem S Bakr, Ruichao Ma, M Eric Tai, Philipp M Preiss, and Markus Greiner. Quantum simulation of antiferromagnetic spin chains in an optical lattice. *Nature*, 472(7343):307–312, 2011.

[28] Sai Vinjanampathy and Janet Anders. Quantum thermodynamics. *arXiv preprint arXiv:1508.06099*, 2015.

[29] Ronnie Kosloff. Quantum thermodynamics: a dynamical viewpoint. *Entropy*, 15(6):2100–2128, 2013.

[30] Edwin T Jaynes. Information theory and statistical mechanics. *Physical review*, 106(4):620, 1957.

[31] Rolf Landauer. Irreversibility and heat generation in the computing process. *IBM journal of research and development*, 5(3):183–191, 1961.

[32] Lidia Del Rio, Johan Åberg, Renato Renner, Oscar Dahlsten, and Vlatko Vedral. The thermodynamic meaning of negative entropy. *Nature*, 474(7349):61–63, 2011.

[33] John Goold, Marcus Huber, Arnau Riera, Lídia del Rio, and Paul Skrzypczyk. The role of quantum information in thermodynamics—a topical review. *Journal of Physics A: Mathematical and Theoretical*, 49(14):143001, 2016.

[34] Johannes Roßnagel, Samuel T Dawkins, Karl N Tolazzi, Obinna Abah, Eric Lutz, Ferdinand Schmidt-Kaler, and Kilian Singer. A single-atom heat engine. *Science*, 352(6283):325–329, 2016.

[35] Gerhard Huber, Ferdinand Schmidt-Kaler, Sebastian Deffner, and Eric Lutz. Employing trapped cold ions to verify the quantum jarzynski equality. *Physical review letters*, 101(7):070403, 2008.

[36] Shuoming An, Jing-Ning Zhang, Mark Um, Dingshun Lv, Yao Lu, Junhua Zhang, Zhang-Qi Yin, HT Quan, and Kihwan Kim. Experimental test of the quantum jarzynski equality with a trapped-ion system. *Nature Physics*, 2014.

[37] Jukka P Pekola. Towards quantum thermodynamics in electronic circuits. *Nature Physics*, 11(2):118–123, 2015.

[38] Marcos Rigol, Vanja Dunjko, and Maxim Olshanii. Thermalization and its mechanism for generic isolated quantum systems. *Nature*, 452(7189):854–858, 2008.

[39] Mari Carmen Bañuls, J Ignacio Cirac, and Matthew B Hastings. Strong and weak thermalization of infinite nonintegrable quantum systems. *Physical review letters*, 106(5):050405, 2011.

[40] Lorenzo Maccone. Quantum solution to the arrow-of-time dilemma. *Physical review letters*, 103(8):080401, 2009.

[41] Juan MR Parrondo, Christian Van den Broeck, and Ryoichi Kawai. Entropy production and the arrow of time. *New Journal of Physics*, 11(7):073008, 2009.

[42] Jonathan J Halliwell, Juan Pérez-Mercader, and Wojciech Hubert Zurek. *Physical origins of time asymmetry*. Cambridge University Press, 1996.

[43] Antoine Bérut, Artak Arakelyan, Artyom Petrosyan, Sergio Ciliberto, Raoul Dillenschneider, and Eric Lutz. Experimental verification of landauer/'s principle linking information and thermodynamics. *Nature*, 483(7388):187–189, 2012.

[44] Robert Alicki, Michał Horodecki, Paweł Horodecki, and Ryszard Horodecki. Thermodynamics of quantum information systems—hamiltonian description. *Open Systems & Information Dynamics*, 11(03):205–217, 2004.

[45] Sybren Ruurds De Groot and Peter Mazur. *Non-equilibrium thermodynamics*. Courier Corporation, 2013.

[46] Lars Onsager. Reciprocal relations in irreversible processes. i. *Physical review*, 37(4):405, 1931.

[47] Obinna Abah, Johannes Rossnagel, Georg Jacob, Sebastian Deffner, Ferdinand Schmidt-Kaler, Kilian Singer, and Eric Lutz. Single-ion heat engine at maximum power. *Physical review letters*, 109(20):203006, 2012.

[48] S Gustavsson, R Leturcq, B Simovič, R Schleser, T Ihn, P Studerus, K Ensslin, DC Driscoll, and AC Gossard. Counting statistics of single electron transport in a quantum dot. *Physical review letters*, 96(7):076605, 2006.

[49] Yasuhiro Utsumi, DS Golubev, Michael Marthaler, Keiji Saito, Toshimasa Fujisawa, and Gerd Schön. Bidirectional single-electron counting and the fluctuation theorem. *Physical Review B*, 81(12):125331, 2010.

[50] Michele Campisi, Peter Hänggi, and Peter Talkner. Colloquium: Quantum fluctuation relations: Foundations and applications. *Reviews of Modern Physics*, 83(3):771, 2011.

[51] Christopher Jarzynski. Nonequilibrium equality for free energy differences. *Physical Review Letters*, 78(14):2690, 1997.

[52] Peter Talkner and Peter Hänggi. The tasaki–crooks quantum fluctuation theorem. *Journal of Physics A: Mathematical and Theoretical*, 40(26):F569, 2007.

[53] Massimiliano Esposito, Upendra Harbola, and Shaul Mukamel. Nonequilibrium fluctuations, fluctuation theorems, and counting statistics in quantum systems. *Reviews of modern physics*, 81(4):1665, 2009.

[54] Fernando GSL Brandao, Michał Horodecki, Jonathan Oppenheim, Joseph M Renes, and Robert W Spekkens. Resource theory of quantum states out of thermal equilibrium. *Physical review letters*, 111(25):250404, 2013.

[55] Dominik Janzing, Pawel Wocjan, Robert Zeier, Rubino Geiss, and Th Beth. Thermodynamic cost of reliability and low temperatures: tightening landauer's principle and the second law. *International Journal of Theoretical Physics*, 39(12):2717–2753, 2000.

[56] Fernando Brandão, Michał Horodecki, Nelly Ng, Jonathan Oppenheim, and Stephanie Wehner. The second laws of quantum thermodynamics. *Proceedings of the National Academy of Sciences*, 112(11):3275–3279, 2015.

[57] Esteban A Martinez and Juan Pablo Paz. Dynamics and thermodynamics of linear quantum open systems. *Physical review letters*, 110(13):130406, 2013.

[58] Amikam Levy, Robert Alicki, and Ronnie Kosloff. Quantum refrigerators and the third law of thermodynamics. *Physical Review E*, 85(6):061126, 2012.

[59] Luis A Correa, José P Palao, Gerardo Adesso, and Daniel Alonso. Performance bound for quantum absorption refrigerators. *Physical Review E*, 87(4):042131, 2013.

[60] Heinz-Peter Breuer and Francesco Petruccione. *The theory of open quantum systems*. Oxford University Press on Demand, 2002.

[61] Amir O Caldeira and Anthony J Leggett. Path integral approach to quantum brownian motion. *Physica A: Statistical mechanics and its Applications*, 121(3):587–616, 1983.

[62] Bei Lok Hu, Juan Pablo Paz, and Yuhong Zhang. Quantum brownian motion in a general environment: Exact master equation with nonlocal dissipation and colored noise. *Physical Review D*, 45(8):2843, 1992.

[63] Juan Pablo Paz and Wojciech Hubert Zurek. Environment-induced decoherence and the transition from quantum to classical. In *Coherent atomic matter waves*, pages 533–614. Springer, 2001.

[64] Goran Lindblad. On the generators of quantum dynamical semigroups. *Communications in Mathematical Physics*, 48(2):119–130, 1976.

[65] Gaston Floquet. Sur les équations différentielles linéaires à coefficients périodiques. In *Annales scientifiques de l'École normale supérieure*, volume 12, pages 47–88, 1883.

[66] Gerald Teschl. *Ordinary differential equations and dynamical systems*, volume 140. American Mathematical Society Providence, RI, 2012.

[67] Francis J Poulin and Glenn R Flierl. The stochastic mathieu's equation. In *Proceedings of the Royal Society of London A: Mathematical, Physical and Engineering Sciences*, volume 464, pages 1885–1904. The Royal Society, 2008.

[68] Sigmund Kohler, Thomas Dittrich, and Peter Hänggi. Floquet-markovian description of the parametrically driven, dissipative harmonic quantum oscillator. *Physical Review E*, 55(1):300, 1997.

[69] Michal Kolář, David Gelbwaser-Klimovsky, Robert Alicki, and Gershon Kurizki. Quantum bath refrigeration towards absolute zero: Challenging the unattainability principle. *Physical review letters*, 109(9):090601, 2012.

[70] Armen E Allahverdyan, Karen V Hovhannisyan, and Guenter Mahler. Comment on "cooling by heating: Refrigeration powered by photons". *Physical review letters*, 109(24):248903, 2012.

[71] Bart Cleuren, Bob Rutten, and Christian Van den Broeck. Cooling by heating: Refrigeration powered by photons. *Physical review letters*, 108(12):120603, 2012.

[72] Jürgen Eschner, Giovanna Morigi, Ferdinand Schmidt-Kaler, and Rainer Blatt. Laser cooling of trapped ions. *JOSA B*, 20(5):1003–1015, 2003.

[73] MG Raizen, JM Gilligan, JC Bergquist, WM Itano, and DJ Wineland. Ionic crystals in a linear paul trap. *Physical Review A*, 45(9):6493, 1992.

[74] R. Blatt and D. Wineland. Entangled states of trapped atomic ions. *Nature*, 453(7198):1008–1015, 2008.

[75] H. Häffner, W. Hänsel, C. F. Roos, J. Benhelm, et al. Scalable multiparticle entanglement of trapped ions. *Nature*, 438(7068):643–646, 2005.

[76] R. Islam, C. Senko, W. C. Campbell, S. Korenblit, J. Smith, A. Lee, E. E. Edwards, C-CJ. Wang, J. K. Freericks, and C. Monroe. Emergence and frustration of magnetism with variable-range interactions in a quantum simulator. *Science*, 340(6132):583–587, 2013.

[77] K Pyka, J Keller, HL Partner, R Nigmatullin, T Burgermeister, DM Meier, K Kuhlmann, A Retzker, MB Plenio, WH Zurek, et al. Topological defect formation and spontaneous symmetry breaking in ion coulomb crystals. *Nature communications*, 4, 2013.

[78] T. Pruttivarasin, M. Ramm, I. Talukdar, A. Kreuter, and H. Häffner. Trapped ions in optical lattices for probing oscillator chain models. *New J. Phys.*, 13(7):075012, 2011.

[79] G. D. Lin and L. M. Duan. Equilibration and temperature distribution in a driven ion chain. *New J. Phys.*, 13(7):075015, 2011.

[80] A. Bermudez, M. Bruderer, and M. B. Plenio. Controlling and measuring quantum transport of heat in trapped-ion crystals. *Phys. Rev. Lett.*, 111(4):040601, 2013.

[81] D. Manzano, M. Tiersch, A. Asadian, and H. J. Briegel. Quantum transport efficiency and fourier's law. *Phys. Rev. E*, 86(6):061118, 2012.

[82] JP Schiffer. Phase transitions in anisotropically confined ionic crystals. *Physical review letters*, 70(6):818, 1993.

[83] Shmuel Fishman, Gabriele De Chiara, Tommaso Calarco, and Giovanna Morigi. Structural phase transitions in low-dimensional ion crystals. *Physical Review B*, 77(6):064111, 2008.

[84] Gabriele De Chiara, Adolfo del Campo, Giovanna Morigi, Martin B Plenio, and Alex Retzker. Spontaneous nucleation of structural defects in inhomogeneous ion chains. *New Journal of Physics*, 12(11):115003, 2010.

[85] Alexei Bylinskii, Dorian Gangloff, and Vladan Vuletić. Tuning friction atom-by-atom in an ion-crystal simulator. *Science*, 348(6239):1115–1118, 2015.

[86] yD Leibfried, R Blatt, C Monroe, and D Wineland. Quantum dynamics of single trapped ions. *Reviews of Modern Physics*, 75(1):281, 2003.

[87] Klaus Mølmer and Anders Sørensen. Multiparticle entanglement of hot trapped ions. *Physical Review Letters*, 82(9):1835, 1999.

[88] Gerald T Moore. Quantum theory of the electromagnetic field in a variable-length one-dimensional cavity. *Journal of Mathematical Physics*, 11(9):2679–2691, 1970.

[89] SA Fulling and PCW Davies. Radiation from a moving mirror in two dimensional space-time: conformal anomaly. In *Proceedings of the Royal Society of London A: Mathematical, Physical and Engineering Sciences*, volume 348, pages 393–414. The Royal Society, 1976.

[90] CM Wilson, Göran Johansson, Arsalan Pourkabirian, Michael Simoen, JR Johansson, Tim Duty, F Nori, and Per Delsing. Observation of the dynamical casimir effect in a superconducting circuit. *Nature*, 479(7373):376–379, 2011.

[91] Pasi Lähteenmäki, GS Paraoanu, Juha Hassel, and Pertti J Hakonen. Dynamical casimir effect in a josephson metamaterial. *Proceedings of the National Academy of Sciences*, 110(11):4234–4238, 2013.

[92] Giuliano Benenti and Giuliano Strini. Dynamical casimir effect and minimal temperature in quantum thermodynamics. *Physical Review A*, 91(2):020502, 2015.

[93] Walther Nernst. *The new heat theorem*. Methuen and Company, Ltd, 1926.

[94] Francesco Ticozzi and Lorenza Viola. Quantum resources for purification and cooling: fundamental limits and opportunities. *Scientific reports*, 4, 2014.

[95] Liliana Arrachea, Eduardo R Mucciolo, Claudio Chamon, and Rodrigo B Capaz. Microscopic model of a phononic refrigerator. *Physical Review B*, 86(12):125424, 2012.

[96] BR Mollow. Power spectrum of light scattered by two-level systems. *Physical Review*, 188(5), 1969.

[97] Ch Roos, Th Zeiger, H Rohde, HC Nägerl, J Eschner, D Leibfried, F Schmidt-Kaler, and R Blatt. Quantum state engineering on an optical transition and decoherence in a paul trap. *Physical Review Letters*, 83(23):4713, 1999.

[98] Joseph Fourier. *Theorie analytique de la chaleur, par M. Fourier*. Chez Firmin Didot, père et fils, 1822.

[99] Z Rieder, JL Lebowitz, and E Lieb. Properties of a harmonic crystal in a stationary nonequilibrium state. *Journal of Mathematical Physics*, 8(5):1073–1078, 1967.

[100] A Asadian, D Manzano, M Tiersch, and HJ Briegel. Heat transport through lattices of quantum harmonic oscillators in arbitrary dimensions. *Physical Review E*, 87(1):012109, 2013.

[101] Hiroshi Nakazawa. On the lattice thermal conduction. *Progress of Theoretical Physics Supplement*, 45:231–262, 1970.

[102] Dibyendu Roy and Abhishek Dhar. Heat transport in ordered harmonic lattices. *Journal of Statistical Physics*, 131(3):535–541, 2008.

[103] Lik Wee Lee and Abhishek Dhar. Heat conduction in a two-dimensional harmonic crystal with disorder. *Physical review letters*, 95(9):094302, 2005.

[104] Keiji Saito and Abhishek Dhar. Heat conduction in a three dimensional anharmonic crystal. *Physical review letters*, 104(4):040601, 2010.

[105] J. Labaziewicz, Y. Ge, P. Antohi, D. Leibrandt, K. R. Brown, and I. L. Chuang. Suppression of heating rates in cryogenic surface-electrode ion traps. *Phys. Rev. Lett.*, 100(1):013001, 2008.

[106] M. Niedermayr, K. Lakhmanskiy, M. Kumph, S. Partel, J. Edlinger, M. Brownnutt, and R. Blatt. Cryogenic surface ion trap based on intrinsic silicon. *New J. Phys.*, 16(11):113068, 2014.

[107] J. I. Cirac, R. Blatt, P. Zoller, and W. D. Phillips. Laser cooling of trapped ions in a standing wave. *Phys. Rev. A*, 46(5):2668, 1992.

[108] A. Chaudhuri, A. Kundu, D. Roy, A. Dhar, J. L. Lebowitz, and H. Spohn. Heat transport and phonon localization in mass-disordered harmonic crystals. *Phys. Rev. B*, 81(6):064301, 2010.

[109] F. Tisseur and K. Meerbergen. The quadratic eigenvalue problem. *SIAM Review*, 43(2):235–286, 2001.

[110] Kirill A Velizhanin, Chih-Chun Chien, Yonatan Dubi, and Michael Zwolak. Intrinsic thermal conductance, extended reservoir simulations, and kramers transition rate theory. *arXiv preprint arXiv:1312.5422*, 2013.

[111] A. Dhar. Heat transport in low-dimensional systems. *Advances in Physics*, 57(5):457–537, 2008.

[112] S. Lepri, R. Livi, and A. Politi. Thermal conduction in classical low-dimensional lattices. *Physics Reports*, 377(1):1–80, 2003.

[113] D. Stick, W. K. Hensinger, S. Olmschenk, M. J. Madsen, K. Schwab, and C. Monroe. Ion trap in a semiconductor chip. *Nature Physics*, 2(1):36–39, 2006.

[114] S. Seidelin, J. Chiaverini, R. Reichle, J. J. Bollinger, D. Leibfried, J. Britton, J. H. Wesenberg, R. B. Blakestad, R. J. Epstein, D. B. Hume, et al. Microfabricated surface-electrode ion trap for scalable quantum information processing. *Phys. Rev. Lett.*, 96(25):253003, 2006.

[115] M. Enderlein, T. Huber, C. Schneider, and T. Schaetz. Single ions trapped in a one-dimensional optical lattice. *Phys. Rev. Lett.*, 109(23):233004, 2012.

[116] Andrew Lucas. Ising formulations of many np problems. *arXiv preprint arXiv:1302.5843*, 2013.

[117] Edward Farhi, Jeffrey Goldstone, Sam Gutmann, Joshua Lapan, Andrew Lundgren, and Daniel Preda. A quantum adiabatic evolution algorithm applied to random instances of an np-complete problem. *Science*, 292(5516):472–475, 2001.

[118] Matthias Vojta. Quantum phase transitions. *Reports on Progress in Physics*, 66(12):2069, 2003.

[119] AP Young, S Knysh, and VN Smelyanskiy. First-order phase transition in the quantum adiabatic algorithm. *Physical review letters*, 104(2):020502, 2010.

[120] Per Bak. Commensurate phases, incommensurate phases and the devil's staircase. *Reports on Progress in Physics*, 45(6):587, 1982.

[121] Michael E Fisher and Walter Selke. Infinitely many commensurate phases in a simple ising model. *Physical Review Letters*, 44(23):1502, 1980.

[122] Walter Selke. The annni model—theoretical analysis and experimental application. *Physics Reports*, 170:213–264, 1988.

[123] Sei Suzuki, Jun-ichi Inoue, and Bikas K Chakrabarti. *Quantum Ising phases and transitions in transverse Ising models*, volume 862. Springer, 2012.

[124] Matteo Beccaria, Massimo Campostrini, and Alessandra Feo. Evidence for a floating phase of the transverse annni model at high frustration. *Physical Review B*, 76(9):094410, 2007.

[125] A Filinov, NV Prokof'Ev, and M Bonitz. Berezinskii-kosterlitz-thouless transition in two-dimensional dipole systems. *Physical review letters*, 105(7):070401, 2010.

[126] Amir Erez and Yigal Meir. Proposed measurement of spatial correlations at the berezinski-kosterlitz-thouless transition of superconducting thin films. *Physical review letters*, 111(18):187002, 2013.

[127] Zoran Hadzibabic, Peter Krüger, Marc Cheneau, Baptiste Battelier, and Jean Dalibard. Berezinskii–kosterlitz–thouless crossover in a trapped atomic gas. *Nature*, 441(7097):1118–1121, 2006.

[128] Jingfu Zhang, Tzu-Chieh Wei, and Raymond Laflamme. Experimental quantum simulation of entanglement in many-body systems. *Physical review letters*, 107(1):010501, 2011.

[129] R. Storn and K. Price. Differential evolution – a simple and efficient heuristic for global optimization over continuous spaces. *Journal of Global Optimization*, 11(4):341–359, 1997.

[130] Peter S Riseborough, Peter Hanggi, and Ulrich Weiss. Exact results for a damped quantum-mechanical harmonic oscillator. *Physical Review A*, 31(1):471, 1985.

[131] Nahuel Freitas and Juan Pablo Paz. Analytic solution for heat flow through a general harmonic network. *Physical Review E*, 90(4):042128, 2014.